

# Deliverable 2.6: “Generating Compact Models for Linear and Nonlinear Thermo-Mechanical Finite Element Models in Microelectronics”

COMPAS

**Compact** modelling of high-tech systems for health management and optimization along the supply chain

<b>Lead beneficiary:</b>	Jade
<b>WP. no, title</b>	WP2, Main achievements of WP2
<b>Contributing task(s)</b>	T2.1 Projection-based MOR for linearized thermo-mechanical models T2.2 Projection-based model order reduction for nonlinear thermo-mechanical models T2.3 Model order reduction via machine learning methods
<b>Dissemination level</b>	Public
<b>Delivery date</b>	M32
<b>Status</b>	Final

Leading Authors		
<i>Name</i>	<i>Beneficiary name</i>	<i>Contact email</i>
Ibrahim Zawra Chengdong Yuan Chisom Umunnakwe Arwed Schütz	Jade University of Applied Sciences.	<a href="mailto:tamara.bechtold@jade-hs.de">tamara.bechtold@jade-hs.de</a>

Tamara Bechtold		
<b>Co-Authors</b>		
<i>Name</i>	<i>Beneficiary Name</i>	<i>Contact email</i>
Ghanshyam Gadhiy	Fraunhofer	<a href="mailto:ghanshyam.gadhiya@enas.fraunhofer.de">ghanshyam.gadhiya@enas.fraunhofer.de</a>
Pascal den Boef	Eindhoven University of Technology	<a href="mailto:p.d.boef@tue.nl">mailto:p.d.boef@tue.nl</a>
Diana Manvelyan	Siemens Germany	<a href="mailto:diana.manvelyan@siemens.com">diana.manvelyan@siemens.com</a>
Frank Naets	KU Leuven	<a href="mailto:frank.naets@kuleuven.be">mailto:frank.naets@kuleuven.be</a>
Michiel van Soestbergen	NXP Semiconductors B.V	<a href="mailto:michiel.van.soestbergen@nxp.com">michiel.van.soestbergen@nxp.com</a>
Martin Niessner	Infineon AG	<a href="mailto:martin.niessner@infineon.com">martin.niessner@infineon.com</a>

# Table of contents

Table of contents .....	3
Table of Figures .....	5
Executive Summary .....	10
1. Introduction.....	12
2. Reduction of Linearized Weakly-Coupled Thermo-Mechanical Models .....	13
2.1. Introduction .....	13
2.2. Sequential MOR.....	14
2.3. Decoupled Domains MOR.....	15
2.4. System Level Simulation and Validation of ROMs Accuracy.....	17
3. Reduction of Linearized Strongly-Coupled Thermal Transient and Mechanical Quasi-Static Models.....	20
3.1. Introduction .....	20
3.2. Case study: a packaged chip model from Infineon.....	20
3.3. Coupled quasi-static thermo-mechanical system .....	21
3.4. Krylov subspace-based model order reduction .....	22
3.5. MOR of the packaged chip model in ANSYS .....	23
3.6. Stress outputs from the ROM using the expansion pass method .....	24
3.7. System-level simulation and validation of ROM .....	24
4. Generation of Boundary Condition Independent Compact Thermo-Mechanical Models. ...	26
4.1. Introduction .....	26
4.2. pMOR for Infineon model with parametrized film coefficient $h$ in the convection boundary condition.....	26
4.3. pMOR for NXP model with parametrized Young's modulus in the solder joints.....	30
5. Development of New DoE-RSM Schemes for Nonlinear Compact Modelling. ....	39
5.1. Introduction .....	39
5.2. Compact model generation using SoS (Statistics on Structures) .....	39
5.3. Compact model generation using StaticROM Builder.....	41
6. Reduction of Linearized Strongly-Coupled Dynamic Thermo-Mechanical Models. ....	43
6.1. Introduction .....	43
6.2. Coupling strategy .....	43
6.3. Toolchain overview .....	47
6.4. Model Order Reduction of a Strongly-Coupled Dynamic Thermo-Mechanical Infineon Package Model in ANSYS.....	52

6.5.	ROM Verification in ANSYS Twin Builder.....	56
7.	Reduction of Nonlinear Thermo-Mechanical Models by Piecewise Linear Approximation .	57
7.1.	Introduction .....	57
7.2.	Trajectory Piece Wise-Linear approach. ....	57
7.3.	Simplified electronics case study with Ball Grid Array.....	58
7.4.	MEMS beam actuator.....	59
7.5.	Extension to thermomechanical practical difficulties and possibilities. ....	61
8.	Development of a Data-Based Reduced Order Modelling .....	63
8.1.	Introduction .....	63
8.2.	Method.....	63
8.3.	Results.....	65
9.	Conclusion and Outlook.....	67
10.	Bibliography.....	69

## Table of Figures

FIGURE 1: EXPLODED MODEL GEOMETRY WITH SELECTED OUTPUT NODE FOR RESULT COMPARISON.....	13
FIGURE 2: WORKFLOW FOR THE SEQUENTIAL THERMO-MECHANICAL REDUCTION.....	14
FIGURE 3: REPRESENTATION OF COUPLING OF THERMAL AND MECHANICAL ROMS AT SYSTEM LEVEL.....	16
FIGURE 4: PROJECT SCHEMATIC IN ANSYS WORKBENCH FOR GENERATING TWO SINGLE-DOMAIN ROMS (THERMAL AND MECHANICAL).....	16
FIGURE 5: SEQUENTIAL MOR SYSTEM LEVEL SIMULATION SETUP.....	17
FIGURE 6: DEFORMATION COMPARISON (LEFT) AND ERROR PLOT (RIGHT) BETWEEN SEQUENTIAL ROM AND FOM.....	18
FIGURE 7: COMPONENT STRESS COMPARISON (LEFT) AND ERROR PLOT (RIGHT) BETWEEN SEQUENTIAL ROM AND FOM.....	18
FIGURE 8: DECOUPLED DOMAINS ROMS SYSTEM LEVEL SIMULATION SETUP.....	19
FIGURE 9: DEFORMATION COMPARISON (LEFT) AND ERROR PLOT (RIGHT) BETWEEN DECOUPLED DOMAINS ROM AND FOM.....	19
FIGURE 10: EXECUTED WORKFLOW FOR MOR FOR LINEARIZED COUPLED QUASI-STATIC THERMO-MECHANICAL MODEL.....	20
FIGURE 11: EXPLODED VIEW OF MODEL GEOMETRY.....	21
FIGURE 12: PROJECT SCHEMATIC UTILISED FOR COUPLED DOMAIN THERMO-MECHANICAL REDUCTION.....	23
FIGURE 13: DETAILS OF ANALYSIS SYSTEM A, EXPORT RESULTS FROM THE FOM.....	23
FIGURE 14: DETAILS OF ANALYSIS SYSTEM B, GENERATE THE ROM.....	23
FIGURE 15: DETAILS OF ANALYSIS SYSTEM C, ADD STRESS COEFFICIENTS TO THE OUTPUT MATRIX.....	24
<i>FIGURE 16: SYSTEM-LEVEL SIMULATION SET-UP OF THE ROM IN TWIN BUILDER.....</i>	<i>24</i>
FIGURE 17: VALIDATION OF ROM WITH FOM.....	25
FIGURE 18 CRACK IN THE SOLDER BALL DUE TO THERMAL LOADING [21].....	26
FIGURE 19 AN EXPLODED VIEW OF THE INFINEON TRAINING MODEL PG-TDSON-8.....	27
FIGURE 20 SIMULATION OF THE PARAMETRIC REDUCED ORDER MODEL IN ANSYS TWIN BUILDER.....	29
FIGURE 21 COMPARISON OF THE RESULTS FROM FULL ORDER AND PARAMETRIC REDUCED ORDER MODELS.....	30
FIGURE 22 AN EXPLODED VIEW OF THE WAVER CHIP-SCALE PACKAGE.....	31
FIGURE 23 VOLUMETRIC MESH SECTIONED THROUGH THE WHOLE MODEL.....	31
FIGURE 24 THE SCHEMATIC OF A SYSTEM LEVEL SIMULATION IN THE REDUCED SPACE, WHILE B0, B1, B2, E1 AND E2 ARE CONSISTENT WITH THE DEFINITIONS IN THE EQUATIONS IN THE PREVIOUS SECTIONS. THE OUTPUTS ON THE RIGHT-HAND SIDE ARE ARBITRARY THREE POINTS DIRECTIONAL DISPLACEMENTS. 'SBOTTOM' AND 'STOP' ARE TWO POINTS CHOSEN ARBITRARILY IN THE SOLDER MATERIAL DOMAIN, WHILE CHIP IS IN THE SILICON MATERIAL DOMAIN.....	35

FIGURE 25 A COMPARISON BETWEEN THE FULL ORDER MODEL AND PARAMETRIC REDUCED MODEL IN RESPONSE TO TEMPERATURE CYCLING. THE RESPONSE IS THE DISPLACEMENT IN X-DIRECTION AT THE NODE 'SBOTTOM' DEFINED IN FIGURE 20. ....	36
FIGURE 26 VALIDATION FOR A SINGLE DOMAIN PARAMETRIC REDUCED ORDER MODEL. THE CHOSEN EXPANSION POINT IS 2.9E10 PA. ....	37
FIGURE 27 THE INFLUENCE OF CHOOSING THE EXPANSION POINT ON RELATIVE ERROR, THE HORIZONTAL AXIS IS THE EXPANSION POINT OF THE FIRST PARAMETER (YOUNG'S MODULUS) AND THE VERTICAL AXIS IS THE EXPANSION POINT OF THE SECOND PARAMETER, WHILE THE COLOR REPRESENTS THE ERROR. ....	37
FIGURE 28 THE RELATION BETWEEN THE RELATIVE ERROR AND THE SIZE OF THE REDUCED SPACE. ON THE HORIZONTAL AXIS IS THE NUMBER OF VECTORS GENERATED FOR EACH PARAMETER MATRIX.....	37
FIGURE 29 OPTISLANG SET-UP FOR GENERATING TRAINING DATA FOR SOS.....	39
FIGURE 30 SOS GUI .....	40
FIGURE 31 : RESULTS FROM SOS .....	41
FIGURE 32 STATIC ROM GENERATION .....	42
FIGURE 33 STATIC ROM VALIDATION.....	42
FIGURE 34: ASSEMBLED STIFFNESS MATRIX OF THE CIRCUIT BOARD WITH THE NXP CHIP CONNECTED VIA FIVE SOLDER BALLS .....	43
FIGURE 35: ILLUSTRATION OF THE DESCRIBED INTERFACE WITH THE NXP CHIP. RED DOTS INDICATE THE DETECTED CLOSEST NODES TO THE SOLDER BALLS. PCB IS DISCRETIZED USING AN 8-NODE LINEAR SOLID ELEMENT TYPE. ....	44
FIGURE 36: ILLUSTRATION OF THE DESCRIBED INTERFACE WITH THE INFINEON CHIP. BLUE AND PINK DOTS RESPECTIVELY INDICATE THE DETECTED CLOSEST NODES TO THE SOLDER PARTS TO THE CHIP AND PCB. ....	45
FIGURE 37: ASSEMBLED STIFFNESS AND MASS MATRICES OF THE INFINEON PG-TDSON-8 MODEL.....	45
<i>FIGURE 38: EIGENMODES FOR THE FIRST THREE MODES FOR THE ROM OF INFINEON PG-TDSON-8 .....</i>	<i>46</i>
FIGURE 39: ASSEMBLED STIFFNESS AND MASS MATRICES OF THE COUPLED THERMO-MECHANICAL PG-TDSON-8 MODEL .....	46
FIGURE 40: RE-POSITIONING THE NXP AND INFINEON CHIPS ON THE PCB .....	46
FIGURE 41: EIGENMODES OF THE ROM CIRCUIT BOARD WITH THE NXP AND INFINEON CHIPS.....	47
FIGURE 42: FINITE ELEMENT MODEL OF THE CIRCUIT BOARD WITH THE PCB AND INFINEON CHIPS IN SIMCENTER .....	47
FIGURE 43: MATLAB INTERFACE TO IMPORT VARIOUS CHIP, SOLDER AND PCB MODELS ....	48
FIGURE 44: FOM EXTRACTION FROM NX NASTRAN.....	48
FIGURE 45: INTERFACE EXTRACTION FOR SOLDERS (TOP AND BOTTOM SURFACE) .....	48
FIGURE 46: INTERFACE IDENTIFICATION FOR CHIP AND PCB.....	48
FIGURE 47: INFINEON SYSTEM GEOMETRY AND INTERFACES.....	49
FIGURE 48: SIEMENS SIMCENTER INTERFACE FOR PCB-CHIP ASSEMBLY CONSTRUCTION. ....	49
<i>FIGURE 49: ROM GENERATION INTERFACE WITH STOCHASTIC LOAD MODES .....</i>	<i>49</i>

FIGURE 50: SINGULAR VALUE DECAY IN STOCHASTIC LOAD MODES FOR INFINEON CHIP AND PCB MODEL ..... 50

FIGURE 51: SINGULAR VALUE DECAY IN STOCHASTIC LOAD MODES FOR THREE SOLDER PATCHES IN INFINEON MODEL  $\mu$  ..... 50

FIGURE 52: FULL SYSTEM LEVEL MODEL DESCRIPTION COMBINING CHIPS, PCBs, SOLDERS AND CORRESPONDING CONNECTIONS. .... 50

FIGURE 53: MODEL ASSEMBLY ROUTINE ..... 51

FIGURE 54: ASSEMBLED ROMS FOR FULL INFINEON SYSTEM MODEL ..... 51

FIGURE 55: EIGENVALUES EVALUATED FOR INFINEON SYSTEM FROM THE ASSEMBLED REDUCED ORDER MODEL. .... 51

FIGURE 56: MODE SHAPES OBTAINED FROM INFINEON SYSTEM MODEL..... 52

FIGURE 57: (A) AN EXPLODED VIEW OF THE INFINEON TRAINING MODEL PG-TDSON-8. (B) THE MESH OF GENERATED IN THE MODEL. THERE ARE 13216 NODES IN TOTAL AND EACH NODE CONTAINS 4 DEGREE OF FREEDOMS: UX, UY, UZ, TEMP. .... 52

FIGURE 58: (A) HEAT FLOW INPUT APPLIED ON THE TOP SURFACE OF THE CHIP. (B) HEAT FLOW INPUT VALUE INCREASES FROM 0 TO 0.1 AT 5E-4 S. THE INPUT VALUE IS CONSTANT AT 0.1 BETWEEN 5E-4 S AND 0.1 S. .... 53

FIGURE 59: (A) CONVECTION BOUNDARY CONDITION APPLIED ON THE EXTERNAL SURFACES OF THE MODEL. (B) FILM COEFFICIENT IS DEFINED AS CONSTANT 1E6 W/M<sup>2</sup>°C. THE AMBIENT TEMPERATURE IS INCREASED FROM 22 °C TO 125 BETWEEN 2E-2 AND 3E-2 S..... 53

FIGURE 60: (A) VIBRATIONAL DISPLACEMENT INPUT APPLIED ON TWO VERTICES AT THE BOTTOM SURFACE. (B) SINE WAVE INPUT VALUES WITH AMPLITUDE 5E-5 M AND FREQUENCY 100 HZ..... 54

FIGURE 61: MODEL SETUPS FOR THE GENERATION OF THE ROM IN ANSYS MECHANICAL.. 55

FIGURE 62: ROM FILES GENERATED FROM ANSYS MECHANICAL VIA 'MODEL REDUCTION INSIDE ANSYS'..... 55

FIGURE 63: SIMULATION OF THE ROM IN ANSYS TWIN BUILDER WITH FORCE, HEAT FLOW, REFERENCE TEMPERATURE, AND AMBIENT TEMPERATURE INPUTS. .... 56

FIGURE 64: COMPARISON OF THE DISPLACEMENT AND TEMPERATURE RESULTS FROM THE SELECTED OUTPUT NODE..... 56

FIGURE 65 GENERATION OF THE LINEARIZED MODELS (S1, S2,...,SN) ALONG A TRAJECTORY OF A NONLINEAR SYSTEM IN A TWO-DIMENSIONAL STATE SPACE [23]..... 58

FIGURE 66 LEFT: A SCHEMATIC REPRESENTATION OF A GEOMETRIC MODEL DELINEATING DISTINCT MATERIAL DOMAINS AND PRESCRIBING DIRICHLET BOUNDARY CONDITIONS ON THE LOWER SURFACE OF THE PRINTED CIRCUIT BOARD (PCB) AT THREE SPECIFIED CORNER POINTS A MECHANICAL COMPRESSION FORCE IS APPLIED AS A DISTRIBUTED LOAD ON THE UPPER SURFACE OF THE CHIP. RIGHT: THE COLOR MAP REPRESENTS THE SOLDER PLASTIC STRAIN, MEASURED IN MILLIMETERS PER METER, ATTAINED DURING THE FINAL LOAD STEP, PROVIDING INSIGHTS INTO THE DEFORMATION BEHAVIOR OF THE MATERIAL UNDER MECHANICAL LOAD CONDITIONS. .... 59

FIGURE 67 A COMPARISON BETWEEN THE REDUCED ORDER MODEL GENERATED BY APPLYING TPWL AND THE FULL ORDER MODEL (FOM) WITH THE ERROR PLOT INSIDE. .... 59

FIGURE 68 OPERATING PRINCIPLE OF THE MICROSYSTEM [4] [5]:A SPHERICAL CAP RESTS ON FOUR ELECTROSTATIC BEAM ACTUATORS. ACTUATING THE BEAMS INTO PULL-IN

TRANSFERS MOMENTUM TO THE SPHERICAL CAP. AFTER A FREE FLIGHT PHASE, THE MIRROR IS CAUGHT INTO ITS STABLE RESTING ..... 60

FIGURE 69 WORKFLOW OF MODELING: FEM MODELS THE BEAM ACTUATOR AS A HIGH-DIMENSIONAL SYSTEM OF ORDINARY DIFFERENTIAL EQUATIONS. SUBSEQUENTLY, MOR CONSTRUCTS AN ACCURATE SURROGATE MODEL OF DRASTICALLY SMALLER DIMENSION. .... 60

FIGURE 70 THE CONCEPT OF THE TPWL APPROXIMATION. THE LOAD CASE ILLUSTRATED IN THE TOP ROW RELIES ON MECHANICAL CONTACT, RENDERING THE MODEL NONLINEAR. THE TPWL APPROXIMATION REPLACES THE ORIGINAL SYSTEM WITH A COMBINATION OF LINEARIZED ONES, WHICH ARE OBTAINED AT DIFFERENT STATES ALONG THE TRAJECTORY. THE LINEARIZED MODELS' RANGE OF VALIDITY IS INDICATED BY CIRCLES AT THEIR LINEARIZATION STATES. .... 60

FIGURE 71 COMPARISON OF THE BEAM'S VERTICAL TIP DISPLACEMENT OVER THE NORMALIZED LOAD. THE FEM SOLUTION CONSTITUTES THE REFERENCE, WHICH THE TPWL MODEL AND ITS REDUCED VERSION APPROXIMATE. THE PLOT ALSO HIGHLIGHTS SAMPLING POSITIONS FOR LINEARIZED MODELS UTILIZED..... 61

FIGURE 72 THE SCHEMATIC DEPICTS THE WORKFLOW FOR EACH TIME STEP IN ANSYS. NOTABLY, THE USER LACKS CONTROL OVER NON-MECHANICAL LOADS, ENCOMPASSING THERMAL LOADS..... 62

FIGURE 73: OVERVIEW OF THE EXAMPLE APPLICATION OF THE NONLINEAR MOR TECHNIQUE. WE CONSIDER THE PROBLEM OF MODELLING SOLDER JOINT – WHICH BEHAVE NONLINEARLY AND ARE CRITICAL FOR ASSESSING STRUCTURAL INTEGRITY OF COMPONENTS IN AUTOMOTIVE SYSTEMS. .... 63

FIGURE 74: 1D MODELLING OF SOLDER JOINT USING FINITE DIFFERENCE METHOD (FDM). 65

FIGURE 75: ACCURACY OF THE ROM FOR A SAMPLE OF THE TRAINING DATASET ..... 66

FIGURE 76: ACCURACY OF THE ROM FOR THE VALIDATION DATASET ..... 66

## List of abbreviations and acronyms

BC	Boundary Condition
DOF	Degrees of Freedom
FE	Finite Element
FOM	Full Order Model
MOR	Model Order Reduction
MORiA	Model Order Reduction inside ANSYS
ROM	Reduced Order Model
POD	Proper Orthogonal Decomposition
TPWL	Trajectory Piece Wise Linear Approximation

### Partner acronyms

Atlas	Atlas Technologies B.V.		MSC	MSC Software	
FhG-ENAS	Fraunhofer ENAS		NXP	NXP Semiconductors B.V.	
Eesy	Eesy-Innovation		Reden	Reden B.V.	
IFAG	Infineon		SIEM	Siemens Munich	
JADE	JADE Hochschule		SISW	Siemens Industry Software	 
KU Leuven	Katholieke Universiteit Leuven		TUD	Delft University of Technology	
MCE	MicroConsult Engineering		Tue	Eindhoven University of Technology	

## Executive Summary

High-tech systems integrate numerous highly complex components. Simulations are necessary at various stages of their design process, to ensure mechanical robustness and reliability. Within this context, the EU project COMPAS aims to develop novel compact models and ultra-compact digital twins for the supply chain of those systems. COMPAS investigates the thermo-mechanical reliability of high-tech systems, such as motor control units for automated factories, smart infrastructures (streetlights, power grids) or autonomous vehicles, using computer simulations.

Mathematical methods of model order reduction (MOR) can speed-up the simulation time significantly and enable system level simulation, efficient design optimization and finally exchange of component models along the supply chain without disclosing the IP. This report describes the achievements of COMPAS consortium on advancing and adapting the MOR methodology towards the microelectronic applications.

Chapter 2 documents how MOR can be applied to linearized weakly-coupled thermo-mechanical models with outstanding accuracy. Two approaches are carried out 'sequential MOR', which generates a single coupled-domain reduced order model (ROM), and 'decoupled domains MOR', which generates single-domain thermal and mechanical ROMs, which are coupled at the system level. Validation of both methods by comparison with full order finite element models (FOMs) demonstrates excellent accuracy.

Chapter 3 describes reduction of linearized strongly-coupled thermal transient and mechanical quasi-static models. The case study is an Infineon thermo-mechanical packaged chip (PG-TDSON-8) model, in which the thermal domain is transient with time-varying boundary conditions and thermal load. In addition, the structural domain of the model is approximated as quasi-static which denotes the negligence of the effects of inertia. By long exposure of such packaged chip system to high varying temperature environment, the solder connections between the packaged chip and the PCB may fail due to the mismatch in thermal expansion of materials. Compact modelling technique using the Krylov-subspace-based method is utilised for efficient studies of the thermal impact on the solder joints. Temperature, mechanical stresses, and displacements are investigated at a given node on the solder joint as outputs in the ROM. The ROM is validated with the original full-scale FEA model and an excellent comparison is observed.

Chapter 4 explains the generation of boundary condition independent compact thermo-mechanical models (detailed report is in D2.4). For efficient studies of the temperature impact on the solder joints, we present a successful application of parametric model order reduction for constructing a compact model starting from the full order finite element model. Temperature dependent Young's modulus, a parameter, which appears on both the left-hand and the right-hand side of the spatially discretized model, is preserved in the symbolic form within this compact model. In addition, we present another application in which we enable to set the film coefficient and the ambient temperature in the convection boundary condition as the parameters in the reduced-order model level.

Chapter 5 gives an overview of available DoE-RSM schemes for nonlinear compact modelling in different Ansys tools, like SoS (Statistics on Structures) and StaticROM Builder. The Infineon package FE model delivers training from static thermo-mechanical analysis considering different material nonlinearities (e.g. viscoelasticity, creep, plasticity). Training data required for testing these tools are generated using virtual DoE simulation set-up developed for different temperature cycles (reported in D3.2).

Chapter 6 deals with reduction of linearized strongly-coupled dynamic thermos-mechanical models. The proposed substructuring approach aims to circumvent the computational challenges

associated with the dynamic analysis of coupled thermo-mechanical circuit models, which commonly have large numbers of degrees-of-freedom. The approach involves dividing the chip, solder, and PCB meshes into various substructures using Simcenter, and developing a novel assembly approach for the ROMs that is tailored to the structure of circuit boards. A novel coupling scheme is also developed to account for the non-conforming interface conditions between the different substructures using a penalty-based enforcement of the interface conditions. The resulting model can be used in an eigenvalue analysis or a time-domain simulation to predict the dynamic behaviour of the system. Furthermore, in this chapter the workflow of generating a ROM of a strongly-coupled dynamic thermo-mechanical Infineon package model from ANSYS Mechanical is presented.

Chapter 7 describes the results of applying the trajectory piece wise linear approximation for reduction of nonlinear FE models in Ansys. Our case studies are a simplified Ball Grid Array (BGA) and a micro-mechanical beam actuator, both implemented in Ansys FE simulation software. The initial results show that both case studies could be reduced with satisfying accuracy. The reduction of coupled-domain thermo-mechanical models in Ansys remains a challenge.

Chapter 8 describes the development of machine data-based reduced order modelling. This technique is non-intrusive, i.e., it only requires snapshots of simulation. This makes it particularly attractive for integration with commercial finite element analysis (FEA) software packages, which often do not provide access to the model equations. Simulation snapshots are always available.

Chapter 9 concludes the presented work and gives an outlook to the future research.

## 1. Introduction

In this comprehensive report, we delve into a multifaceted exploration of advanced model order reduction techniques within the domain of thermo-mechanical modeling. Our investigation unfolds across seven distinct sections, each contributing uniquely to the overarching goal of enhancing the efficiency and applicability of these reduction methodologies.

Section 2 delves into the intricacies of reducing linearized weakly-coupled thermo-mechanical models, shedding light on methods to streamline these systems while preserving accuracy. Following this, Section 3 focuses on the reduction of linearized thermal transient and mechanical quasi-static models, introducing nuanced approaches to address dynamic and quasi-static aspects concurrently.

Section 4 navigates the generation of boundary condition-independent compact thermo-mechanical models, offering insights into techniques that transcend traditional dependencies. In Section 5, we explore the development of novel Design of Experiments-Response Surface Methodology (DoE-RSM) schemes tailored for nonlinear compact modeling, unveiling innovative approaches to capturing nonlinearity within reduced models.

The subsequent sections, 6 and 7, tackle the reduction techniques for dynamically coupled linearized thermo-mechanical models and the development of structure-preserving model order reduction techniques for nonlinear multi-physics models, respectively. These sections underscore the report's commitment to advancing reduction methodologies across diverse thermo-mechanical scenarios.

Collectively, this report provides a comprehensive survey of cutting-edge techniques, contributing to the evolution of model order reduction strategies and their application to complex thermo-mechanical systems.

## 2. Reduction of Linearized Weakly-Coupled Thermo-Mechanical Models

### 2.1. Introduction

In this report, we consider a linearized thermo-mechanical training model from Infineon (PG-TDSON-8). FOM is simulated in ANSYS Workbench (version 2021 R2, Ansys Inc.) and time-varying nodal displacements, temperatures and stresses are determined, in response to transient thermal loads. Material properties are temperature-independent and linear elasticity is assumed. In order to generate ROM, a Krylov-subspace based Block-Arnoldi reduction algorithm is used [1]. Furthermore, software “Model Reduction inside ANSYS” (MORiA) [2] has been extended to allow for mechanical stress outputs at the system level.

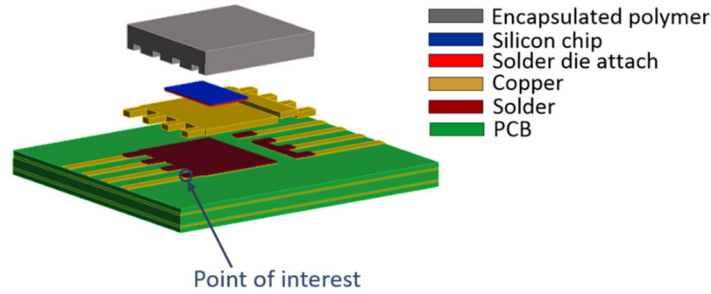


Figure 1: Exploded model geometry with selected output node for result comparison.

For the comparison between the FOM and ROM, a node defined as point of interest is selected (see Figure 1). Mechanical deformation due to thermal expansion is investigated.

MOR is a numerical technique that enables an automated generation of accurate, low-dimensional models directly from high-dimensional finite element models [3]. Krylov-subspace based MOR aims at approximating the transfer function of the original model by model of much smaller order. In this work, the spatially discretized and linearized thermo-mechanical system is approximated as a mechanical-quasi-static model in the following form:

$$\underbrace{\begin{bmatrix} 0 & 0 \\ 0 & E_T \end{bmatrix}}_E \underbrace{\begin{Bmatrix} \dot{U} \\ \dot{T} \end{Bmatrix}}_{\dot{x}} + \underbrace{\begin{bmatrix} K_U & K_{UT} \\ 0 & K_T \end{bmatrix}}_K \underbrace{\begin{Bmatrix} U \\ T \end{Bmatrix}}_x = \underbrace{\begin{Bmatrix} F \\ Q \end{Bmatrix}}_{B \cdot u} \quad (1)$$

$y = Cx$

where the state vector  $x \in \mathbb{R}^n$  contains nodal displacements  $U$  and nodal temperatures  $T$ . The term  $K_{UT}$  couples the thermal and the mechanical DOFs. For linear thermo-mechanical applications, Block Arnoldi method [1], which is implemented in MORiA, has already been proved to be successful in generating extremely accurate ROMs [4]. The approximation of (3) is attained by projecting it onto an appropriate low-dimensional subspace  $V$ . The full-scale state vector is approximated as  $x \approx V \cdot x_r$ , where  $x_r \in \mathbb{R}^r$ ,  $r \ll n$ , can be considered as a vector of generalized coordinates leading to the reduced system of the form:

$$\underbrace{\frac{V^T E V}{E_r}} \dot{x}_r(t) + \underbrace{\frac{V^T K V}{K_r}} x_r(t) = \underbrace{\frac{V^T B}{B_r}} \cdot u(t)$$

$$y(t) = \underbrace{C V}_{C_r} x_r(t) \quad (2)$$

In the Laplace domain, the transfer function of (3)  $H(s) = C\{sE + K\}^{-1}B$  is thus, reduced to  $H_r(s) = C_r\{sE_r + K_r\}^{-1}B_r$ . It can be proven that if  $V$  is chosen as a basis of the right-Krylov subspace

associated with (1),  $V = \text{span}\{\tilde{B}, A\tilde{B}, A^2\tilde{B}, \dots, A^{r-1}\tilde{B}\}$  where  $\tilde{B} = K^{-1}B$  and  $A = -K^{-1}E$ . The first  $r$  moments in the Taylor series expansion of the full- and reduced system's transfer function match.

## 2.2. Sequential MOR

Given a fully coupled thermo-mechanical system in mechanical-quasi-static form:

$$\begin{bmatrix} 0 & 0 \\ 0 & E_T \end{bmatrix} \begin{Bmatrix} \dot{U} \\ \dot{T} \end{Bmatrix} + \begin{bmatrix} K_U & K_{UT} \\ 0 & K_T \end{bmatrix} \begin{Bmatrix} U \\ T \end{Bmatrix} = \begin{Bmatrix} 0 \\ Q \end{Bmatrix} \quad (3)$$

Note that there is no damping and mechanical load exists in the system. This means that the temperature results influence directly on the nodes containing mechanical DOFs via the thermal expansion effect, in which the coefficient of thermal expansion is not zero.

We can rewrite the equation (3) into two domains with the output equations:

$$\text{Mechanical: } \begin{cases} K_U \cdot U = -K_{UT} \cdot T \\ y_U = C_U \cdot U \end{cases} \quad (4)$$

$$\text{Thermal: } \begin{cases} E_T \cdot \dot{T} + K_T \cdot T = Q \\ y_T = C_T \cdot T \end{cases} \quad (5)$$

Firstly, the thermal model (5) is reduced. The full-scale temperature state vector  $T$  is approximated by  $T \approx V \cdot z$  and the reduced thermal ROM is written as:

$$\begin{cases} V^T E_T V \cdot \dot{z} + V^T K_T V \cdot z = V^T Q \\ y_T = C_T V \cdot z \end{cases} \quad (6)$$

To obtain the static deformation results from the mechanical domain, equation (4) becomes:

$$\begin{cases} U = -K_U^{-1} K_{UT} V \cdot z \\ y_U = C_U \cdot U = \underbrace{-C_U K_U^{-1} K_{UT} V}_{\tilde{C}_U} \cdot z \end{cases} \quad (7)$$

where the mechanical outputs  $y_U$  can now be computed and added to the output equation in (6):

$$\begin{cases} V^T E_T V \cdot \dot{z} + V^T K_T V \cdot z = V^T Q \\ y = \begin{bmatrix} y_T \\ y_U \end{bmatrix} = \begin{bmatrix} C_T V \\ \tilde{C}_U \end{bmatrix} z \end{cases} \quad (8)$$

The following project schematic is utilized in ANSYS Workbench:

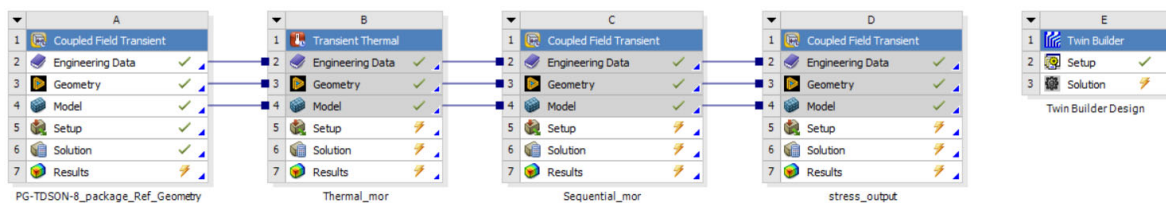


Figure 2: Workflow for the sequential thermo-mechanical reduction.

As presented in Figure 2, analysis system A includes the material properties, geometry, and mesh data. Full thermo-mechanical model is simulated in A and the results are exported as the reference for comparison. It is coupled with the transient thermal analysis system B, where MOR is made firstly for the thermal model. Then, the sequential MOR is done in C. The ROM with stress outputs is generated in D. The system level-simulation of the ROM is performed in ANSYS Twin Builder in E.

The model setups in ANSYS Workbench can be seen from the figure at the right-hand side of this page. In analysis system B, we first make the model reduction by using the macro from MORiA:

```
mor_driver_thermal_mor, '-N 30 -b -v -  
tml',,,, 'outname',,,, 'convtemp',,,, 'heatflow'
```

where `-tml` is a new flag used to generate the matrices, which are necessary to be transferred to the next stage of reduction. These matrices are written in binary form and saved to files named:

`mor.tmV`  
`mor.tmVnv`

where `mor.tmV` is the projection matrix used for the reduction of thermal model and `mor.tmVnv` contains the information of the nodes, which is used to obtain the submatrices  $K_U$  and  $K_{UT}$  from the coupled field analysis system C. The sequential MOR is done in analysis system C by using the macro:

```
mor_thermomech_mor, '-v', 'names'
```

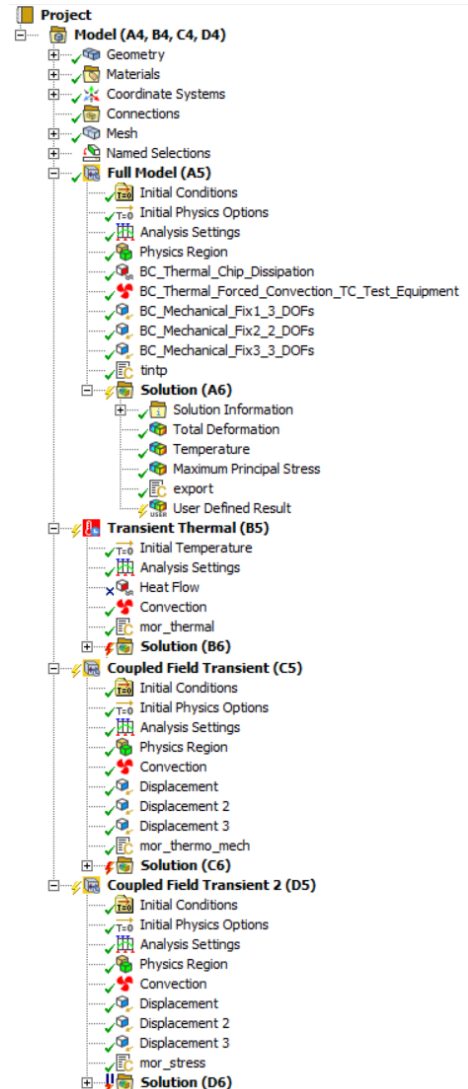
This macro reads the `mor.tmV` and `mor.tmVnv` files and adds the mechanical outputs to the output matrix of the thermal ROM as presented in equation (8). Then, the reduced model is regenerated and system-level files are created. Please find the details of all macros used in this project in **Fehler! Verweisquelle konnte nicht gefunden werden. A**.

### 2.3. Decoupled Domains MOR

The goal is to generate two ROMs from thermal and mechanical domains, separately, and couple them at the system level. As shown in Figure 3, the reduction of the thermal model will be carried out firstly. The thermal ROM like Equation (6) is obtained:

$$\begin{cases} V^T E_T V \cdot \dot{z} + V^T K_T V \cdot z = V^T Q \\ y_T = C_T V \cdot z \end{cases} \quad (9)$$

Note that, temperatures in all FE nodes are defined as outputs; i.e.  $C_T$  is a unity matrix of dimension  $n$ . Furthermore, it holds:



$$T \approx V \cdot z = \underbrace{\begin{bmatrix} V_{11} & \dots & V_{1r} \\ \vdots & \ddots & \vdots \\ V_{N1} & \dots & V_{Nr} \end{bmatrix}}_V \underbrace{\begin{bmatrix} z_1 \\ \vdots \\ z_r \end{bmatrix}}_z \quad (10)$$

which implies that the full temperature state vector  $T$  is expressed as a linear combination of the reduced states  $z$  and the columns of the projection matrix  $V$  are the coefficients. Those columns are applied as thermal loads to the full order mechanical model, which is also reduced by projection. The mechanical ROM is expressed as follows:

$$\begin{cases} \tilde{V}^T K_U \tilde{V} \cdot q = \tilde{V}^T \tilde{B} \underbrace{V \cdot z}_T \\ y_U = C_U \tilde{V} \cdot q \end{cases} \quad (11)$$

where  $\tilde{B}$  is the input distribution array, which translates nodal temperatures into mechanical forces as described in [5],  $\tilde{V}$  is the projection matrix constructed as an orthonormal basis of the Krylov subspace  $\mathcal{K}_r \{-K_U^{-1} M_U, K_U^{-1} \tilde{B}\}$  and  $q$  is a reduced state-vector, where  $M_U$  is a dummy mass matrix used only for practical considerations. In this way, the full reduction subspace  $V$  is integrated in the mechanical reduced input matrix  $\tilde{B}_r = \tilde{V}^T \tilde{B} V$  and mechanical ROM has  $r$  inputs. The primary output of the mechanical ROM are the nodal displacements caused by the thermal expansion effect. Furthermore, mechanical stresses can also be observed at the system-level, as will be shown in the next section. Please note, that the coupling does not occur in the system matrices but through the input/output vectors. We refer to this as weak-coupling.

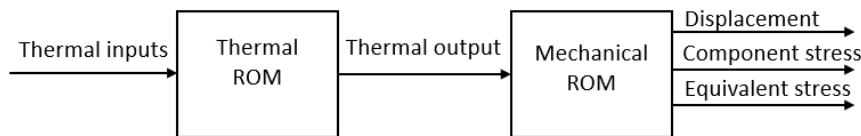


Figure 3: Representation of coupling of thermal and mechanical ROMs at system level.

The advantage of this method is that the ROMs are generated for single domain models only, on the other hand side, multiple inputs and outputs have to be generated for both ROMs.

The project schematic in ANSYS Workbench is shown in Figure 4:

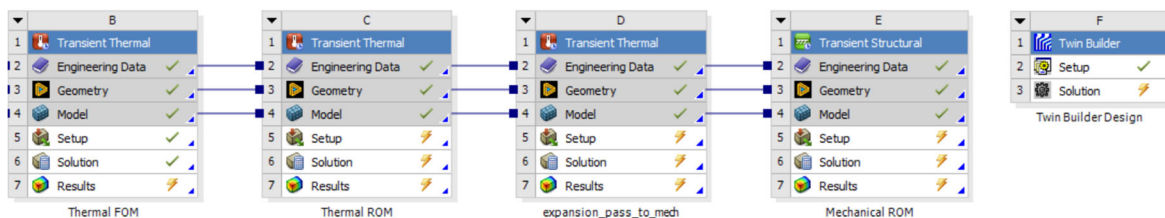


Figure 4: Project schematic in ANSYS Workbench for generating two single-domain ROMs (thermal and mechanical).

Firstly, the thermal ROM is generated from thermal system C. After the reduction has been concluded, one must generate full projection matrix of the thermal system using the macro:

```
mor_driver_thermal_mor, '-N 30 -b -v', '1,,', 'outname', 'convtemp', 'heatflow'
```

where the flag '1' in the command tells MORiA to write out the full expansion pass in the file *mor.expand*. In system D, an ANSYS readable expansion pass is generated in *expand.ans*. In order

to feed the columns from the expansion pass as inputs to the mechanical system, some manipulations need to be done in *expand.ans*:

- The Dirichlet BC command 'D' is changed to body force 'BF' for ANSYS to recognize it as a thermal load in the mechanical system.
- A null and a very high frequency (0 and 1e10 Hz) is used in harmonic analysis to obtain the full system matrices of the mechanical model.
- 30 full files are written out which correspond to the number of columns in the expansion pass. These 30 full files represent the 30 inputs of the mechanical system.

These necessary steps are automated in a python function called `ManipulateExpandAns` in *post4mor.py* which accepts *expand.ans* as an argument for treatment. This function is called in system D and generates file *header.txt*.

The next step is to copy all the lines from *header.txt* file, which is automatically generated from system D, into the 'Commands' object in transient structural analysis E. Then, MORiA is called to write all the full files and a system-level simulation file of the ROM will be generated.

Please find in **Fehler! Verweisquelle konnte nicht gefunden werden.** B the macros used for this section.

## 2.4. System Level Simulation and Validation of ROMs Accuracy

MORiA has the capability to generate different system level simulation files such as the Modelica (.mo), Simplorer (.smf), Very High-Speed Integrated Circuit Hardware Description Language (.vhd), Statespace and Circuit (.cir) files. In this project, the VHDL file is used in the ANSYS Twin Builder environment. It is important to note that the same transient setups as those of the FOM were used in the system-level simulation

### 2.4.1. Sequential Thermo-Mechanical MOR

In the Figure 5 below, The ROM contains 3 inputs (ambient temperature in convection BC, heat flow applied on chip, and initial temperature) and 11 outputs (temperature, displacement in x, y, z-directions, component stresses, and the Von-Mises equivalent stress from the selected node). Heat flow and ambient temperature inputs are both time dependent. Therefore, the values of these inputs are defined using 'Datapairs'.

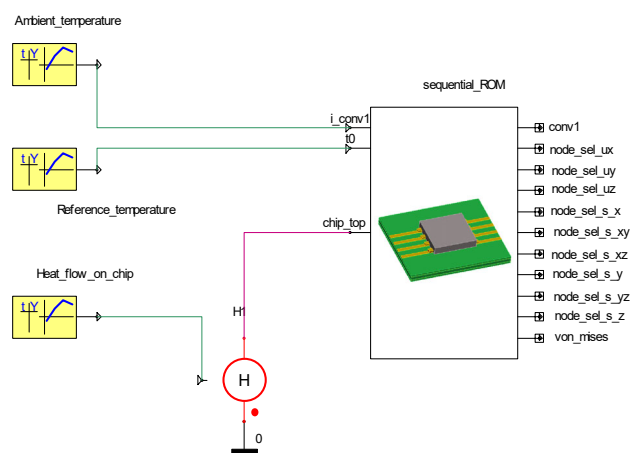


Figure 5: Sequential MOR System Level Simulation Setup.

The validation of ROM results is based on the comparison with the FOM (see figures below). In this report, two outputs (x-directional deformation and S<sub>yz</sub> component stress) are compared with the FOM. An error plot is made to show the discrepancies between results.

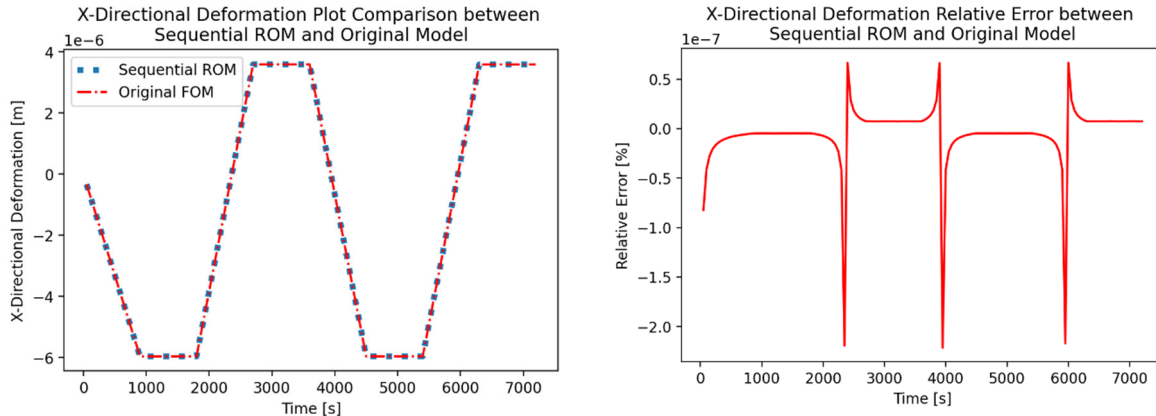


Figure 6: Deformation comparison (left) and error plot (right) between sequential ROM and FOM.

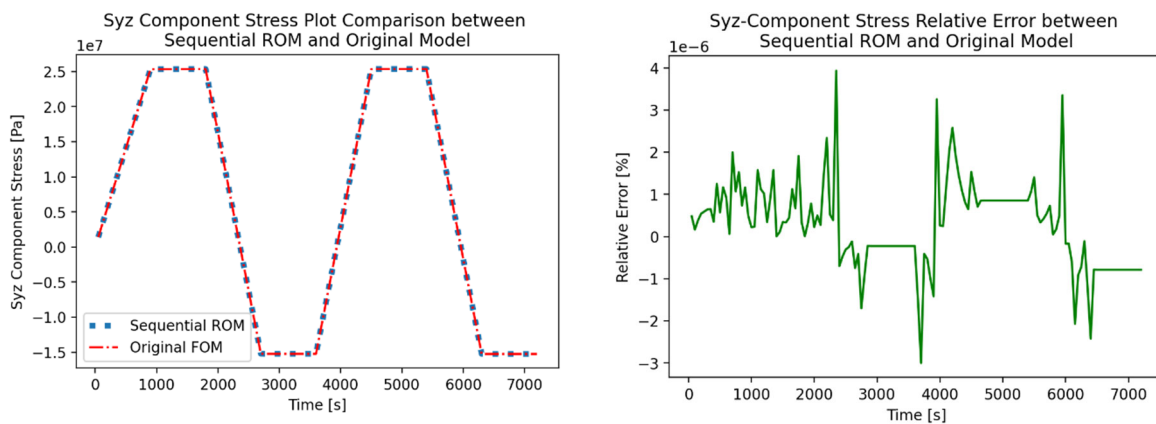


Figure 7: Component stress comparison (left) and error plot (right) between sequential ROM and FOM.

As can be seen in Figure 6 and Figure 7, the sequential ROM matched accurately with the FOM and with negligible error.

#### 2.4.2. Decoupled Thermo-Mechanical ROMs

Both thermal and mechanical ROMs are imported into Twin Builder for the transient analysis. The same analysis setup for the transient simulation in ANSYS is used in Twin Builder. Figure 8 below gives a visualization of the system level simulation setup:

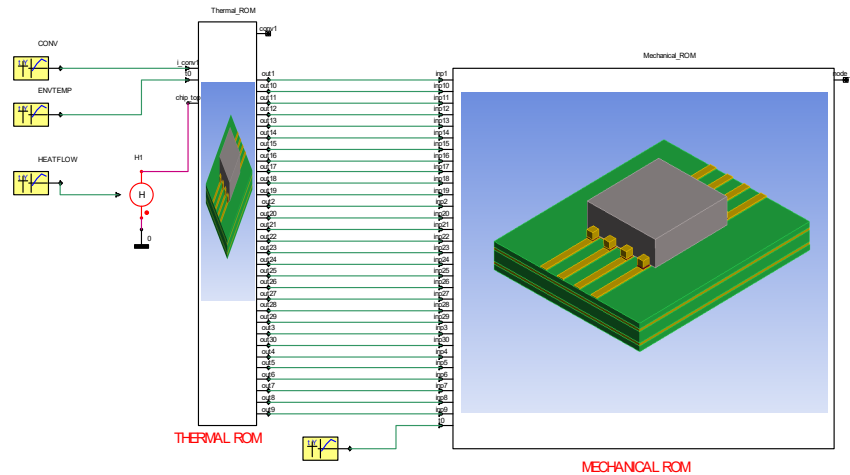


Figure 8: Decoupled Domains ROMs System Level Simulation Setup.

The thermal ROM receives the heatflow, the ambient temperature in convection BC, and the initial temperature as inputs. Thirty output pins from the thermal ROM are connected to the mechanical ROM and acts as inputs to the mechanical system. The dynamical behavior of the mechanical system is investigated through a selected node. A plot which shows the comparison of the deformation between the FOM ('fully coupled') and the ROMs ('decoupled systems') is shown in Figure 9. The error plot for this analysis is also made, where a maximum error of 4.85% is observed.

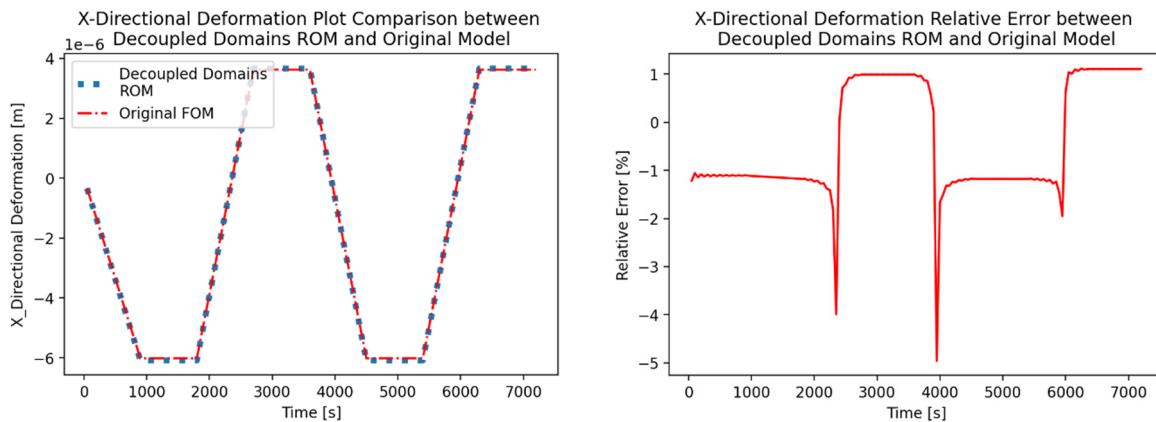


Figure 9: Deformation comparison (left) and error plot (right) between decoupled domains ROM and FOM.

It can be observed that the error in the decoupled domains ROMs is higher than the former sequential ROM (though negligible). This error could be further reduced by increasing the number of input vectors from the thermal domain at the expense of computational costs.

### 3. Reduction of Linearized Strongly-Coupled Thermal Transient and Mechanical Quasi-Static Models

#### 3.1. Introduction

Microelectronic components, such as packaged chips, undergo thermal cycling tests in order to examine their thermo-mechanical reliability. For performing such life assessment tests, the packaged chips are exposed to accelerated temperature cycles ranging from  $-40^{\circ}\text{C}$  to  $125^{\circ}\text{C}$ . Heat, having a significant influence on the package reliability, can lead to structural failures such as solder joint fatigue, die cracking, and delamination [6]. The silicon product chip may also be damaged by the mismatch in thermal expansion of materials or external force-induced stress [7]. Computer-based simulations are necessary to account for various real-life test cases of such accelerated tests. However, due to the expensive nature of finite element simulations, there is a need for generating a compact model from the original full-scale thermo-mechanical model through the MOR techniques.

In this document, we present a systematic study of the applicability of MOR to the linearized thermo-mechanical model from Infineon Technologies. Figure 10 shows the flowchart utilised in performing MOR on the Infineon coupled thermo-mechanical model. We adopted a linear compact modelling technique, the Krylov-subspace-based MOR [8], and applied it to reduce the linear thermal transient and mechanical quasi-static model. The temperature, displacements, and thermally caused mechanical stresses from a selected node on a joint solder are observed as outputs from the ROM. Comparison and error plots presented in Section 3.7 show excellent results between the FOM and the ROM.

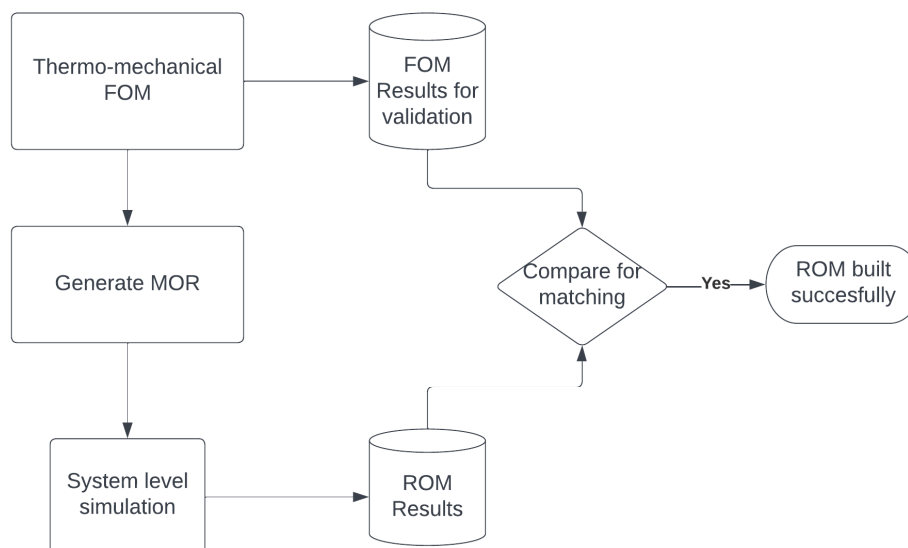


Figure 10: Executed workflow for MOR for linearized coupled quasi-static thermo-mechanical model.

#### 3.2. Case study: a packaged chip model from Infineon

The case study is a training-model "PG-TDSON-8" which comprises a packaged chip installed on a PCB. In this document, the packaged chip denotes an embodiment of a silicon chip and its housing. Figure 11 below shows an illustration of the case study. It is worth knowing that the

geometry, mesh data, simulation setups, boundary conditions, and material properties are all already made available. The material properties of the model are linear-elastic only and have no dependence on temperature.

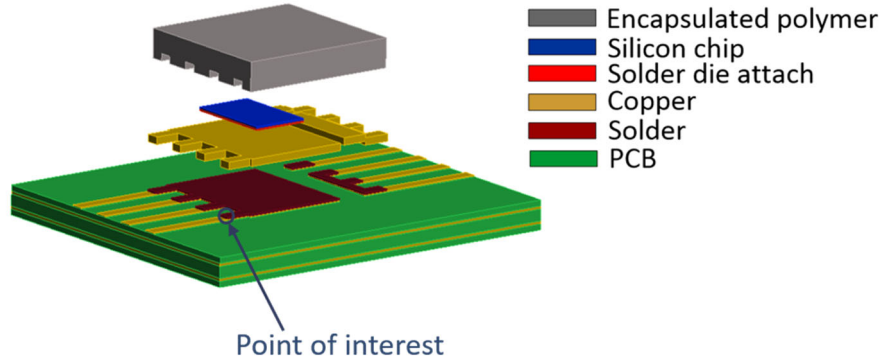


Figure 11: Exploded view of model geometry.

In order to have a basis for comparison between the ROM and the FOM, it is necessary to run the FOM simulation. A coupled field transient analysis was undergone using ANSYS Workbench (version 2021 R2) and a thermal load step ranging from 900 to 7200 seconds was imposed. This yielded the time-varying results, e.g., displacement, temperature, and stress, in response to transient loads. Forced convective boundary conditions on the external surfaces of the model and the displacement boundary conditions on three edges of the model to avoid rigid body motions were induced. For more details of the model setups, please check the report on the COMPAS SharePoint [9]. The machine utilised for the computation has 8 physical cores, 64 GB RAM, with a Broadwell Intel core 3.0 GHz processor. The original FOM has 1.2 million DOFs and took 11 hours for computation.

### 3.3. Coupled quasi-static thermo-mechanical system

After spatial discretization and matrices assembly of the finite element method, a given thermo-mechanical model is represented by a system of ordinary differential equations:

$$\begin{cases} M\ddot{x}(t) + E\dot{x}(t) + Kx(t) = Bu(t) \\ y(t) = Cx(t) \end{cases} \quad (12)$$

where  $x(t) \in \mathbb{R}^n$  is the unknown state vector.  $M, E$ , and  $K \in \mathbb{R}^{n \times n}$  are the mass, damping, and stiffness system matrices.  $B \in \mathbb{R}^{n \times m}$  is the input matrix, and  $C \in \mathbb{R}^{p \times n}$  is the output matrix which specifies the user interested states.  $u(t) \in \mathbb{R}^m$  is the vector of input functions. Our goal is to project the high-dimensional full order dynamic system (12) onto a much lower-dimensional space  $r$ , which is far smaller than  $n$ . In this case, the spatially discretized and linearized thermo-mechanical system can be approximated as transient-thermal and mechanical-quasi-static as follows since there is no damping and no mechanical load in the model:

$$\Sigma_n: \begin{cases} \begin{bmatrix} 0 & 0 \\ 0 & E_T \end{bmatrix} \begin{Bmatrix} \dot{U} \\ \dot{T} \end{Bmatrix} + \begin{bmatrix} K_U & K_{UT} \\ 0 & K_T \end{bmatrix} \begin{Bmatrix} U \\ T \end{Bmatrix} = \begin{Bmatrix} 0 \\ Q \end{Bmatrix} \\ y(t) = Cx \end{cases} \quad (13)$$

where the state vector  $x$  contains nodal displacement state vector  $U$  and nodal temperature state vector  $T$ . The coupling term  $K_{UT}$  couples the thermal and mechanical parts. This means that the temperature results influence directly the nodes containing mechanical DOFs via thermal strain, in which the coefficient of thermal expansion is not zero.

### 3.4. Krylov subspace-based model order reduction

Krylov subspace-based MOR aims at approximating the transfer function of a full-order original model with a model of a much smaller order. That is, we would like to construct a reduced model of smaller dimension which approximates the input-output behaviour of the original model. In order to achieve this approximation, the original dynamical system is projected onto a lower dimensional subspace  $x \approx Vz$  via the projection basis  $V \in \mathbb{R}^{n \times r}$ , where  $r \ll n$ . The target here is to find the low dimensional subspace  $V$  in such a way that it could accurately approximate the original dynamic system.

In this work, we applied the Block Arnoldi method suggested in [8] to build the projection matrix. For a first-order system like in (13), its transfer function is obtained as follows:

$$\begin{aligned} G(s) &= \frac{Y(s)}{U(s)} = C(sE + K)^{-1}B = C(sE + K + s_{0E} - s_{0E})^{-1}B \\ &= C[(s - s_{0E})E + (K + s_{0E})]^{-1}B \\ &= C\{I - [-(K + s_{0E})]^{-1}E(s - s_{0E})\}^{-1}(K + s_{0E})^{-1}B \end{aligned} \quad (14)$$

According to the Neumann series  $\sum_{i=0}^{\infty} T^i = (I - T)^{-1}$ , the transfer function (14) can be rewritten as:

$$G(s) = \sum_{i=0}^{\infty} \left\{ \underbrace{C[-(K + s_{0E})]^{-1}E]^i (K + s_{0E})^{-1}B}_{\{m_i, i=0,1,2,\dots\}} \cdot (s - s_{0E})^i \right\} \quad (15)$$

where  $m_i$  are the moments of the transfer function of the FOM. The Krylov subspace is then generated based on the moments  $m_i$  and orthogonalized by the Block Arnoldi method:

$$\text{colspan}\{V\} = \text{mathcal}\{K\}_{r, -(K + s_{0E})^{-1}E, (K + s_{0E})^{-1}B} \quad (16)$$

In this case,  $V$  is the projection matrix constructed around the expansion point  $s_0 = 0$  and the full order model (13) is reduced to the system as follows [10]:

$$\Sigma_r: \begin{matrix} \{\text{matrix}\} \\ \{E_r\}z(t) \end{matrix} \begin{matrix} \{V^{TEV}\} \\ \{K_r\}z(t) \end{matrix} + \begin{matrix} \{V^{TKV}\} \\ \{B_r\}u(t) \end{matrix} = \begin{matrix} \{V^{TB}\} \\ \{B_r\}u(t) \end{matrix} y(t) = \begin{matrix} \{CV\} \\ \{C_r\}z(t) \end{matrix} \{\text{matrix}\} \quad (17)$$

In the Laplace domain, the transfer function of the reduced system (17) is obtained as follows:

$$G_r(s) = \sum_{i=0}^{\infty} \left\{ \underbrace{C \begin{bmatrix} i(K_r + s_{0E_r})^{-1}B_r \\ r[-(K_r + s_{0E_r})^{-1}E_r] \end{bmatrix}}_{\{m_i^r, i=0,1,2,\dots\}} \cdot (s - s_{0E})^i \right\} \quad (18)$$

where  $m_i^r$  are the moments of the transfer function of the ROM. It can be proven as shown in [8] that if  $V$  is chosen as a basis of the right-Krylov subspace as shown in equation (16), the first  $r$  moments of the full and reduced system's transfer function match.

### 3.5. MOR of the packaged chip model in ANSYS

The general workflow used in generating ROM of the packaged chip model in ANSYS is shown in Figure 12 below. The workflow is divided into four detailed parts with their separate functionalities.

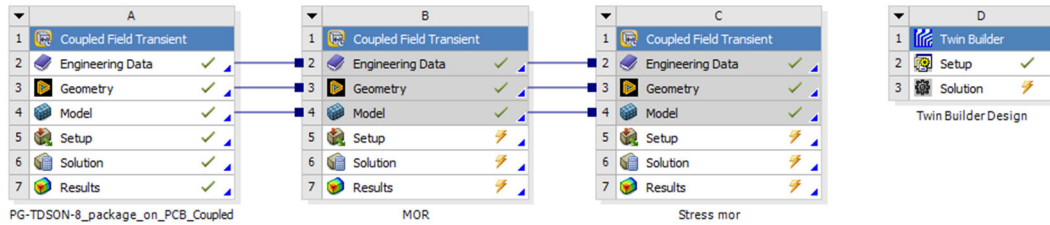


Figure 12: Project schematic utilised for coupled domain thermo-mechanical reduction.

- a) **Analysis system A:** the FOM is simulated with defined boundary conditions and loads. The FOM results for the interested states as well as the Von-Mises stresses are extracted at the selected node. These extracted FOM results will be used as a comparison with the ROM.

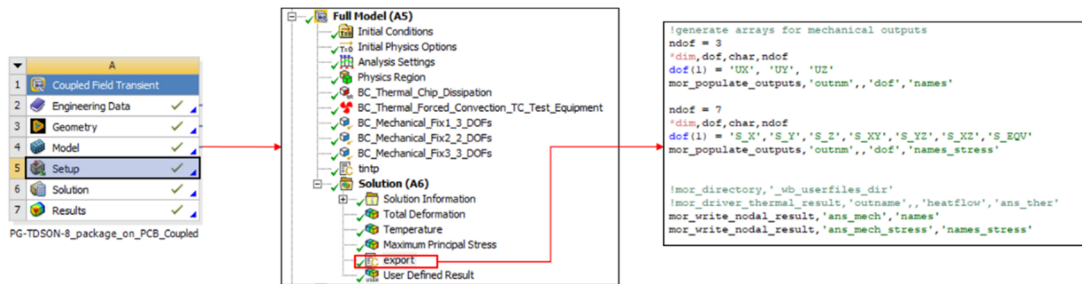


Figure 13: Details of Analysis system A, export results from the FOM.

Figure 13 shows how the developed APDL macros are used to write the nodal mechanical displacements and mechanical stresses results from the FOM. These transient results are saved as '.txt files' in the 'user\_files' directory.

- b) **Analysis system B:** this is where the model order reduction of the full coupled quasi-static thermo-mechanical system is performed, see Figure 14. Furthermore, system-level simulation files, such as the VHDL, Modelica, and state space files are generated. These files will come in handy in the analysis system D.

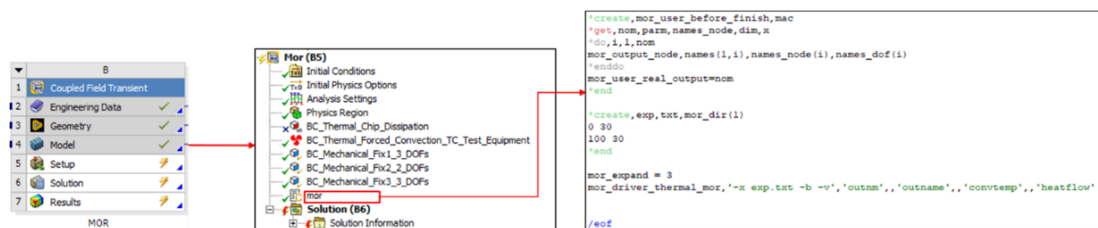


Figure 14: Details of Analysis system B, generate the ROM.

- c) **Analysis system C:** here the expansion pass method is used to compute the stress coefficients which are later being added to the output matrix C, see Figure 15. This enables the calculation of the stress outputs from the ROM at the system level. More details of this part are shown in Section 3.6.

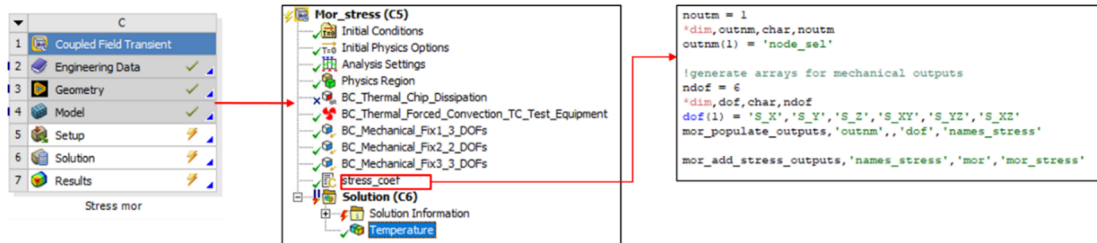


Figure 15: Details of Analysis system C, add stress coefficients to the output matrix.

- d) **Analysis system D:** here the system-level simulation is performed in ANSYS Twin Builder (version 2021 R2). It is important that the same transient setups which are used in the FOM simulation should be preserved, such as the time step and integration scheme. The system-level simulation files are imported into ANSYS Twin Builder where the simulation and comparison between the ROM results and FOM results are performed. More details of this part are shown in Section 3.7.

### 3.6. Stress outputs from the ROM using the expansion pass method

We assume that the stress and strain are a linear combination of the deformation. As such, one can have it as output in the reduced model. We use the ANSYS expansion pass as a back substitution method to evaluate the full model stress/strain. By doing that, we obtain the stress output coefficients needed to be added to the output matrix C. To carry out this approach, ANSYS APDL and macros from MORiA [11] were utilised. The tutorial on how to carry out this procedure can be found in COMPAS SharePoint [12].

### 3.7. System-level simulation and validation of ROM

A ROM in VHDL format was imported into ANSYS Twin-Builder for system-level simulation. Transient solution with the same parameters as the full simulation in terms of run time and time step was setup. The temperature as well as displacements and stresses results from the selected node are defined as outputs from the ROM. The inputs to the ROM are the ambient temperature in the convection boundary condition and the thermal loads in the chip. The results obtained from the ROM are validated with the FOM as shown in Figure 16.

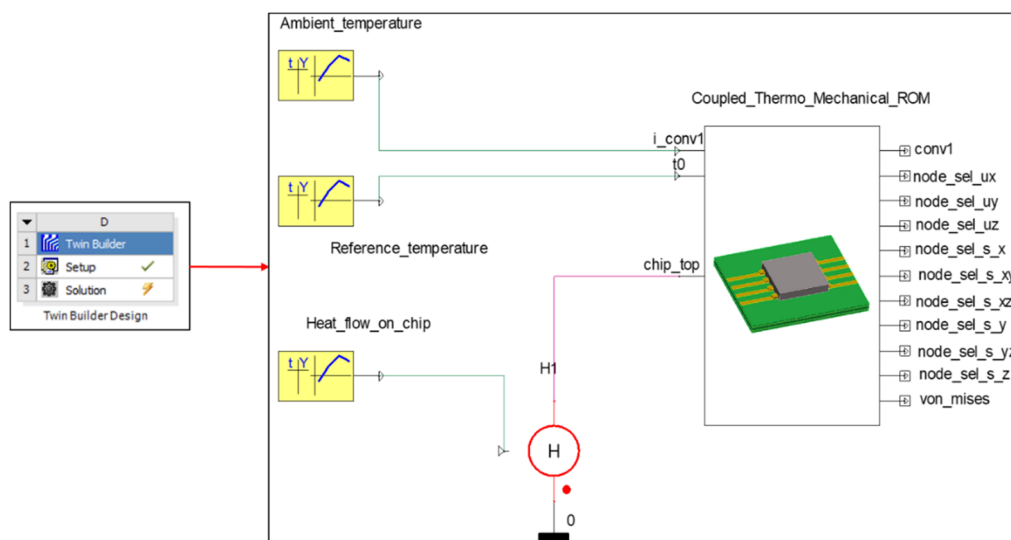
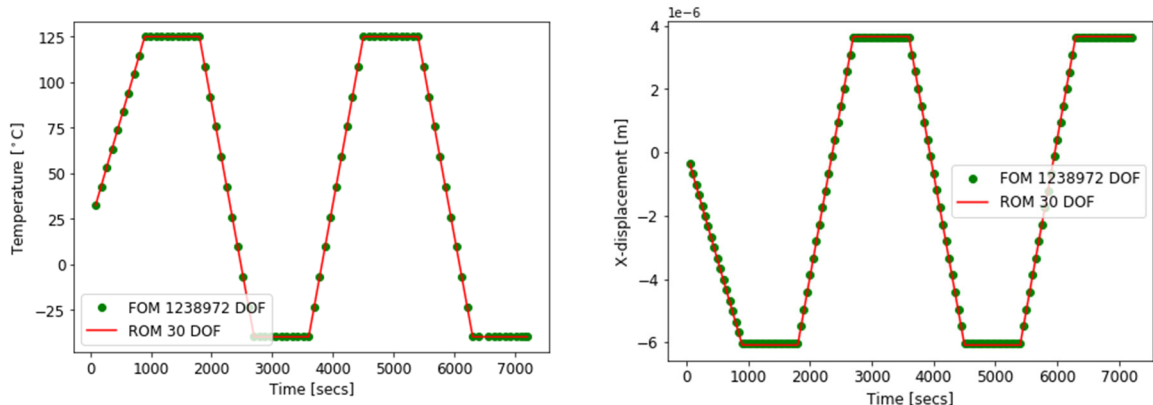
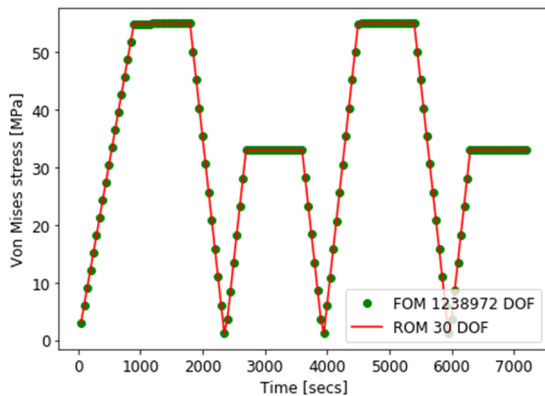


Figure 16: System-level simulation set-up of the ROM in Twin Builder.

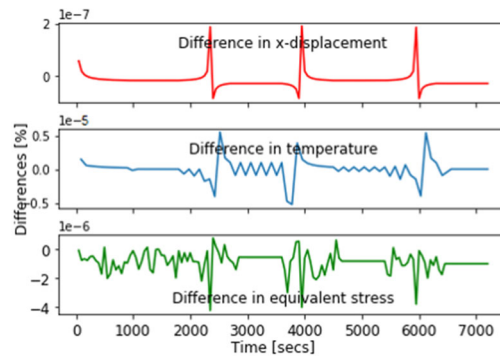


a) Temperature comparison at the selected node.

b) X-displacement comparison at the selected node.



a) Stress comparison at the selected node.



a) Error plots between FOM and ROM.

Figure 17: Validation of ROM with FOM.

Based on the plots above, it can be observed that the ROM is fully validated as the results of the FOM and ROM match each other with negligible errors. This shows how accurate the applied reduction technique is. With respect to computational efforts, Table 1 below shows how the computational cost is reduced by a factor of 5410. The machine utilised is a virtualised Intel®Core Processor (Broadwell) @ 3.0 GHz, 64 GB RAM.

Table 1 Computational cost comparison between FOM and ROM.

	FOM	ROM
DOFs	1,238,972	30
ROM generation time	n.a	7 seconds
Simulation time	11 hours	0.32 seconds

## 4. Generation of Boundary Condition Independent Compact Thermo-Mechanical Models.

### 4.1. Introduction

To solve this issue, the methodology of model order reduction (MOR) has been introduced [13] [14]. Starting from a high-dimensional finite element model, MOR enables the automatic generation of a lower dimensional but still accurate surrogate, which significantly reduces the computational cost and enables the system-level simulation. Conventional MOR methods already proved successful for linear single physical-domain models [15]. However, microelectronic components require coupled domain thermo-mechanical simulations and exhibit temperature dependent material properties. To deal with that, parametric model order reduction (pMOR) methods have been developed, which enable to preserve the parameters in the symbolic form within the reduced order model [16] [17] [18] [14] [19] [20]. The European project COMPAS aims to develop novel compact models and ultra-compact digital twins for predicting the thermo-mechanical reliability issues in high-tech systems, which integrate numerous highly complex components. The project starts with a test model of a wafer level chip-scale package provided by NXP Semiconductors. One major failure mode in such hardware is the solder connection fatigue (see Figure 18). The mismatch between the coefficients of thermal expansion (CTE) of the package and of the printed circuit board (PCB) causes mechanical stress within the solder connection and leads to the solder fatigue and ultimate failure. In this work, we successfully apply pMOR to the wafer level chip-scale package model for constructing a parametric reduced order model (pROM). The temperature dependent Young's modulus in the solder connection is defined as a parameter and preserved in the symbolic form within the compact model. This enables efficient reliability analysis. The report is organized as follows. Two parts, the first part presents the Infineon model with the preservation of film coefficient (Boundary independent MOR) in the reduced space. The second part describes the NXP model and material property dependency preservation in the reduced space.

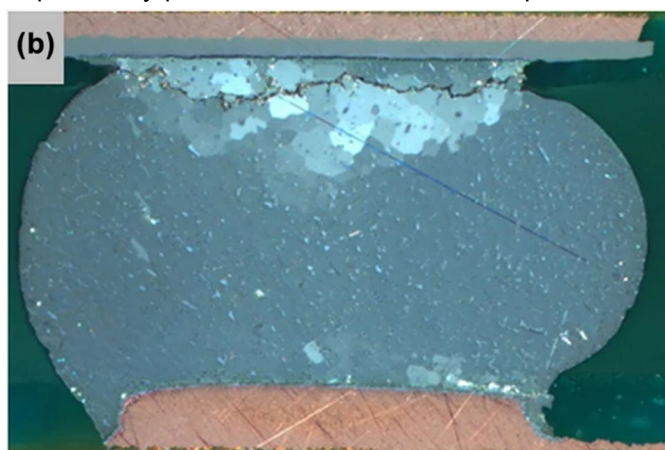


Figure 18 Crack in the solder ball due to thermal loading [21].

### 4.2. pMOR for Infineon model with parametrized film coefficient $h$ in the convection boundary condition

#### 4.2.1. Case study: Infineon Training Model PG-TDSON-8

Figure 19 presents the schematic of the Infineon training model, which consists of the PCB, solders, copper, package chip, and molding compound. Three nodes noted in Figure 19 are

assigned with the Dirichlet boundary conditions. The model is simulated with an initial uniform temperature of 22 °C in the thermo-mechanical domain. It is also noted as the reference temperature. A heat flow input is defined in the chip and a convection boundary condition is assigned to the external surfaces of the model. The material properties used in this model are linear-elastic only as shown in Figure 19.

$$u_0(x, y, z) = (0,0,0), u_1(x, y, z) = (0, y, 0), u_2(x, y, z) = (x, y, 0) \quad (19)$$

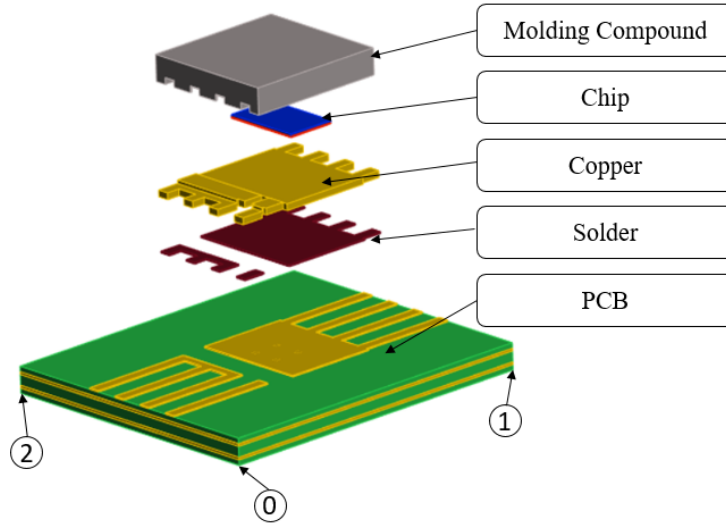


Figure 19 An exploded view of the Infineon training model PG-TDSON-8

Table 2 Material properties used in the model (CTE: Coefficient of Thermal Expansion).

Material/body	Young's modulus [GPa]	CTE [ppm/K]	Poisson's Ration
Copper	130	17	0.34
Silicon (Chip)	169	3	0.34
Solder (lead) in side package	20	28	0.4
Polymer (Molding compound)	30	6	0.3
Solder SAC on PCB	40	21	0.34
FR4 (PCB)	26	16	0.2

The full-order model is approximated in quasi-static format and written as:

$$\Sigma_N: \left\{ \begin{array}{l} \left[ \begin{array}{cc} 0 & 0 \\ E_{TU} & E_T \end{array} \right] \begin{array}{l} \dot{U} \\ \dot{T} \end{array} + \left[ \begin{array}{cc} K_U & K_{UT} \\ 0 & K_T \end{array} \right] \begin{array}{l} U \\ T \end{array} = \underbrace{\left\{ \begin{array}{l} F + K_{UT}\{T_{ref}\} \\ Q \end{array} \right\}}_{B \cdot u} \\ y = Cx \end{array} \right. \quad (20)$$

where the state vector  $x \in \mathbb{R}^{N \times N}$  contains nodal displacement state  $U \in \mathbb{R}^{N_1}$  and nodal temperature state  $T \in \mathbb{R}^{N_2}$ ,  $N = N_1 + N_2$ .  $K_U \in \mathbb{R}^{N_1 \times N_1}$  is the stiffness matrix in the mechanical domain and  $E_T \in \mathbb{R}^{N_2 \times N_2}$ ,  $K_T \in \mathbb{R}^{N_2 \times N_2}$  are the heat capacity and conductivity matrices in the thermal domain. The

coupling term  $K_{UT} \in \mathbb{R}^{N_1 \times N_2}$  couples the thermal and mechanical parts. This means that the temperature results influence directly the nodes containing mechanical DOFs via thermal strain, in which the coefficient of thermal expansion is not zero.  $T_{ref}$  is the reference temperature for thermal expansion. It is normally set as  $T_{ref} = 0$  °C for the generation of the reduced order model.  $E_{TU} \in \mathbb{R}^{N_2 \times N_1} = 0$  because the thermoelastic damping effect is turned off in this case.  $Q$  and  $F$  are the thermal and mechanical loads in the model, where  $F = 0$  in this case.  $C \in \mathbb{R}^{p \times N}$  is the output matrix defined by the users, which gives  $p$  outputs in the output vector  $y$ .  $B \in \mathbb{R}^{N \times m}$  and  $u \in \mathbb{R}^m$  are the input matrix and vector with  $m$  inputs.

#### 4.2.2. Parametric Model Order Reduction

In this case study, we aim to generate a parametric reduced-order model, in which the film coefficient and the ambient temperature in the convection boundary condition are the parameters. Therefore, the full-order model as shown in Equation.(20) can be rewritten in a parametric form:

$$\Sigma_N: \begin{cases} E \cdot \dot{x} + (K_0 + h \cdot K_1) \cdot x = B \cdot \begin{bmatrix} q \\ h \cdot T_{amb} \\ u \end{bmatrix} \\ y = Cx \end{cases} \quad (21)$$

where  $h$  and  $T_{amb}$  are the film coefficient and ambient temperature in the convection boundary condition, respectively.  $K_0, K_1 \in \mathbb{R}^{N \times N}$  are the parameter-independent and parameter-dependent parts, respectively.  $q$  is the heat flow input applied on the chip. Therefore, the goal of parametric model order reduction is to construct a projection matrix  $V \in \mathbb{R}^{N \times r}$ . The full state vector can be projected onto a lower dimension subspace  $x = V \cdot z$ , where  $z \in \mathbb{R}^r$  is the reduced state vector,  $r \ll N$ . The boundary condition independent parametric reduced order model can be written as:

$$\Sigma_r: \begin{cases} \frac{V^T E V}{E_r} \cdot \dot{z} + \left( \frac{V^T K_0 V}{K_{0r}} + h \cdot \frac{V^T K_1 V}{K_{1r}} \right) \cdot z = \frac{V^T B}{B_r} \cdot \begin{bmatrix} q \\ h \cdot T_{amb} \\ u \end{bmatrix} \\ y = \underbrace{C V}_{C_r} z \end{cases} \quad (22)$$

The transfer function of Equation (21) is written as follows:

$$G(s, h) = C[sE + (K_0 + h \cdot K_1)]^{-1}B \quad (23)$$

where  $s$  is the frequency. In this case, we have two parameters that are not physically correlated. Two disjoint Krylov subspaces where one parameter is kept constant, while the Krylov subspace is generated for another parameter and vice versa. On basis of the transfer function, we are able to construct the projection matrix as follows:

**Step 1:** Fix  $h = h_0$ , and rewrite the transfer function with parameter  $s$  at the expansion point  $s_0$ .

$$\begin{aligned} G(s, h_0) &= C[sE + (K_0 + h_0 \cdot K_1)]^{-1}B \\ &= C[sE + K(h_0) + s_0E - s_0E]^{-1}B \\ &= C[(s - s_0)E + K(h_0) + s_0E]^{-1}B \\ &= C\{I - [-(K(h_0) + s_0E)]^{-1}E(s - s_0)\}(K(h_0) + s_0E)^{-1}B \\ &= \sum_{i=0}^{\infty} \frac{C[-(K(h_0) + s_0E)]^{-1}E]^i (K(h_0) + s_0E)^{-1}B (s - s_0)^i}{m_i^s} \end{aligned} \quad (24)$$

where  $m_i^s$ ,  $i = 0,1,2, \dots$ , are the moments of the transfer function  $G(s, h_0)$ . Then the projection matrix for parameter  $s$  is constructed on basis of the Krylov subspace:

$$\text{colspan}\{V_s\} = \mathcal{K}_{r_1}\{-(K(h_0) + s_0E))^{-1}E, (K(h_0) + s_0E)^{-1}B\} \quad (25)$$

**Step 2:** Fix  $s = s_0$ , and rewrite the transfer function with parameter  $h$  at the expansion point  $h_0$ .

$$\begin{aligned} G(s_0, h) &= C[s_0E + (K_0 + h \cdot K_1)]^{-1}B \\ &= C[s_0E + (K_0 + h \cdot K_1 + h_0 \cdot K_1 - h_0 \cdot K_1)]^{-1}B \\ &= C[s_0E + (K_0 + h_0 \cdot K_1) + (h - h_0)K_1]^{-1}B \\ &= C\{I - [(K(h_0) + s_0E))^{-1}K_1(h - h_0)]\}(K(h_0) + s_0E)^{-1}B \\ &= \sum_{i=0}^{\infty} \frac{C[-(K(h_0) + s_0E))^{-1}K_1]^i (K(h_0) + s_0E)^{-1}B (h - h_0)^i}{m_i^h} \end{aligned} \quad (26)$$

where  $m_i^h$ ,  $i = 0,1,2, \dots$ , are the moments of the transfer function  $G(s_0, h)$ . Then the projection matrix for parameter  $h$  is constructed on basis of the Krylov subspace:

$$\text{colspan}\{V_h\} = \mathcal{K}_{r_2}\{-(K(h_0) + s_0E))^{-1}K_1, (K(h_0) + s_0E)^{-1}B\} \quad (27)$$

**Step 3:** Merging the orthonormal bases of  $V_s$  and  $V_h$  into a single projection matrix  $V$ :

$$\text{colspan}\{V_h\} = \text{colspan}\{V_s, V_h\} \quad (28)$$

### 4.2.3. Numerical Results

The parametric reduced order model is generated with expansion points  $s_0 = 0$  and  $100$ ,  $h_0 = 15$ . It is transformed in VHDL format and imported into system-level simulation software ANSYS Twin Builder (see Figure 20). The computational efficiency of the parametric reduced-order model is shown in Table 3. The computational time for performing the simulations of the FOM and ROM on the server within Intel Core Processor (Broadwell) @3.0 GHz, 128 GB RAM. The accuracy of the parametric reduced order model is shown in Figure 21. **Fehler! Verweisquelle konnte nicht gefunden werden..** The parametric reduced order model is more accurate with film coefficient  $h = 15$  because it is generated around the expansion point  $h_0 = 15$ .  $h = 30$  is away from the expansion point and the results give larger.

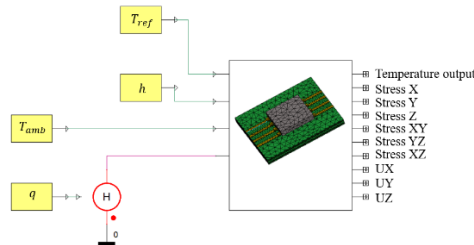


Figure 20 Simulation of the parametric reduced order model in ANSYS Twin Builder.

Table 3 The computational time for performing the simulations of the FOM and ROM on the server within Intel Core Processor (Broadwell) @3.0 GHz, 128 GB RAM.

	FOM	pROM
Total DOFs	43,760	51
CPU Time (s)	588	0.126

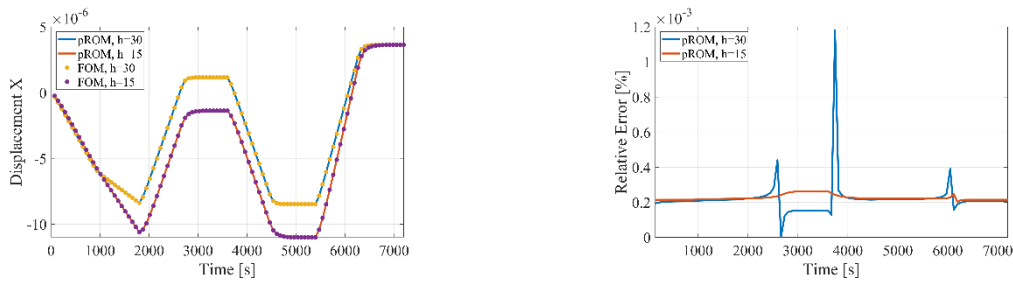


Figure 21 Comparison of the results from full order and parametric reduced order models.

### 4.3. pMOR for NXP model with parametrized Young's modulus in the solder joints

#### 4.3.1. Case Study: Wafer Level Chip-Scale Package

Figure 22 displays the model assembly that contains the PCB, solders, copper, passivation, chip and coating. The model consists of six elastic material domains and the parameter of interest is the Young's modulus of the solder domain. It is to be preserved in symbolic form within the reduced order model. Furthermore, Young's modulus of the silicon chip domain can also be preserved in the symbolic form. The three points demarked in Figure 22 with  $\{0,1,2\}$  on the border  $\partial\Omega$  of computational domain  $\Omega$  are subjected to the following mechanical Dirichlet boundary conditions, where point one is totally fixed, point two is free only in the x direction and point three is only fixed in z-direction:

$$u_0(x, y, z) = [0,0,0], \quad u_1(x, y, z) = [x, 0,0], \quad u_2(x, y, z) = [x, y, 0] \text{ on } \partial\Omega \quad (29)$$

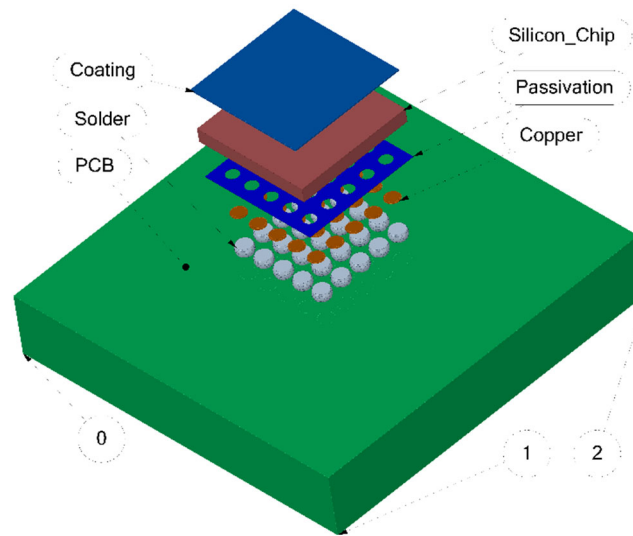


Figure 22 An exploded view of the wafer chip-scale package.

The reliability tests for these devices are performed inside an oven under homogeneous temperature cycles. This temperature cycling leads to mechanical deformations and stresses. Usually, such tests are performed in a passive regime, that is, without turning on the Chip. This means that one can assume the homogeneous temperature distribution across the chip (corresponding to the temperature cycling) and describe it with a static finite element model. We use ANSYS® R 21.2. In Figure 23 and Table 4, the finite element mesh and its statistics are displayed. The governing partial differential equations of linear elasticity over a continuous domain  $\Omega$ , considering infinitesimal strain theory and isotropic materials can be written as follow:

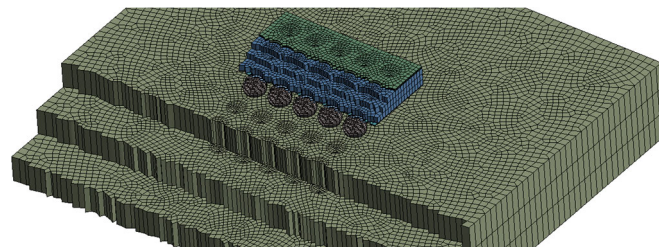


Figure 23 Volumetric mesh sectioned through the whole model.

Table 4 Mesh statistics of the model.

Body name	Nodes	Elements	Type
Coating	12272	9123	Solid
Silicon Chip	12272	9123	Solid
Passivation	9172	6048	Solid
Copper	10375	7500	Solid
Solder	11725	8850	Solid
PCB	40152	29919	Solid
Total	84232	70563	Solid

The total number of degrees of freedoms amounts to 252690

$$\begin{aligned}
 -\nabla\sigma(u) &= f \text{ in } \Omega \\
 \sigma(u) &= \lambda\text{tr}(\varepsilon(u))\mathbf{I} + 2\mu\varepsilon(u) \\
 \varepsilon(u) &= \frac{1}{2}(\nabla u + (\nabla u)^T)
 \end{aligned} \tag{30}$$

where  $u$  is the state vector and represents the displacement vector field in the domain  $\Omega$ ,  $\sigma(u)$  and  $\varepsilon(u)$  are the stress and strain-rate tensors,  $f$  is the body force per unit volume,  $\lambda$  and  $\mu$  are elasticity parameters of materials in  $\Omega$ ,  $\mathbf{I}$  is the identity tensor,  $\text{tr}$  is the trace operator on a tensor. Finite elements based spatial discretization of Equation (30) leads to the following element matrices and element load vectors:

$$\begin{aligned}
 \{\sigma\} &= [D]\{\varepsilon^{el}\} \\
 \{\varepsilon^{el}\} &= \{\varepsilon\} - \{\varepsilon^{th}\}, \{\varepsilon^{th}\} = \Delta T[\alpha_x^{se} \alpha_y^{se} \alpha_z^{se} 000]^T
 \end{aligned} \tag{31}$$

$$\begin{aligned}
 ([K_e] + [K_e^f])\{u\} &= \{F_e^{th}\} \\
 [K_e] &= \int_{vol} [B]^T [D] [B] d(\text{vol}) \\
 [K_e^f] &= k \int_{area} [N_n]^T [N_n] d(\text{area}_f) \\
 \{F_e^{th}\} &= \int_{vol} [B]^T [D] \{\varepsilon^{th}\} d(\text{vol})
 \end{aligned} \tag{32}$$

$$[D] = \frac{E}{(1+\nu)(1-2\nu)} \begin{bmatrix} 1-\nu & \nu & \nu & 0 & 0 & 0 \\ \nu & 1-\nu & \nu & 0 & 0 & 0 \\ \nu & \nu & 1-\nu & 0 & 0 & 0 \\ 0 & 0 & 0 & \frac{1-2\nu}{2} & 0 & 0 \\ 0 & 0 & 0 & 0 & \frac{1-2\nu}{2} & 0 \\ 0 & 0 & 0 & 0 & 0 & \frac{1-2\nu}{2} \end{bmatrix} \tag{33}$$

Where  $D$  is the generalized Hook's law fourth order tensor, material property, which relates to stress.  $E$  and  $\nu$  are Young's modulus and Poisson's ratio.  $\varepsilon^{el}$  is the elastic strain,  $\alpha_x^{se}$  is the first component of secant coefficient of thermal expansion vector,  $\Delta T = T - T_{ref}$  while  $T_{ref}$  is the strain free temperature,  $[B]$  strain-displacement matrix, based on the element shape functions,  $\{u\}$  nodal displacement vector,  $[K_e]$  is element stiffness matrix,  $[K_e^f]$  is the element foundation stiffness matrix,  $[N_n]$  is the matrix of shape functions for normal motions at the surface and  $\{F_e^{th}\}$  is the element thermal load vector. From Equation (32) the system stiffness matrix  $K$  is assembled and the parameter of interest ( $E$ ) can be factorized see Equation (33). Note that it would be not so simple to factorize the Poisson's ratio as a parameter, because it enters the system matrix in a non-linear way. The same holds true for geometrical parameters.

#### 4.3.2. Parametric Model Order Reduction

In this chapter, we will define the linear parametric system arising from the finite element model defined in Section 4.2. Furthermore, the parametric reduced order model, which preserves inputs, outputs and the Young's modulus in symbolic form is defined. Many studies in the field of parametric model order reduction focus on treating dynamical systems, in which solely left-hand side is

parameter-independent. However, the parametric system arising in this work contains parameters also at right hand side. Finally, we will describe the multi-point moment matching property of the MOR algorithm. In this case, we can say that the reduced model is a partial realization or Pade-type approximation of the full order model.

#### 4.3.3. Arising Parametric System

As discussed in Section 4.2 we can write the parametric full order model for a single material parameter as follows:

$$\Sigma_N: \begin{cases} \underbrace{(K_0 + E \cdot K_1)}_{=:K(E)} \cdot x = \underbrace{(B_0 + E \cdot B_1)}_{=:B(E)} \cdot u(t) \\ y = C \cdot x \end{cases} \quad (34)$$

where  $N$  is the dimension of the full order model and is equivalent to the number of the degrees of freedoms defined in Table 4 ( $N= 252690$ ),  $K \in \mathbb{R}^{N \times N}$  is the system's stiffness matrix with factorized Young's modulus and  $K_0, K_1 \in \mathbb{R}^{N \times N}$  are its parameter-independent and the parameter-dependent parts respectively.  $u \in \mathbb{R}^m$ ,  $y \in \mathbb{R}^o$  are the input and output vectors.  $B \in \mathbb{R}^{N \times m}$ ,  $C \in \mathbb{R}^{o \times N}$  are the input and output matrices, respectively.  $m, o$  are the number of inputs and user defined outputs.  $x \in \mathbb{R}^N$  is the state vector of unknown displacements and  $E$  is the Young's modulus of the specified material domain.

In general multi-parameter case, the parametric system can be written as follows:

$$\Sigma_N: \begin{cases} \underbrace{(K_0 + E_1 \cdot K_1 + E_2 \cdot K_2 + \dots + E_p \cdot K_p)}_{=:K(E)} \cdot x = \underbrace{(B_0 + E_1 \cdot B_1 + E_2 \cdot B_2 + \dots + E_p \cdot B_p)}_{=:B(E)} \cdot u(t) \\ y = C \cdot x \end{cases} \quad (35)$$

Where the subscript  $p$  denotes the total number of parameters. Physically each parameter can describe the material property of a certain material domain, which enters the system matrices linearly and hence, can be factorized. The goal is to reduce such parameterized system to a compact form, which can be employed within a system level simulation. Single-parameter system Equation (34) can be reduced by Galerkin approximation as follows:

$$\Sigma_r: \begin{cases} \underbrace{V^T(K_0 + E \cdot K_1)V}_{K_r(E)} \cdot x_r = \underbrace{V^T(B_0 + EB_1)}_{B_r} \cdot u(t) \\ y_r = \underbrace{CV}_{C_r} \cdot x_r \end{cases} \quad (36)$$

where  $V \in \mathbb{R}^{N \times r}$ ,  $K_r \in \mathbb{R}^{r \times r}$ ,  $B_r \in \mathbb{R}^{r \times m}$ ,  $C_r \in \mathbb{R}^{o \times r}$  and  $r \ll N$  is the dimension of the reduced order model Note that,  $m, o$  are the same numbers of inputs and user defined outputs, as in the original system Equation(34).  $x \in \mathbb{R}^r$  is the reduced state vector and  $E$  is the Young's modulus of the specified material domain, which now preserved in the reduced space and can be changed at the system level simulation. The remaining question is how to define the projection subspace  $K_r$  with minimal approximation error as it will be demonstrated in the next section.

#### 4.3.4. Moment Matching and Subspace Definition

The transfer function of the parametric system defined in Equation (34) reads:

$$G(E) = Y(s)/U(s) = C[K(E)]^{-1}B(E) \quad (37)$$

This transfer function can be rewritten as follows:

$$G(E) = C[I - [-(E)K_1]K(E)^{-1}]^{-1}K(E)^{-1}[B(E) + (E) \cdot B_1] \quad (38)$$

Then, we apply the Taylor expansion and observe its coefficients (moments) around a chosen expansion point  $E_0$ :

$$G(E) = \underbrace{CK(E)^{-1}B(E)}_{M_0^E} + \sum_{i=1}^{\infty} \underbrace{\{C[-K(E)^{-1}K_1]^i K(E)^{-1}B(E) + C[-K(E)^{-1}K_1]^{i-1}K(E)^{-1}B_1\}}_{M_i^E, i=1,2,\dots} (E)^i \quad (39)$$

Based on these moments we can generate the Krylov subspace as follow:

$$\begin{aligned} \text{colspan}\{V_1\} &= \mathcal{K}_{r_1}\{-K(E)^{-1}K_1, K(E)^{-1}[B(E), B_1]\} \\ B(E) &= B_0 + E \cdot B_1 \end{aligned} \quad (40)$$

$$\begin{aligned} \text{colspan}\{V\} &= \mathcal{K}_{r_2}\{-K(E)^{-1}K_1, K(E)^{-1}[B_0, B_1]\} \\ &= \mathcal{K}_{r_1}\{-K(E)^{-1}K_1, K(E)^{-1}[B(E), B_1]\} \end{aligned} \quad (41)$$

The derivatives included in V can be matched by the reduced system such that:  $M_i^E = V\widehat{M}_j^E$  where  $\widehat{M}_j^E$  are the moments of the reduced system. Thus, we have moments of  $y$  and  $y_r$  are identical [16].

$$\begin{aligned} G(E_1, E_2) &= \underline{G(0,0)} + \underline{\frac{\partial G}{\partial E_1}(0,0)} \cdot E_1 + \underline{\frac{\partial G}{\partial E_2}(0,0)} \cdot E_2 + \frac{1}{2!} \frac{\partial^2 G}{\partial E_1^2}(0,0) \cdot E_1^2 \\ &+ \frac{\partial^2 G}{\partial E_1 \partial E_2}(0,0) \cdot E_1 \cdot E_2 + \frac{\partial^2 G}{\partial E_2 \partial E_1}(0,0) \cdot E_1 \cdot E_2 + \frac{1}{2!} \frac{\partial^2 G}{\partial E_2^2}(0,0) \cdot E_2^2 + \dots \end{aligned} \quad (42)$$

$$\begin{aligned} G_r(E_1, E_2) &= \underline{G_r(0,0)} + \underline{\frac{\partial G_r}{\partial E_1}(0,0)} \cdot E_1 + \underline{\frac{\partial G_r}{\partial E_2}(0,0)} \cdot E_2 + \frac{1}{2!} \frac{\partial^2 G_r}{\partial E_1^2}(0,0) \cdot E_1^2 \\ &+ \frac{\partial^2 G_r}{\partial E_1 \partial E_2}(0,0) \cdot E_1 \cdot E_2 + \frac{\partial^2 G_r}{\partial E_2 \partial E_1}(0,0) \cdot E_1 \cdot E_2 + \frac{1}{2!} \frac{\partial^2 G_r}{\partial E_2^2}(0,0) \cdot E_2^2 + \dots \end{aligned} \quad (43)$$

For a multi-parameter system like in Equation (35) building the reduced space is more complicated. As studied in [14] a comparison between three different algorithms, we here stick to the second proposed method, where building the reduced space is more efficient and robust. However, we apply a correction to deal with parametric right-hand side. In this method, the derivatives are computed separately. For example, Equations (42) and (43) show two parameters expansion reduced, only the underlined moments are matched. For the generalized case, we can define the subspace that preserves moment matching for each parameter  $p_i$  as follow:

$$\begin{aligned} \text{colspan}\{V_{p_i}\} &= \mathcal{K}_{r_i}\{-K(E)^{-1}K_{p_i}, K(E)^{-1}[B(E), B_1]\} \\ V &= \text{span}(V_{p_1}, \dots, V_{p_i}) \end{aligned} \quad (44)$$

#### 4.3.5. Numerical Results

In this chapter, we will demonstrate the efficiency and accuracy of our approach. Table 5 shows the time comparison between the full finite element model and the reduced parameterized model with single material domain parameter. A speed up by a factor of 63 could be reached with maximal

relative error of  $0.2E^{-5}$ . Note that the speed up would be much larger if a transient simulation of the full model is required. A great time reduction in simulating the parametric reduced model over the full finite element model and keeping almost a negligible error. The full model runs in almost half an hour, while the reduced model do the job in a fraction of a second.

Table 5 Time comparison between reduced and full order models at Intel Core Processor (Broadwell) @3.0 GHz, 64 GB.

Model	DOF	Time[s]
Finite element model	252690	2058.9
pROM generation (offline)	86	32.208
pROM (online)	86	0.1600

Figure 24 displays a schematic for the usage of pROM in the system-level simulation. Engineers can define the Young's modulus of different material domains as an arbitrary function of temperature. In our case study, temperature cycles are defined from  $-40^{\circ}\text{C}$  to  $125^{\circ}\text{C}$ . The corresponding mechanical response of the full- and reduced-order model is shown in Figure 25.

Here, we have to define our error criteria, as the input  $u(t)$  is time dependent and each output node in  $y$  is defined by a row-vector in  $C$ . The relative error is defined as:

$$e = \frac{|y - y_r|}{y} \quad e_{\text{vec}} = \begin{bmatrix} \|e_{0j}\|_2 \\ \|e_{1j}\|_2 \\ \dots \\ \|e_{oj}\|_2 \end{bmatrix} \quad e_{\text{rel}} = \|e_{\text{vec}}\|_{\infty} \quad (45)$$

First, we calculate  $e$  which is the defined as the error above, while  $y$  and  $y_r$  are FOM and ROM outputs respectively, then we take the second norm for each row in  $e$ , e.g.  $e_{0j}$  is the first row of  $e$  and  $e_{oj}$  is the last row, which can represent the average error over time. Secondly, we have a vector of these averaged errors,  $e_{\text{vec}}$ , then we compute the infinite norm of it, which can be considered as the maximum relative error,  $e_{\text{rel}}$ , among the selected output nodes.

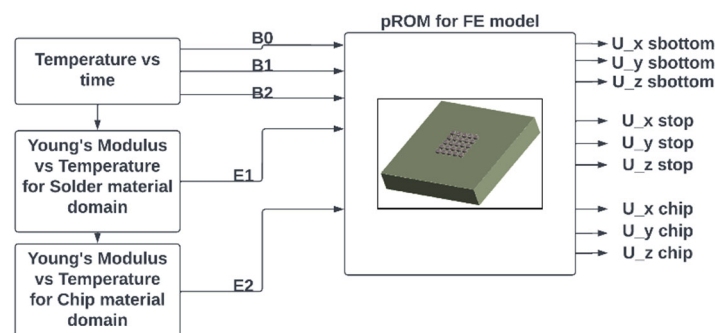


Figure 24 The schematic of a system level simulation in the reduced space, while B0, B1, B2, E1 and E2 are consistent with the definitions in the equations in the previous sections. The outputs on the right-hand side are arbitrary three points directional displacements. 'sbottom' and 'stop' are two points chosen arbitrarily in the solder material domain, while chip is in the silicon material domain.

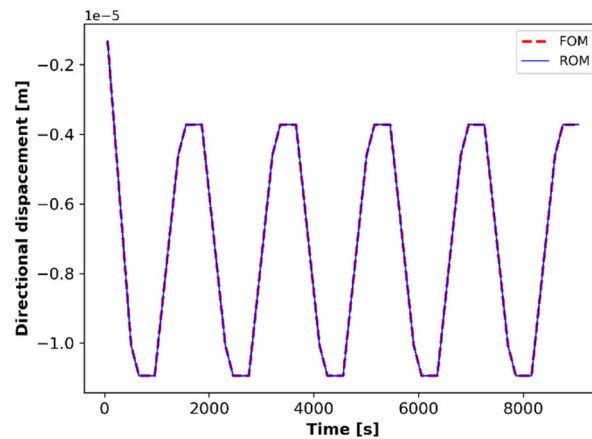


Figure 25 A comparison between the full order model and parametric reduced model in response to temperature cycling. The response is the displacement in x-direction at the node 'sbottom' defined in Figure 20.

Figure 26 shows the relative error between the parametric reduced order model and the full order model over the range of values for Young's modulus. In this case, the single material parameter is observed. As expected, the minimum error is in the vicinity of the chosen expansion point  $E_0 = 2.9E10$  Pa. In the case of Multi-material domain it shows the same conclusion.

Figure 27 shows the effect of using the expansion (extraction) point in chip material domain on the multi-material parametric reduced model. The plot is generated by producing a reduced model with  $K_0$  shown by  $X$  and  $Y$  axis of the plots, with the difference to Figure 26 each point on Figure 27 is a new reduced model. Then the relative error for a cyclic simulation (see Figure 25) is evaluated and plotted. We can clearly observe that error drastically go up when we choose an expansion (extraction) point below the lower bound of the used curve which describes the young's modulus temperature dependency. Despite the fact that mathematically there should be no influence in selecting an extraction point far from the expansion point, Industrial models show many numerical problems here. Also, Optimality algorithm should be applied to identify the optimum choice for the expansion point in each material domain, maybe 'Iterative Rational Krylov Algorithm' [22]. We used the expansion and the extraction point interchangeably. Figure 28 shows how the choice of the subspace can influence the results in multi-material domain study. In contrast to single material parametric case, subspace building has a great influence on the error. As far as we know, the mixing moments absence in building the subspace can be one reason for that.

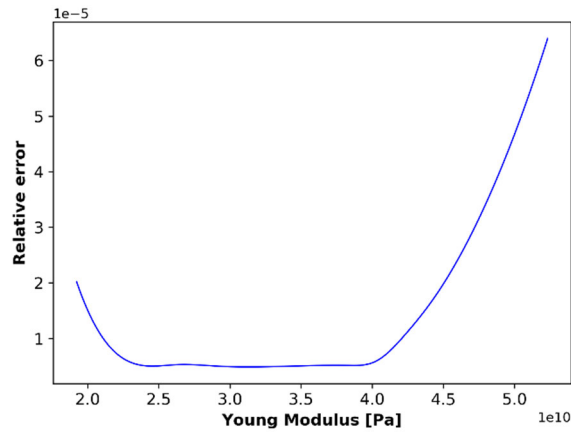


Figure 26 Validation for a single domain parametric reduced order model. The chosen expansion point is 2.9E10 Pa.

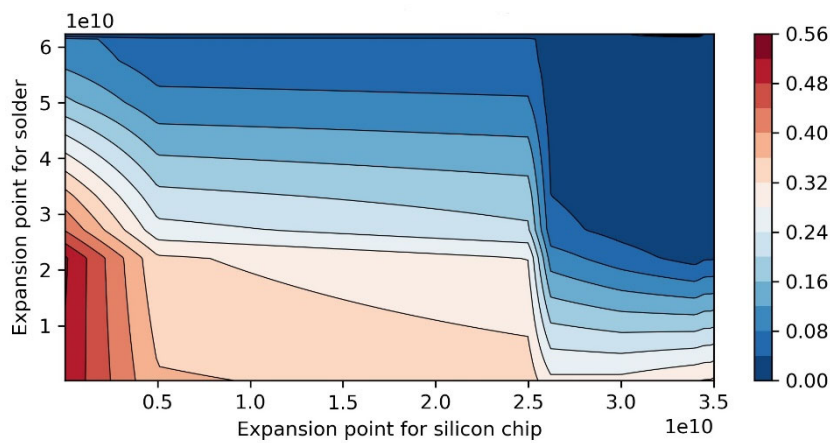


Figure 27 The influence of choosing the expansion point on relative error, the horizontal axis is the expansion point of the first parameter (Young's modulus) and the vertical axis is the expansion point of the second parameter, while the color represents the error.

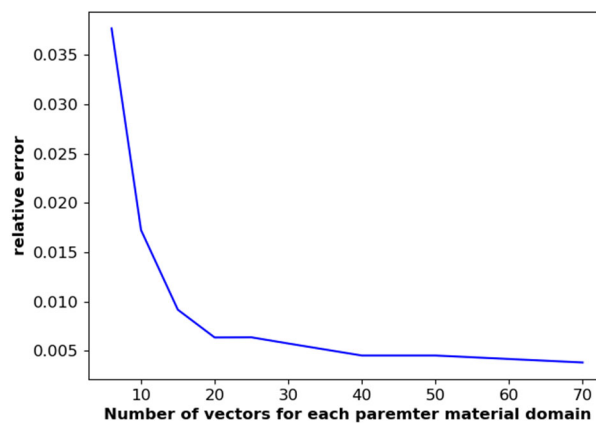


Figure 28 The relation between the relative error and the size of the reduced space. On the horizontal axis is the number of vectors generated for each parameter matrix.

Thus, in this report, we have been able to achieve one of COMPAS project goals, to preserve material properties in symbolic form within a reduced order model. Our next step is to reduce fully nonlinear reliability models.

## 5. Development of New DoE-RSM Schemes for Nonlinear Compact Modelling.

### 5.1. Introduction

ENAS has tested different meta-modelling approach available within ANSYS like SoS (Statistics on Structures) and StaticROM Builder, on the Infineon package FE model based training data using static thermo-mechanical analysis considering different material nonlinearities (e.g. viscoelasticity, creep, plasticity). Training data required for testing these tools are generated using virtual DoE simulation set-up developed for different temperature cycles (reported in D3.2).

Application of SoS and StaticROM Builder for creating nonlinear compact model of Infineon model is explained in following sections.

### 5.2. Compact model generation using SoS (Statistics on Structures)

First of all, Optislang set-up for generating training data for SoS is shown in Figure 29 and necessary results (Stresses, strains and displacements) from all nodes are stored in the .csv file format for 50 designs. Also, geometry mesh file is necessary for SoS. The add-on to convert OMDB file to bin file is also used. These .csv file, .bin file and geometry mesh file is imported in the SoS. SoS GUI is also shown in the Figure 30 where all the imported results could be plotted with imported model mesh.

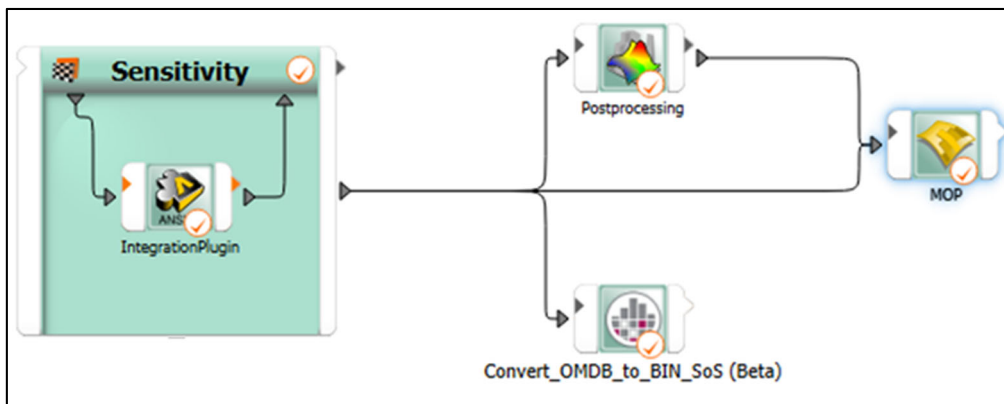


Figure 29 Optislang set-up for generating training data for SoS

SoS tool loads training data (for example, Stress field over all nodes) and decompose the data in mean value field and series expansions where each terms consists of a shape function (which is invariant) and variable ( $z_1, z_2, z_3, \dots$ ). Series terms are sorted by the contribution to the total variation of that field. After decomposition, SoS will generate the sample of  $Z_i$  values corresponding to the respective input parameter sets. Then it use MOP methods from Optislang to generate MOP for each  $Z$  variables. Now, we can use new input data and use this FMOP as a black box to generate new response field as an output. In this case, FMOP provide corresponding  $z$  variable value depending on new input and perform series expansion.

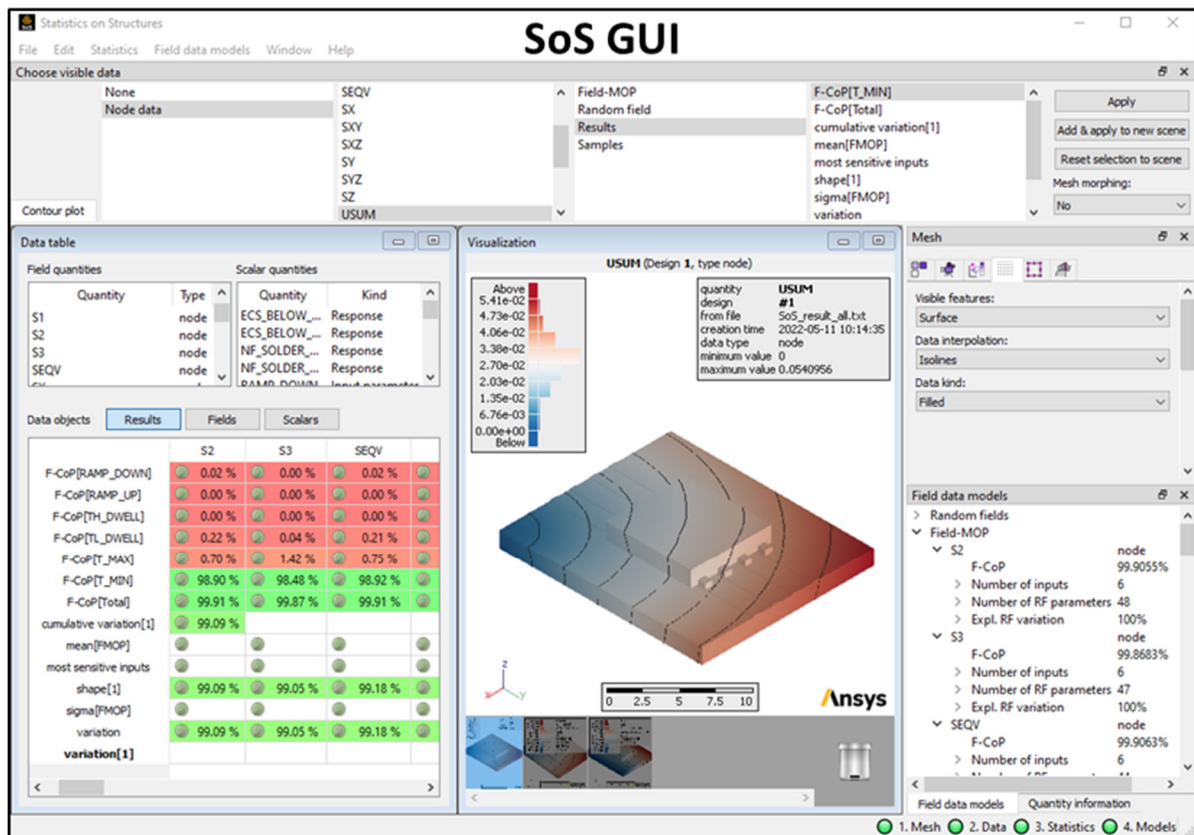


Figure 30 SoS GUI

FMOP is created for selected output parameters within few seconds by following steps described in SoS tool. This FMOP can be used to predict response for the new input which is not included in the training data sets. Predicted creep strain is shown in the solder layers for one training data set.

Also, an accuracy of this FMOP can be verified by comparing the results from FMOP with the reference training data set as shown in the figure for the accumulated equivalent creep strain in the solder layers. The calculated accuracy represents the random field model's ability to reproduce samples as a relative value. When visualized, 100% means exact reproducibility. Values greater than 100% indicate overestimation of the true value.

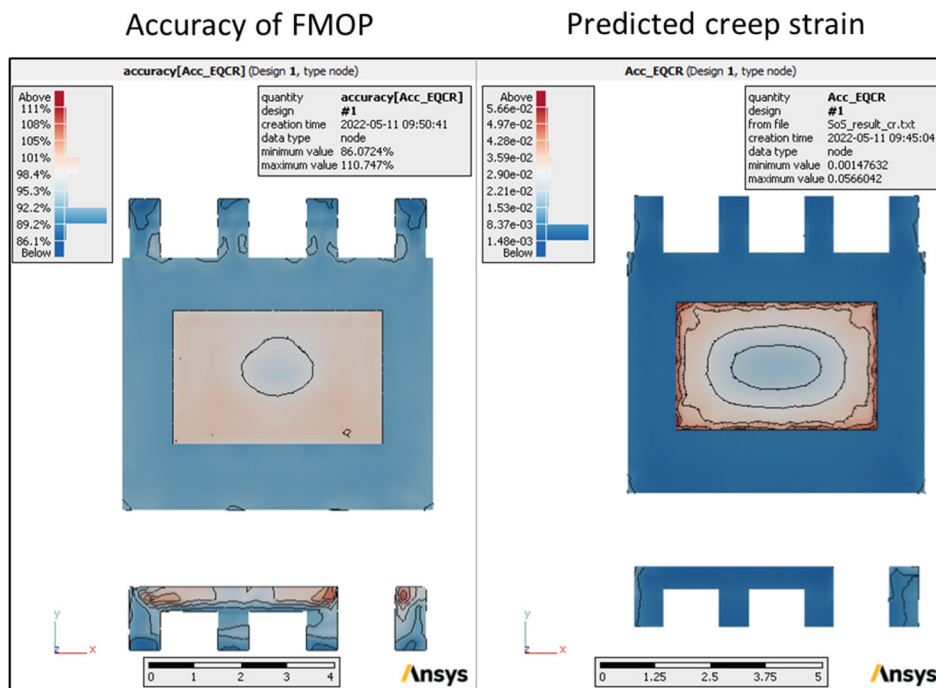


Figure 31 : Results from SoS

### 5.3. Compact model generation using StaticROM Builder

Similar to SoS, StaticROM Builder also generate ROM for field data and static analysis (linear, nonlinear output). This tool uses singular value decomposition method to create parametric nonlinear ROM for field data. It also decomposes input field data into number of static mode shapes  $\Phi_m$  (invariant). The series consist of these mode shapes multiplied by mode coefficients which are function of input parameters. Each mode coefficients are fitted with best metamodel from Optislang. By combination of these mode shapes and mode coefficient values, different response can be predicted for untrained data sets.

There are two main steps for using Static ROM builder: first is generation of Static ROM which requires training data sets in .bin file format. Second step is to use generated ROM as standalone, as Digital Twin and exported as FMU to a third-party system tool.

Compact model generation using Static ROM for Infineon model is illustrated here:

First of all, 27 designs sets are imported in the Static ROM Builder. In the given example, only displacements results are imported. After that, few design sets are selected as a training data out of 27 and remaining sets are kept for validation. After this selection, clicking "Reduce" determines optimal number of modes for ROM using Singular Value Decomposition. Relative reduction error can be checked after this first step. Second step: Clicking 'Build' launches the calculation of the response surface for the mode coefficients and build the ROM. After this step, ROM relative error can be observed and few iteration can be performed by selecting more training data sets.

Once ROM is generated, it can be validated by comparing the relative error or difference between reference and ROM output (nodal value visible as a point-cloud) as shown for the total displacement of the package in the Figure 5. If the error is large, more training data should be used for training the ROM.

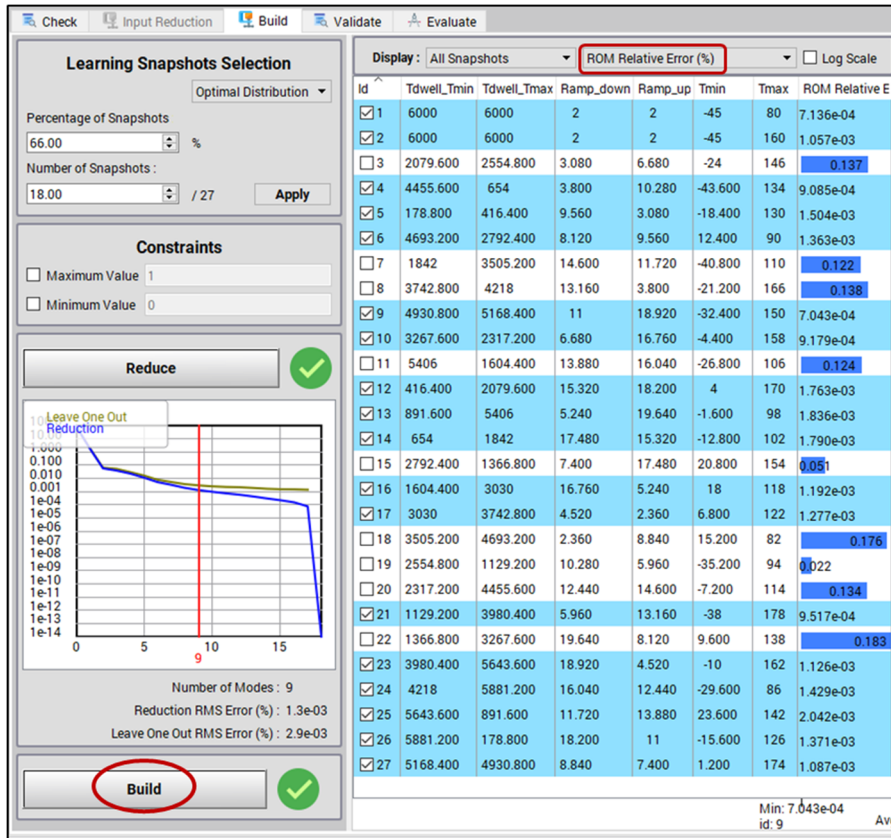


Figure 32 Static ROM generation

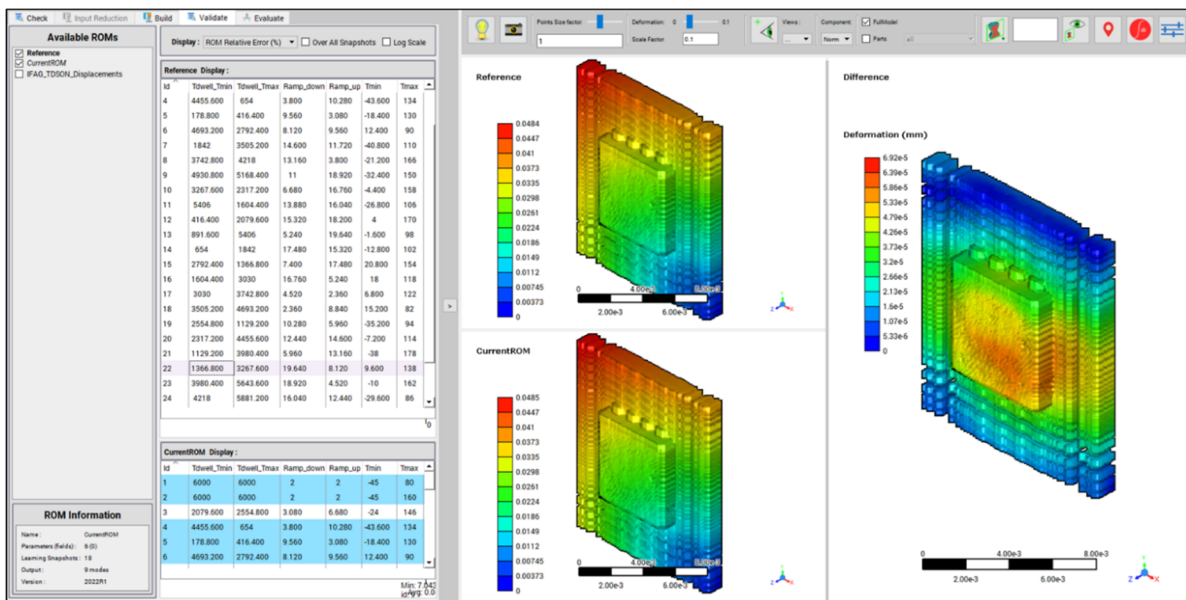


Figure 33 Static ROM validation

## 6. Reduction of Linearized Strongly-Coupled Dynamic Thermo-Mechanical Models.

### 6.1. Introduction

The dynamic analysis of coupled thermo-mechanical circuit models, commonly requires large computational loads. As these systems consist of multiple components, each of which commonly consist of a large number of degrees-of-freedom, the resulting models easily have several million degrees-of-freedom. As a result of this very larger number of degrees-of-freedom, even the definition of a suitable reduced order model can be challenging. In order to circumvent these model size issues, we propose a substructuring approach in this work.

### 6.2. Coupling strategy

The foundation of the reduced order modeling framework is a division of the chip, solder, and PCB meshes into various substructures. Simcenter is used to perform this decomposition, load the initial model, and separate the mesh. Starting from the Reduced Order Models (ROM) for the separate components, a novel assembly approach for the ROMs has been developed which is particularly tailored to the structure of circuit boards, as conceptually outlined in **Figure 34** in the case of the NXP chip.

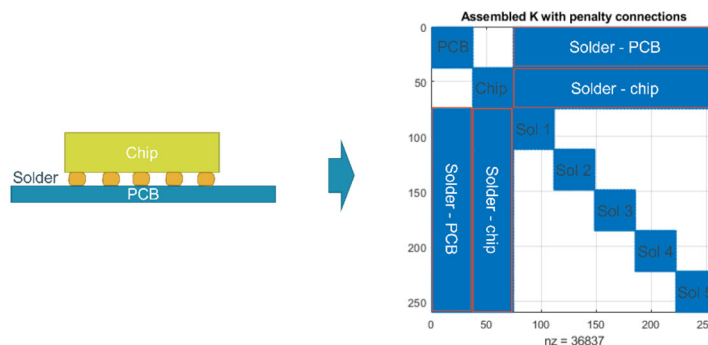


Figure 34: Assembled stiffness matrix of the circuit board with the NXP chip connected via five solder balls

For the PG-TDSON-8 model, the initial model is decomposed in five submodels in Simcenter. These models are i) the chip, ii) three solder patches, iii) and a PCB model.

To account for the non-conforming interface conditions between the different substructures, a novel coupling scheme has been developed starting from a penalty-based enforcement of the interface conditions between the different substructures.

The corresponding Lagrangian  $L$  for a system consisting of two substructure A and B can be written as:

$$L = \frac{1}{2}(\ddot{q}^A)^T \widetilde{M}_{uu}^A \ddot{q}^A + \frac{1}{2}(\ddot{q}^B)^T \widetilde{M}_{uu}^B \ddot{q}^B - \frac{1}{2}(q^A)^T \widetilde{K}_{uu}^A q^A + \frac{1}{2}(q^B)^T \widetilde{K}_{uu}^B q^B - (q^A)^T \widetilde{K}_{uT}^A T^A - (q^B)^T \widetilde{K}_{uT}^B T^B + (q^A)^T \widetilde{f}^A + (q^B)^T \widetilde{f}^B - E_{penalty} \quad (46)$$

The following equation impose the connection constraint on the interfaces between the components by means of penalty method:

$$E_{penalty} = \frac{1}{2} p (\widetilde{C}_{uu}^B q^B - \widetilde{C}_{uu}^A q^A)^T (\widetilde{C}_{uu}^B q^B - \widetilde{C}_{uu}^A q^A) = 0$$

The connection interface between the upper surface of the solder in contact with chip and the lower surface of the solder in contact with the PCB is described for the non-conforming interfaces. For example, in the case of the NXP chip the following steps were taken: A local search scheme to find the closest slave element ID to each of the master nodes in the solder(s) upper and lower surfaces using an element shape function to perform the distance check between the centroid of each slave element and the master nodes. Figure 35 illustrates the closest slave nodes on the PCB (in red color) corresponding to the solder lower surface that represent the contact interface between the solder balls and PCB.

For the PG-TDSON-8 model, the initial model is decomposed in five submodels in Simcenter. These models are i) the chip, ii) three solder patches, iii) and a PCB model.

To account for the non-conforming interface conditions between the different substructures, a novel coupling scheme has been developed starting from a penalty-based enforcement of the interface conditions between the different substructures.

The corresponding Lagrangian  $L$  for a system consisting of two substructure A and B can be written as:

$$L = \frac{1}{2} (\ddot{q}^A)^T \widetilde{M}_{uu}^A \ddot{q}^A + \frac{1}{2} (\ddot{q}^B)^T \widetilde{M}_{uu}^B \ddot{q}^B - \frac{1}{2} (q^A)^T \widetilde{K}_{uu}^A q^A + \frac{1}{2} (q^B)^T \widetilde{K}_{uu}^B q^B - (q^A)^T \widetilde{K}_{uT}^A T^A - (q^B)^T \widetilde{K}_{uT}^B T^B + (q^A)^T \widetilde{f}^A + (q^B)^T \widetilde{f}^B - E_{penalty}$$

The following equation impose the connection constraint on the interfaces between the components by means of penalty method:

$$E_{penalty} = \frac{1}{2} p (\widetilde{C}_{uu}^B q^B - \widetilde{C}_{uu}^A q^A)^T (\widetilde{C}_{uu}^B q^B - \widetilde{C}_{uu}^A q^A) = 0$$

The connection interface between the upper surface of the solder in contact with chip and the lower surface of the solder in contact with the PCB is described for the non-conforming interfaces. For example, in the case of the NXP chip the following steps were taken: A local search scheme to find the closest slave element ID to each of the master nodes in the solder(s) upper and lower surfaces using an element shape function to perform the distance check between the centroid of each slave element and the master nodes. Figure 35 illustrates the closest slave nodes on the PCB (in red color) corresponding to the solder lower surface that represent the contact interface between the solder balls and PCB.

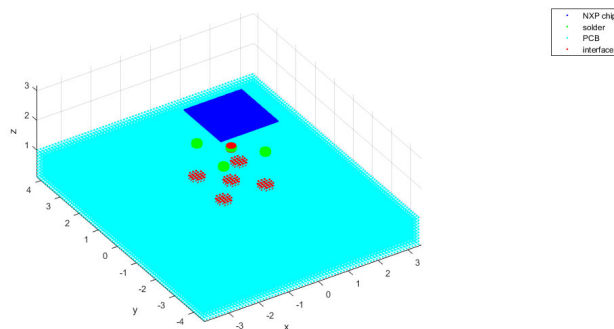


Figure 35: Illustration of the described interface with the NXP chip. Red dots indicate the detected closest nodes to the solder balls. PCB is discretized using an 8-node linear solid element type. Figure 36 illustrates the closest slave nodes on the Infineon chip and (in blue color) corresponding to the solder lower surface that represent the contact interface between the three solder parts and

the chip. This is also the case for the contact interface between the solder parts and PCB denoting in pink.

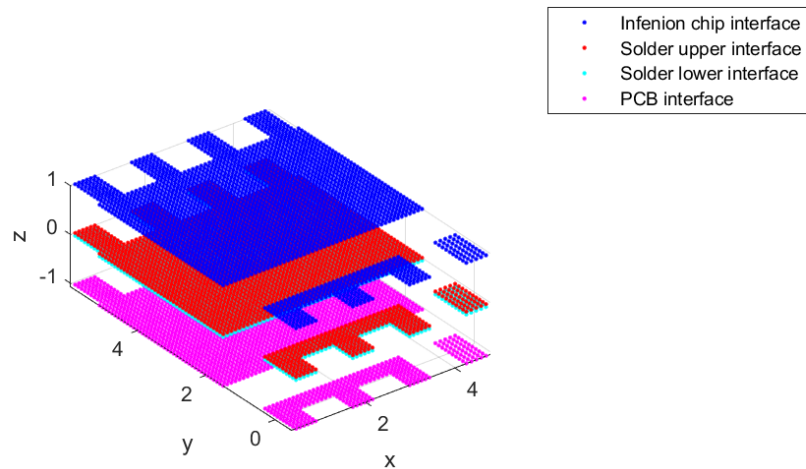


Figure 36: Illustration of the described interface with the Infineon chip. Blue and pink dots respectively indicate the detected closest nodes to the solder parts to the chip and PCB.

Applying Hamilton’s principle, we can extract the resulting dynamic equations for the substructured system, where the penalty terms lead to additional coupling terms within the stiffness matrix. For the PG-TDSON-8 model, **Figure 37** illustrates these coupling terms have the following structure.

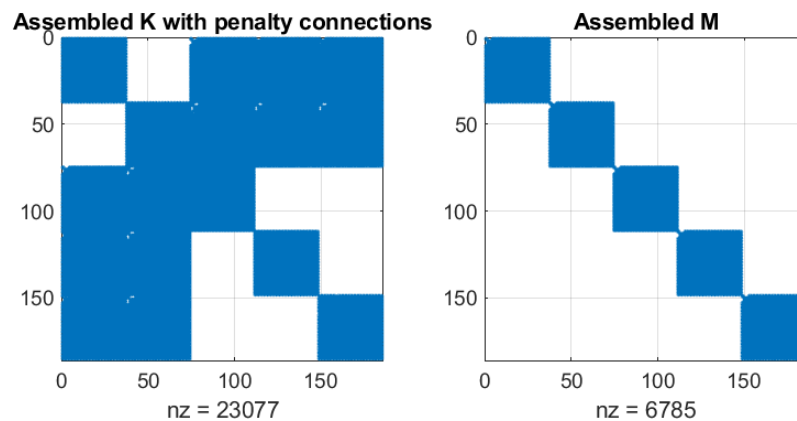


Figure 37: Assembled stiffness and mass matrices of the Infineon PG-TDSON-8 model

Where for the PG-TDSON-8 model, the initial model was decomposed in five sub-models in Simcenter. These models are: the chip, three solder patches, and a PCB model. These different substructures can be recognized as the diagonal block-matrices in this stiffness and mass matrix. The resulting model can e.g. be exploited in an eigenvalue analysis. In the modal analysis the 1<sup>st</sup> bending and torsional and the 2<sup>nd</sup> bending modes for ROM of the structure were investigated. The captured modes are illustrated in **Figure 38**.

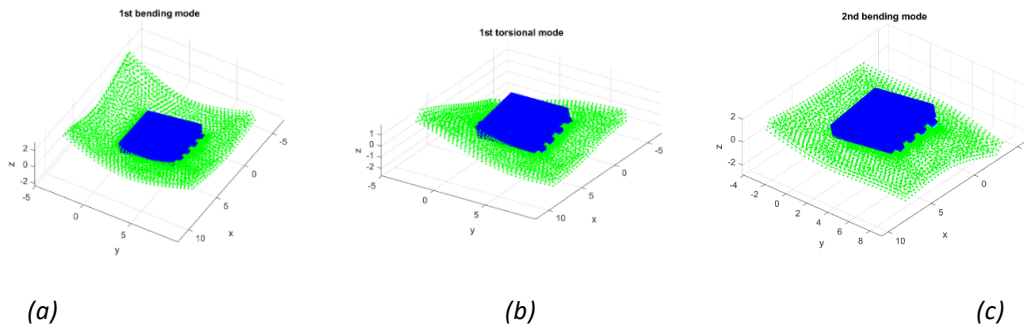


Figure 38: Eigenmodes for the first three modes for the ROM of Infineon PG-TDSON-8

Analogously, the thermal dynamic equations and thermo-mechanical coupling can be assessed. This leads to a set of model equations of the following form:

$$\begin{bmatrix} \tilde{M}_{uu} & 0 \\ 0 & 0 \end{bmatrix} \begin{Bmatrix} \dot{q} \\ \dot{T} \end{Bmatrix} + \begin{bmatrix} 0 & 0 \\ 0 & \tilde{c}_{TT} \end{bmatrix} \begin{Bmatrix} q \\ T \end{Bmatrix} + \begin{bmatrix} \tilde{K}_{uu} & \tilde{K}_{uT} \\ 0 & \tilde{K}_{TT} \end{bmatrix} \begin{Bmatrix} q \\ T \end{Bmatrix} = \begin{Bmatrix} \tilde{f} \\ \tilde{Q} \end{Bmatrix}.$$

The equation above has been assembled according to the procedure illustrated in **Figure 39**.

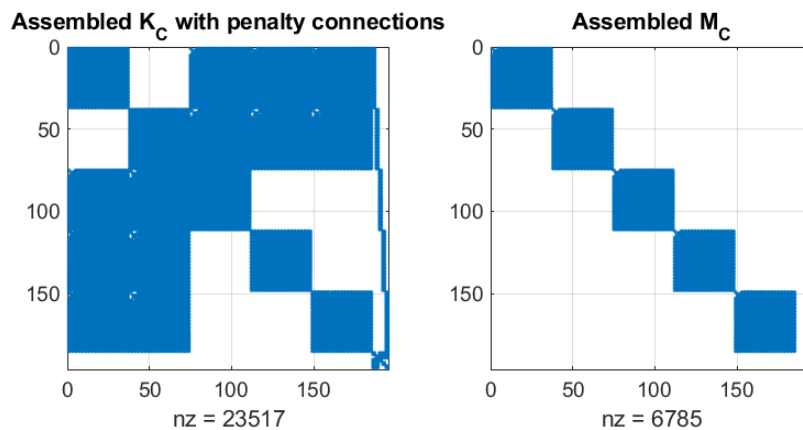


Figure 39: Assembled stiffness and mass matrices of the coupled thermo-mechanical PG-TDSON-8 model

It should be noted that for the considered application, the deformation caused by heat is considered because of one-directional thermo-mechanical coupling.

This assembly procedure enables a flexible treatment of non-conforming interfaces between the various components (chips, solder and PCB) of the circuit board. This in turn then allows us to assemble the reduced order model matrices for the system with the chips in various locations in order to allow a straightforward design analysis. For example, in **Figure 40** we show an exercise where the NXP and Infineon chip are connected to a single PCB. The chips can be easily repositioned on the PCB to enable design analysis.

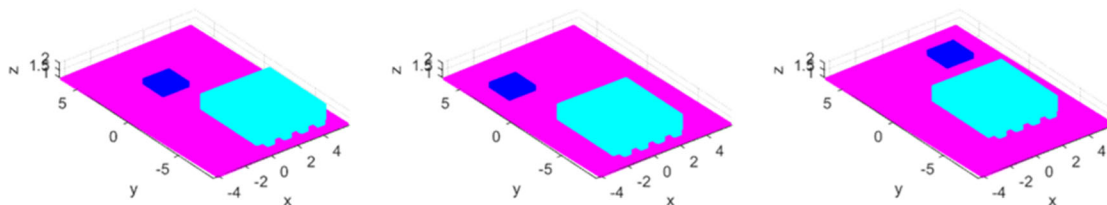


Figure 40: Re-positioning the NXP and Infineon chips on the PCB

Using the resulting substructured models, it becomes feasible to perform e.g. an eigenvalue analysis on the full circuit board, and analysis which previously required super-computer capabilities, as shown in Figure 41.

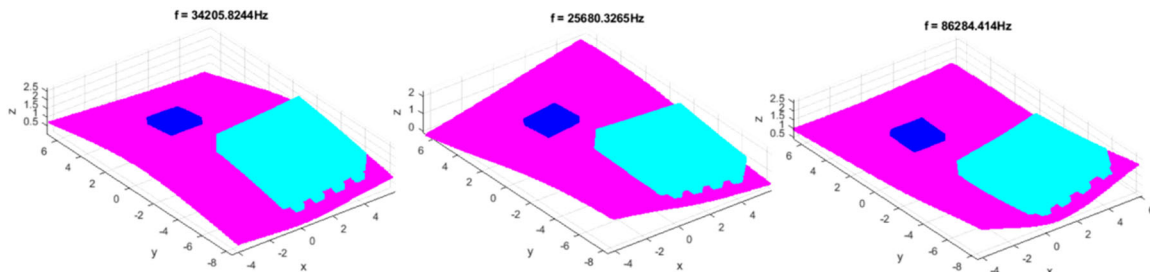


Figure 41: Eigenmodes of the ROM circuit board with the NXP and Infineon chips

### 6.3. Toolchain overview

The simulation procedure starts with building a full finite element model of the circuit board in NASTRAN Simcenter. The main full FE model consists of chip and PCB as shown in the following figure.

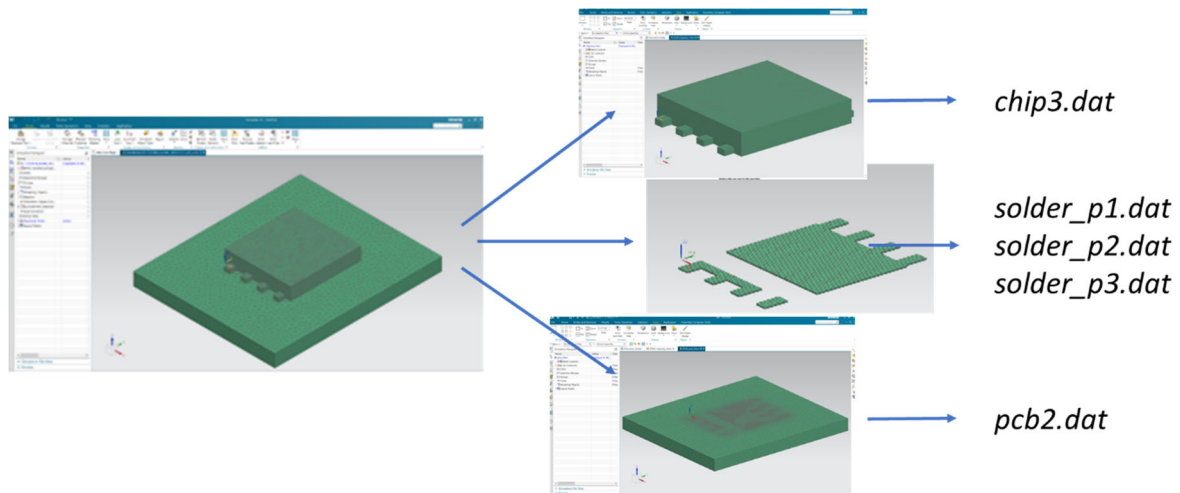


Figure 42: Finite element model of the circuit board with the PCB and Infineon chips in Simcenter

Next, the full system model is split into separate components including PCB, chip and solder parts, as shown in Figure 42. The (five) components are to be imported in ACSIII / text file format such as .DAT / .BDF files (standard Nastran input) to be further processed through a MATLAB-based workflow.

The ACSIII files are imported as dat/bdf file format in MATLAB as illustrated in Figure 43.

```
% Infineon chip
bdfFile = 'I:\COMPAS\InfineonModel\chip3.dat';
[mesh_chip] = GetTMMModel(bdfFile, 'nastran', 'matlab', NastranExec);
% Solder part 1
bdfFile = 'I:\COMPAS\InfineonModel\solder_p1.dat';
[mesh_solder_p1] = GetTMMModel(bdfFile, 'nastran', 'matlab', NastranExec);
% Solder part 2
bdfFile = 'I:\COMPAS\InfineonModel\solder_p2.dat';
[mesh_solder_p2] = GetTMMModel(bdfFile, 'nastran', 'matlab', NastranExec);
% Solder part 3
bdfFile = 'I:\COMPAS\InfineonModel\solder_p3.dat';
[mesh_solder_p3] = GetTMMModel(bdfFile, 'nastran', 'matlab', NastranExec);
% PCB
bdfFile = 'I:\COMPAS\InfineonModel\pcb2.dat';
[mesh_pcb] = GetTMMModel(bdfFile, 'nastran', 'matlab', NastranExec);
```

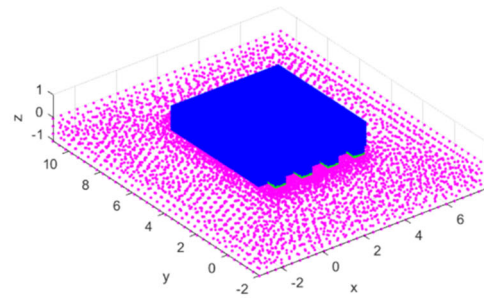


Figure 43: Matlab interface to import various chip, solder and pcb models

In this initial stage, both the mesh information (nodes, elements, materials) are stored in a structure, as well as the corresponding full order model matrices, like the stiffness, mass and thermal matrices. Different approaches can be selected for generating these matrices, where the current toolchain supports direct computation in Matlab (as shown in the previous figure), or extraction from NX Nastran, as shown in the interface below.

```
% Infineon chip
bdfFile = 'I:\COMPAS\InfineonModel\chip3.dat';
[mesh_chip] = GetTMMModel(bdfFile, 'nastran', 'nastran', NastranExec);
```

Figure 44: FOM extraction from NX Nastran.

At this stage of the process, the various components of the system are not connected yet. Next we need to define the interfaces between these components. In circuit boards, the solders are the driving components in the connection, and the toolchain first assess the position of the top and bottom nodes of the solders, and stores these in the 'interface indices', as shown in the figure below.

```
%% Define interfaces on solders
mesh_solder_p1.interface(1).ind = find(abs(mesh_solder_p1.co(:,3))-max(mesh_solder_p1.co(:,3)))<1e-5); % solder-chip
mesh_solder_p1.interface(2).ind = find(abs(mesh_solder_p1.co(:,3))-min(mesh_solder_p1.co(:,3)))<1e-5); % solder-pcb

mesh_solder_p2.interface(1).ind = find(abs(mesh_solder_p2.co(:,3))-max(mesh_solder_p2.co(:,3)))<1e-5); % solder-chip
mesh_solder_p2.interface(2).ind = find(abs(mesh_solder_p2.co(:,3))-min(mesh_solder_p2.co(:,3)))<1e-5); % solder-pcb

mesh_solder_p3.interface(1).ind = find(abs(mesh_solder_p3.co(:,3))-max(mesh_solder_p3.co(:,3)))<1e-5); % solder-chip
mesh_solder_p3.interface(2).ind = find(abs(mesh_solder_p3.co(:,3))-min(mesh_solder_p3.co(:,3)))<1e-5); % solder-pcb
```

Figure 45: interface extraction for solders (top and bottom surface)

Starting from the solder interfaces, a script is called which allows to detect the corresponding degrees-of-freedom on the chip and pcb, and generates corresponding 'constraint matrices', as shown in the script below.

```
[mesh_solder_p1.interface(1).C, mesh_chip.interface(1).C, mesh_chip.interface(1).ind] = GetInterface(mesh_solder_p1, 1, mesh_chip);
[mesh_solder_p2.interface(1).C, mesh_chip.interface(2).C, mesh_chip.interface(2).ind] = GetInterface(mesh_solder_p2, 1, mesh_chip);
[mesh_solder_p3.interface(1).C, mesh_chip.interface(3).C, mesh_chip.interface(3).ind] = GetInterface(mesh_solder_p3, 1, mesh_chip);

[mesh_solder_p1.interface(2).C, mesh_pcb.interface(1).C, mesh_pcb.interface(1).ind] = GetInterface(mesh_solder_p1, 2, mesh_pcb);
[mesh_solder_p2.interface(2).C, mesh_pcb.interface(2).C, mesh_pcb.interface(2).ind] = GetInterface(mesh_solder_p2, 2, mesh_pcb);
[mesh_solder_p3.interface(2).C, mesh_pcb.interface(3).C, mesh_pcb.interface(3).ind] = GetInterface(mesh_solder_p3, 2, mesh_pcb);
```

Figure 46: interface identification for chip and pcb

For the considered Infineon system, with one chip and three solders, the resulting geometry is shown in Figure 47.

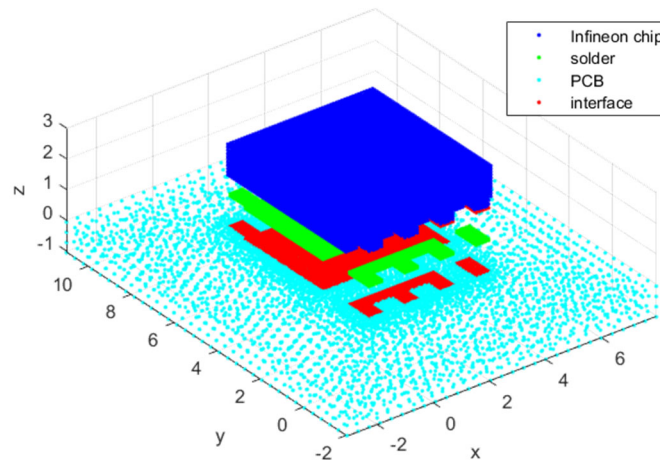


Figure 47: Infineon system geometry and interfaces.

This process has also been integrated in a graphical user-interface in Siemens Simcenter, which make it more accessible for general engineering applications. As shown in Figure 48, this interface allows to select the PCB and chip(s) from existing mesh files, and position them at a desired location. After this positioning, the computational procedure as described before is triggered.

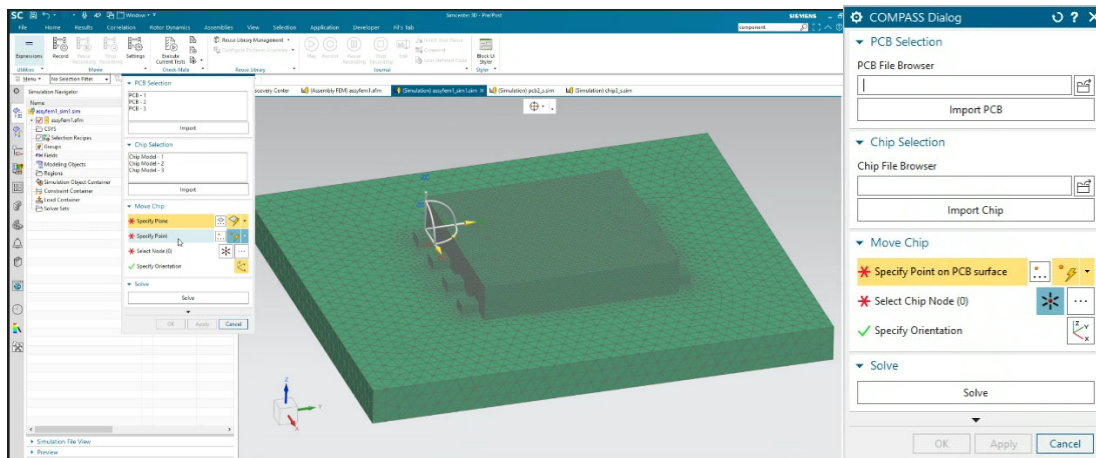


Figure 48: Siemens Simcenter interface for PCB-chip assembly construction

At this point, all information is available to set up the reduced order model. To this end, we employ the *stochastic load mode* approach presented in D2.1. A ROM is generated for each substructure as shown in Figure 49.

```

%% Generate reduced order component models:
% ROM for infineon chip
[ROM_chip.Kr, ROM_chip.Mr, ROM_chip.Tr, ROM_chip.V, ROM_chip.x0, ROM_chip.Vb, ROM_chip.xb0] = ...
    GetReducedComponent(mesh_chip, 3, 40);

% ROMs for solders
[ROM_solder_p1.Kr, ROM_solder_p1.Mr, ROM_solder_p1.Tr, ROM_solder_p1.V, ROM_solder_p1.x0, ROM_solder_p1.Vb, ROM_solder_p1.xb0] = ...
    GetReducedComponent(mesh_solder_p1, 3, 20);
[ROM_solder_p2.Kr, ROM_solder_p2.Mr, ROM_solder_p2.Tr, ROM_solder_p2.V, ROM_solder_p2.x0, ROM_solder_p2.Vb, ROM_solder_p2.xb0] = ...
    GetReducedComponent(mesh_solder_p2, 3, 20);
[ROM_solder_p3.Kr, ROM_solder_p3.Mr, ROM_solder_p3.Tr, ROM_solder_p3.V, ROM_solder_p3.x0, ROM_solder_p3.Vb, ROM_solder_p3.xb0] = ...
    GetReducedComponent(mesh_solder_p3, 3, 20);

% ROM for PCB
[ROM_pcb.Kr, ROM_pcb.Mr, ROM_pcb.Tr, ROM_pcb.V, ROM_pcb.x0, ROM_pcb.Vb, ROM_pcb.xb0] = ...
    GetReducedComponent(mesh_pcb, 3, 30);
    
```

Figure 49: ROM generation interface with stochastic load modes

In this approach, the decay of the singular values of the stochastic load modes indicates the reducibility of the models. **Figure 50** shows the decay of the singular values for the Infineon chip and PCB model, where the strong decay indicates good reducibility, and the presented models with respectively 40 and 30 load modes can be expected to provide good accuracy.

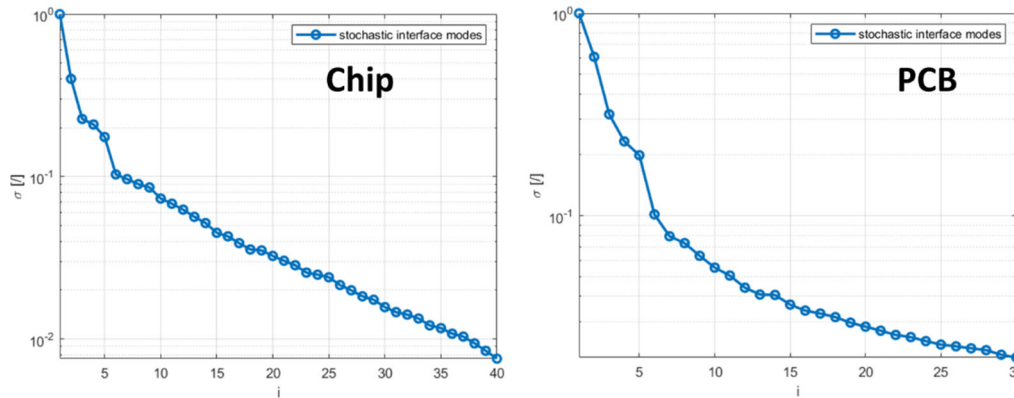


Figure 50: singular value decay in stochastic load modes for Infineon chip and PCB model. Similarly, the singular value decay for the ROM for the solder patches is shown in Figure 51.

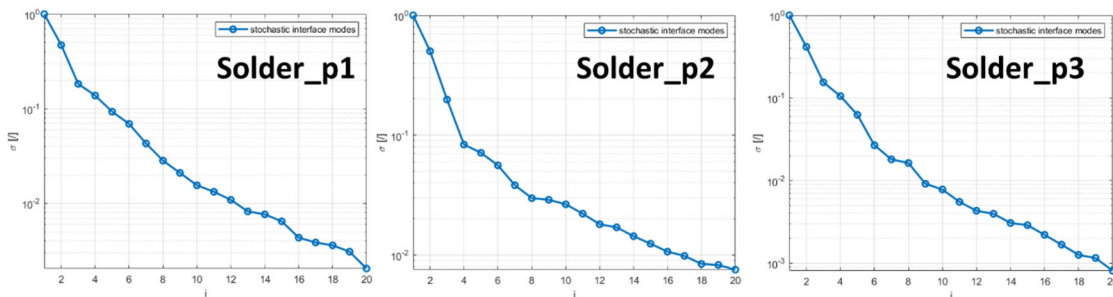


Figure 51: singular value decay in stochastic load modes for three solder patches in Infineon model  $\mu$

Based on the resulting component level ROMs, the full circuit board model is defined, as discussed in the previous section. The corresponding Matlab interface is shown in Figure 52.

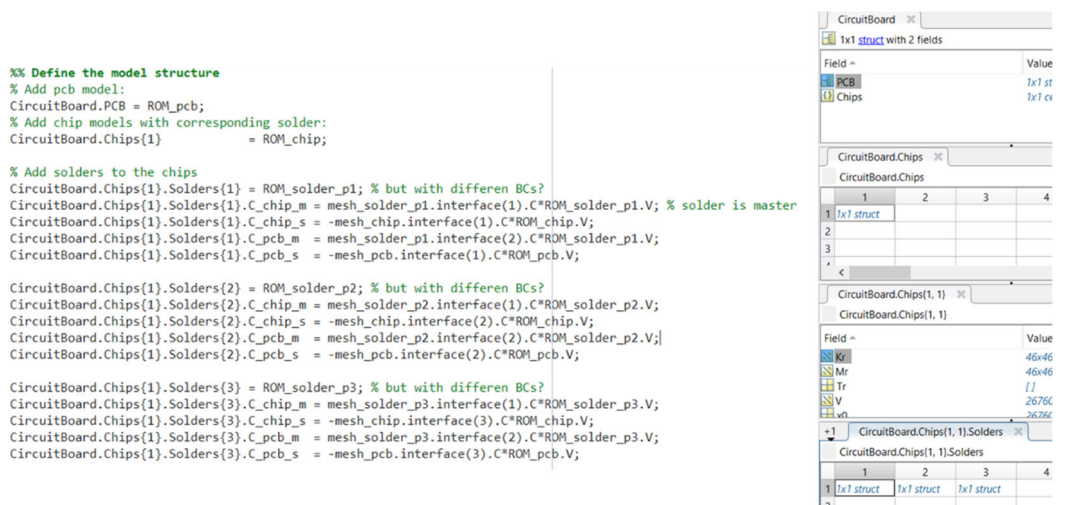


Figure 52: full system level model description combining chips, PCBs, solders and corresponding connections.

Next, the system model assembly can be performed, exploiting the penalty based formulation discussed in the previous section. A simple Matlab interface allows to convert the previously defined 'Circuitboard' into the assembled system matrices, as shown below.

```
% Assemble circuit board model:

p = 1e7; % penalty factor
[K_ass, M_ass] = AssembleCircuitBoardMatrices(CircuitBoard, p);
```

Figure 53: model assembly routine

The structure of the resulting stiffness and mass matrices is shown in the figure below.

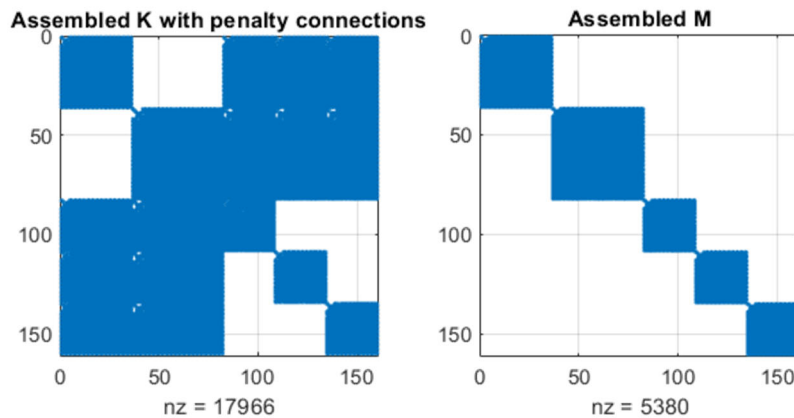


Figure 54: assembled ROMs for full Infineon system model

The resulting full system model is limited to a very low number of reduced degrees-of-freedom, 180 in this case.

This low dimensionality allows for a straightforward evaluation of the dynamic performance of the system under consideration. In this example we perform a modal analysis on the assembled Infineon model. Using the standard Matlab 'eig' command, the obtained eigenvalues are shown in

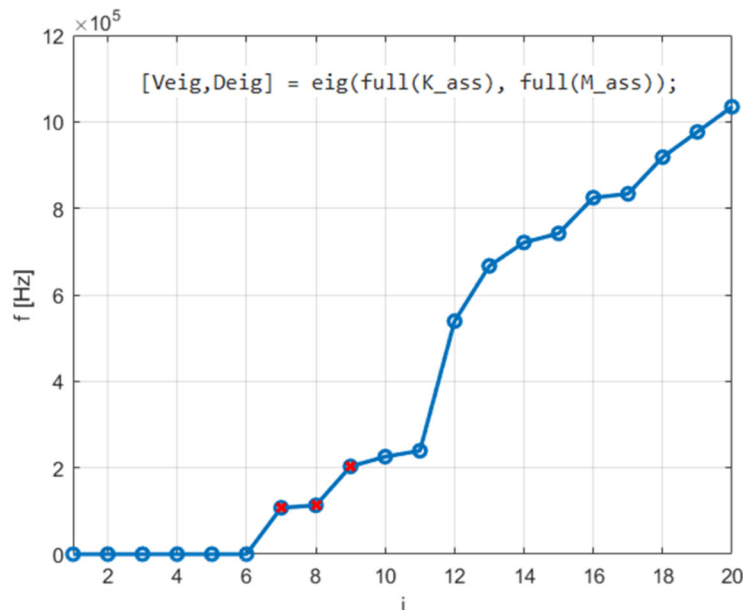


Figure 55: eigenvalues evaluated for Infineon system from the assembled reduced order model.

The computation is performed in less than 0.1seconds on a regular laptop. This analysis shows six rigid body modes, as expected, and a steady increase in the dynamic deformation modes. The corresponding mode shapes obtained for the first three deformation modes (marked in red in Figure 55), are shown in the figure below.

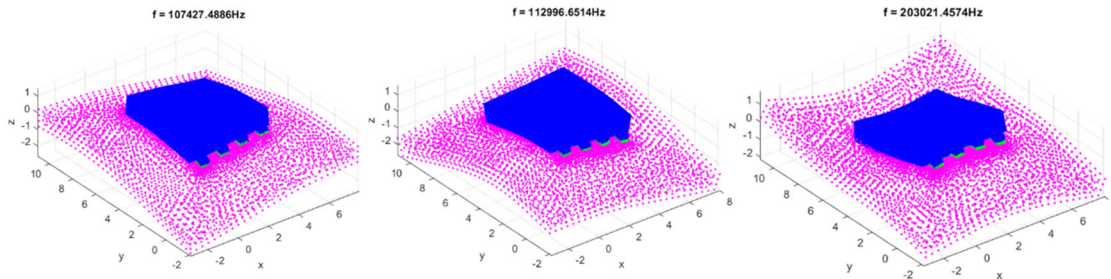


Figure 56: mode shapes obtained from Infineon system model

#### 6.4. Model Order Reduction of a Strongly-Coupled Dynamic Thermo-Mechanical Infineon Package Model in ANSYS

In this section, we present the workflow of generating a ROM of a strongly-coupled dynamic thermo-mechanical Infineon package model from ANSYS Mechanical. On basis of the software 'Model Reduction inside ANSYS', novel APDL scripts are developed to construct the ROM and transform it into VHD format, which can be imported into ANSYS Twin Builder to do system-level simulations.

##### 6.4.1. Case Study

The package model as shown in Figure 57. It presents the schematic of the Infineon training model, which consists of the PCB, solders, copper, package chip, and molding compound. The edge and nodes noted in Figure 57 (A) are assigned with the Dirichlet boundary conditions.

$$u_0(x, y, z) = (x, 0, z), \quad u_1(x, y, z) = (x, y, 0), \quad u_2(x, y, z) = (0, 0, z) \quad (47)$$

The model is simulated with an initial uniform temperature of 22 °C in the thermal domain, which is noted as the reference temperature in the structure domain.

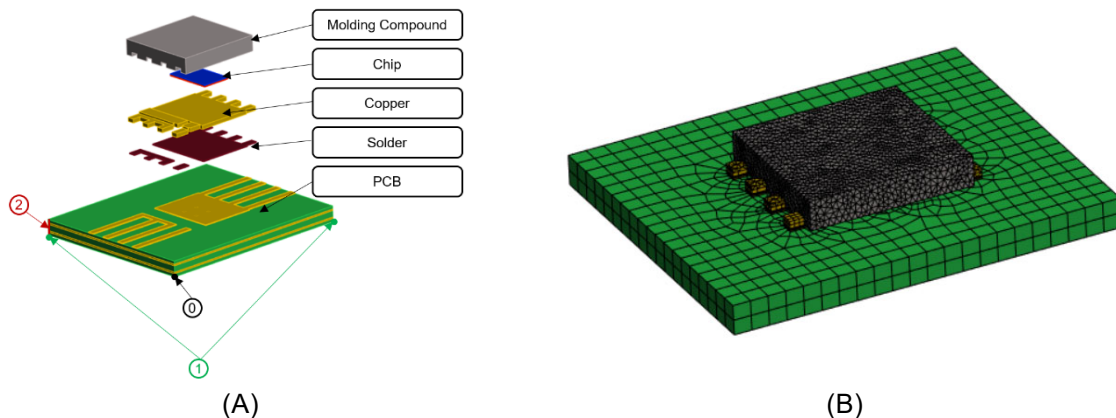
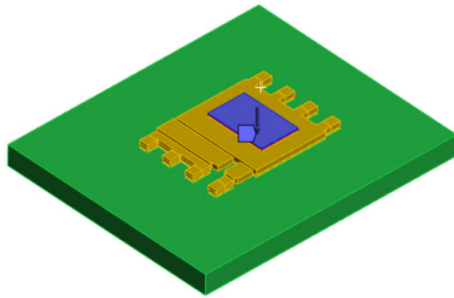


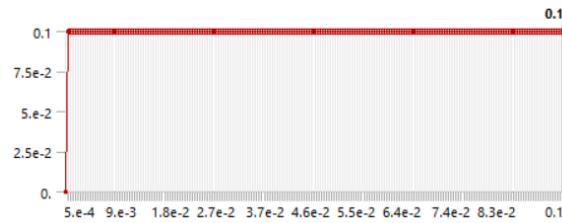
Figure 57: (A) An exploded view of the Infineon training model PG-TDSON-8. (B) The mesh of generated in the model. There are 13216 nodes in total and each node contains 4 degree of freedoms: Ux, Uy, Uz, Temp.

The simulation is performed with a transient analysis. Step end time is 0.1 s with minimum time step  $5e-6$  s and maximum time step  $5e-4$  s.

**A** heat flow is defined in the chip and a convection boundary condition is assigned to the external surfaces of the model as shown in **Figure 58** and **Figure 59**.

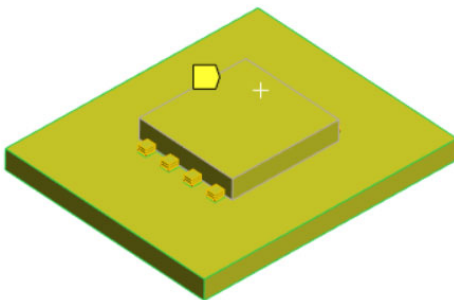


(A)

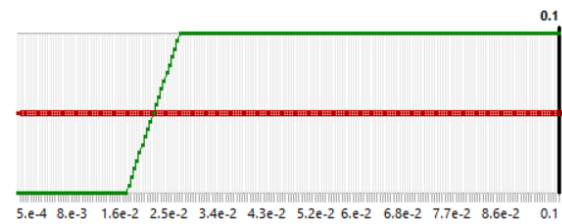


(B)

Figure 58: (A) Heat flow input applied on the top surface of the chip. (B) Heat flow input value increases from 0 to 0.1 at  $5e-4$  s. The input value is constant at 0.1 between  $5e-4$  s and 0.1 s.



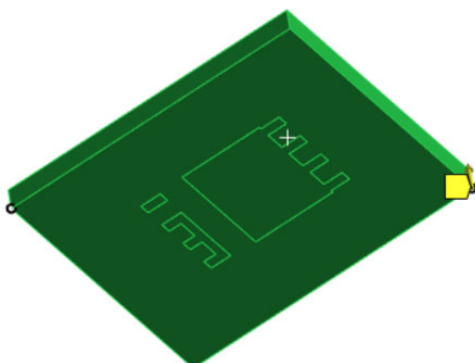
(A)



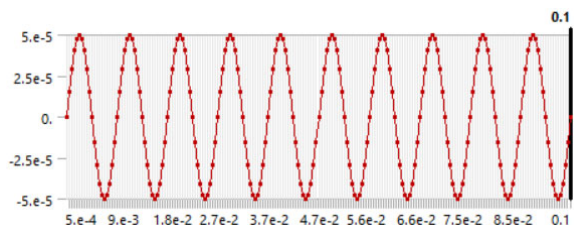
(B)

Figure 59: (A) Convection boundary condition applied on the external surfaces of the model. (B) Film coefficient is defined as constant  $1e6$  W/m<sup>2</sup>°C. The ambient temperature is increased from 22 °C to 125 between  $2e-2$  and  $3e-2$  s.

In addition, in this case study, a vibrational movement is applied on two vertices at the bottom surface of the model as shown in **Figure 60**.



(A)



(B)

Figure 60: (A) Vibrational displacement input applied on two vertices at the bottom surface. (B) Sine wave input values with amplitude 5e-5 m and frequency 100 Hz.

Material/body	Young's modulus [GPa]	CTE [ppm/K]	Poisson's Ration
Copper	130	17	0.34
Silicon (Chip)	169	3	0.34
Solder (lead) in side package	20	28	0.4
Polymer (Molding compound)	30	6	0.3
Solder SAC on PCB	40	21	0.34
FR4 (PCB)	26	16	0.2

Table 6: Material properties used in the model (CTE: coefficient of Thermal Expansion).

The material properties used in this model are all linear-elastic only as shown in Table 6. Therefore, the finite element model of the strongly-coupled dynamic thermo-mechanical model can be expressed as follows:

$$\Sigma_N: \left\{ \underbrace{\begin{bmatrix} M_U & 0 \\ 0 & E_T \end{bmatrix}}_M \underbrace{\begin{Bmatrix} \dot{U} \\ \dot{T} \end{Bmatrix}}_{\dot{x}} + \underbrace{\begin{bmatrix} E_U & 0 \\ 0 & E_T \end{bmatrix}}_E \underbrace{\begin{Bmatrix} \dot{U} \\ \dot{T} \end{Bmatrix}}_{\dot{x}} + \underbrace{\begin{bmatrix} K_U & K_{UT} \\ 0 & K_T \end{bmatrix}}_K \underbrace{\begin{Bmatrix} U \\ T \end{Bmatrix}}_x = \underbrace{\begin{Bmatrix} F + K_{UT}\{T_{ref}\} \\ Q \end{Bmatrix}}_{B \cdot u} \quad (48)$$

$$y = C \cdot x$$

where the state vector  $x \in \mathbb{R}^{N \times N}$  contains nodal displacement state  $U \in \mathbb{R}^{N_1}$  and nodal temperature state  $T \in \mathbb{R}^{N_2}$ ,  $N = N_1 + N_2$ .  $K_U \in \mathbb{R}^{N_1 \times N_1}$  is the stiffness matrix in the mechanical domain and  $E_T \in \mathbb{R}^{N_2 \times N_2}$ ,  $K_T \in \mathbb{R}^{N_2 \times N_2}$  are the heat capacity and conductivity matrices in the thermal domain. The coupling term  $K_{UT} \in \mathbb{R}^{N_1 \times N_2}$  couples the thermal and mechanical parts. This means that the temperature results influence directly the nodes containing mechanical DOFs via thermal strain, in which the coefficient of thermal expansion is not zero.  $T_{ref}$  is the reference temperature for thermal expansion.  $Q$  and  $F$  are the thermal and mechanical loads in the model.  $C \in \mathbb{R}^{p \times N}$  is the output matrix defined by the users, which gives  $p$  outputs in the output vector  $y$ .  $B \in \mathbb{R}^{N \times m}$  and  $u \in \mathbb{R}^m$  are the input matrix and vector with  $m$  inputs.

#### 6.4.2. Model Order Reduction

We aim to generate a ROM of the model presented in Equation (48). The model setups for the ROM generation in ANSYS Mechanical is shown in Figure 61. The reference temperature  $T_{ref}$  for thermal expansion and the ambient temperature in the convection boundary condition are all set as 0 °C. The film coefficient in the convection boundary condition is preserved as the same as that in the full-order model. The vibrational displacement input in the full-order model is replaced by a force input. In addition, an APDL script is developed to invoke the functions from 'Model Reduction inside ANSYS' to generate the ROM.

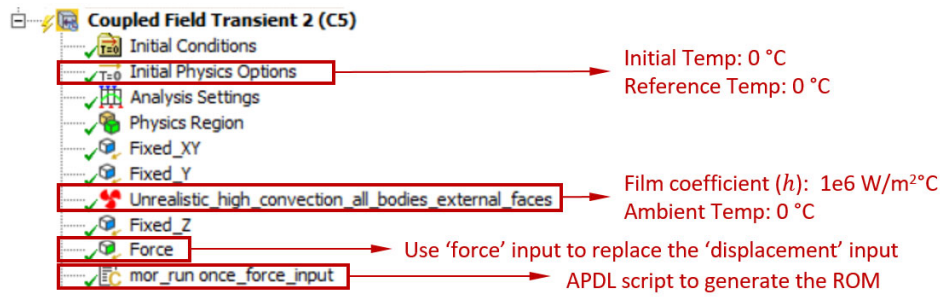


Figure 61: Model setups for the generation of the ROM in ANSYS Mechanical.

Therefore, the full-order model of Equation (48) is rewritten as follows:

$$\Sigma_N: \begin{cases} \begin{bmatrix} M_U & 0 \\ 0 & E_T \end{bmatrix} \begin{Bmatrix} \ddot{U} \\ \ddot{T} \end{Bmatrix} + \begin{bmatrix} E_U & 0 \\ 0 & E_T \end{bmatrix} \begin{Bmatrix} \dot{U} \\ \dot{T} \end{Bmatrix} + \begin{bmatrix} K_U & K_{UT} \\ 0 & K_T \end{bmatrix} \begin{Bmatrix} U \\ T \end{Bmatrix} = B(h) \cdot \begin{bmatrix} f \\ q \\ T_{amb} \end{bmatrix} \\ y = C \cdot x \end{cases} \quad (49)$$

where  $f$  is the force input applied on the vertices at the bottom surface of the PCB,  $q$  is the heat flow input applied on the chip, and  $T_{amb}$  is the ambient temperature in convection boundary condition. It should be noted here that, in the original full-order model  $T_{ref} = 22 \text{ }^\circ\text{C}$ . Therefore, the real temperature  $\hat{T}$  from Equation (49) is calculated as follows:

$$\hat{T} = T + T_{ref} \quad (50)$$

Afterward, second order Arnoldi reduction (SOAR) method is applied to construct a projection matrix  $V \in \mathbb{R}^{N \times r}$  based on the second-order Krylov subspace around expansion point 0 as follows:

$$\text{colspan}\{V\} = \mathcal{K}_r\{-K^{-1}E, -K^{-1}M; -K^{-1}B\} \quad (51)$$

The full state vector can be projected onto a lower dimension subspace  $x = V \cdot z$ , where  $z \in \mathbb{R}^r$  is the reduced state vector,  $r \ll N$ . Thereby, the reduced model of Equation (49) is written as follows:

$$\Sigma_r: \begin{cases} \begin{bmatrix} V^T M V & \\ & V^T E V \end{bmatrix} \cdot \dot{z} + \begin{bmatrix} V^T K V & \\ & V^T B(h) \end{bmatrix} \cdot z = \begin{bmatrix} f \\ q \\ T_{amb} \end{bmatrix} \\ y = \begin{bmatrix} y_{dis} \\ y_{temp} \end{bmatrix} = \begin{bmatrix} C_U \\ C_T \end{bmatrix} \cdot z \end{cases} \quad (52)$$

where  $M_r, E_r, K_r \in \mathbb{R}^{r \times r}$ ,  $B_r \in \mathbb{R}^{r \times m}$  and  $C_r \in \mathbb{R}^{p \times r}$  are reduced system matrices.  $y_{dis}$  is the Uz displacement output and  $y_{temp}$  is the temperature output from a node selected in the solder layer.

The generated files of the ROM are all saved in the 'userfiles' directory of the project. As shown in Figure 62, the full files contains the information of the original full-scale system matrices. They are reduced and saved in 'mor.\*' files and they are further transformed into VHDL format.

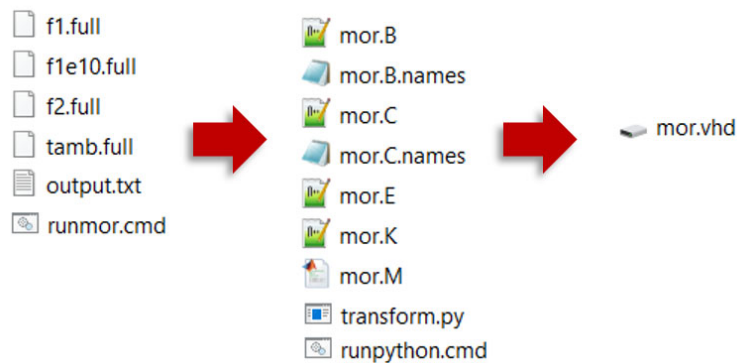


Figure 62: ROM files generated from ANSYS Mechanical via 'Model Reduction inside ANSYS'.

### 6.5. ROM Verification in ANSYS Twin Builder

The reduced model is imported into system-level simulation software ANSYS Twin Builder as presented in Figure 63. The computational efficiency of the ROM is shown in Table 7. The accuracy of the ROM is shown in Figure 64.

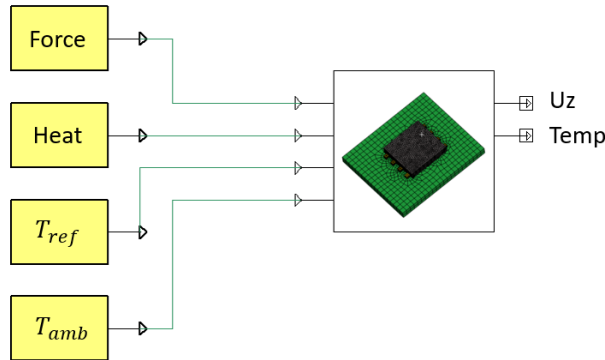


Figure 63: Simulation of the ROM in ANSYS Twin Builder with force, heat flow, reference temperature, and ambient temperature inputs.

	FOM	pROM
Total DOFs	52,853	45
Elapsed Time (s)	1038	7.584

Table 7: The computational time for performing the simulations of the FOM and ROM (on Intel Core Processor i5-7600 CPU @3.0 GHz, RAM 32 GB).

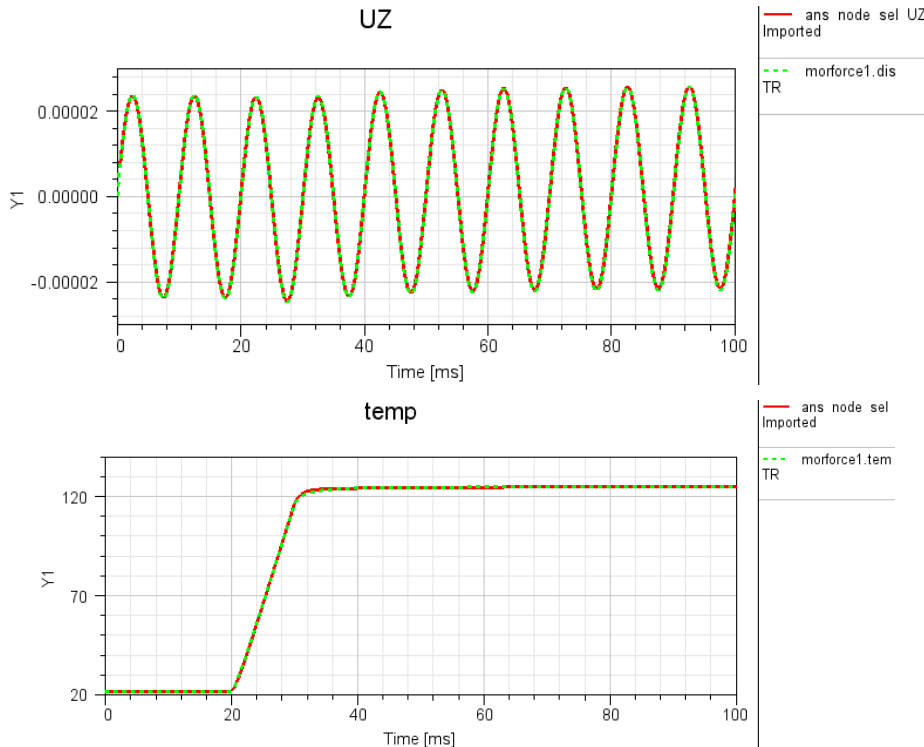


Figure 64: Comparison of the displacement and temperature results from the selected output node.

## 7. Reduction of Nonlinear Thermo-Mechanical Models by Piecewise Linear Approximation

### 7.1. Introduction

This report presents a thorough investigation into the application of advanced model order reduction techniques to nonlinear dynamical systems arising from the spatial discretization in finite element analysis. Utilizing a state-space approach, as defined in [23], the study explores the formulation of nonlinear systems and subsequently focuses on the effective linearization of these systems in the vicinity of multiple equilibrium points. The proposed methodology leverages the high accuracy demonstrated by linear model order reduction, particularly employing proper orthogonal decomposition to derive reduced models. The report exemplifies this approach through an insightful exploration of thermomechanical models, providing a detailed examination of the implemented equations, characteristics, advantages, and disadvantages. Furthermore, the research extends its application to a simplified electronics case study involving a Ball Grid Array (BGA), illustrating the generation of linearized models along a trajectory and the subsequent reconstruction of nonlinear trajectories through a weighted summation technique.

### 7.2. Trajectory Piece Wise-Linear approach.

After the finite element based spatial discretization, the nonlinear dynamical system may be formulated and described using the following state-space approach defined in [23]:

$$\Sigma_N: \begin{cases} \frac{dg(x(t))}{dt} = f(x(t)) + B(x(t))u(t), \\ y(t) = C^T x(t) \end{cases}, \quad (53)$$

where  $x(t) \in R^N$  is a vector of states at time  $t$ ,  $f: R^N \rightarrow R^N$  and  $g: R^N \rightarrow R^N$  are nonlinear vector-valued functions,  $B \in R^{N \times M}$  is a temperature-dependent input matrix,  $u(t) \in R^M$  is an input,  $C \in R^{N \times K}$  is an output matrix and  $y(t) \in R^K$  is the output.

Nonlinear systems of this nature can be effectively linearized in the vicinity of multiple equilibrium points (so called snapshots), permitting a precise representation through linearized models as shown in Figure 65. Given the demonstrated high accuracy of linear model order reduction [13], we can derive reduced models for these systems, by projecting all the linearized systems onto a global projection matrix using proper orthogonal decomposition [3]. The reconstruction of nonlinear trajectories can subsequently be achieved by linearly combining these reduced linear time invariant models through a weighted summation technique.

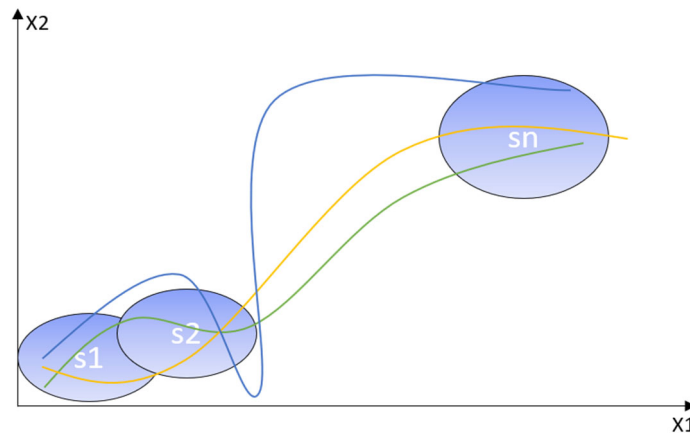


Figure 65 Generation of the linearized models (s1, s2,...,sn) along a trajectory of a nonlinear system in a two-dimensional state space [23].

For a thermomechanical model featuring nonlinear state-dependent terms, Equation. (54) can be written as:

$$\Sigma_N: \begin{cases} M \ddot{x}(t) + E \dot{x}(t) + f(x(t)) = B(x(t)) u(t) \\ y(t) = C^T x(t) \end{cases}, \quad (54)$$

Characteristics/Advantages/Disadvantages:

- Robust method
- Compatible with commercial software
- Only valid for load cases similar to those the model was trained on
- “curse of dimensionality” if multiple different load or parameters
- TPWL-approximated model is still nonlinear due to state-dependent weights, but these are drastically more efficient to evaluate (“Due to these state-dependent
- weighting scheme, the TPWL-approximated system still contains nonlinearities, but they are few and are efficient to evaluate.”)

### 7.3. Simplified electronics case study with Ball Grid Array.

Figure 66 provides a comprehensive depiction of the setup and outcomes of the full order nonlinear FE model under examination. The graphical presentation encapsulates the progressive accumulation of plastic strain within the material as it undergoes the mechanical loading procedure. Figure 2 (right) illustrates the observed relationship between the accuracy of representing the reduced linear systems and the number of singular vectors in the bases. The precision of this representation also depends upon the placement of the snapshots, a detailed discussion of which is reserved for the comprehensive exposition in the full research paper.

Figure 2 (left) shows a complete match between the reduced order model and the full one, except at the initialization discontinuity which can be treated in the full paper.

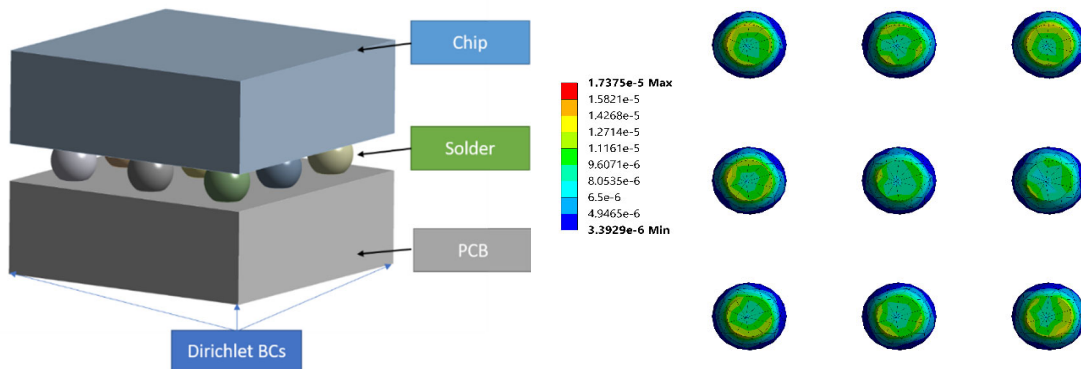


Figure 66 Left: a schematic representation of a geometric model delineating distinct material domains and prescribing Dirichlet boundary conditions on the lower surface of the printed circuit board (PCB) at three specified corner points a mechanical compression force is applied as a distributed load on the upper surface of the chip. Right: the color map represents the solder plastic strain, measured in millimeters per meter, attained during the final load step, providing insights into the deformation behavior of the material under mechanical load conditions.

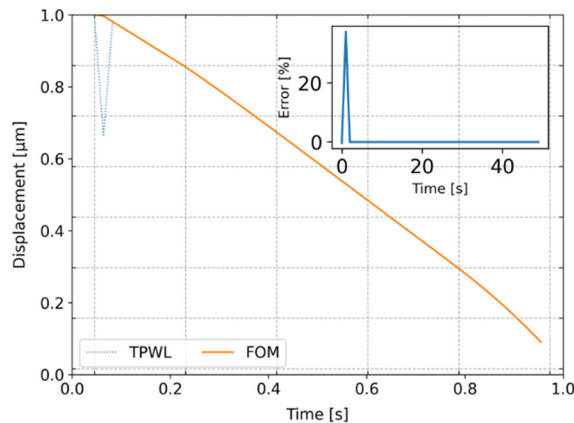


Figure 67 A comparison between the reduced order model generated by applying TPWL and the full order model (FOM) with the error plot inside.

#### 7.4. MEMS beam actuator.

The beam actuator is a subsystem of an innovative design for a quasistatic micromirror [1,2]. Figure 68 illustrates the design and its actuation sequence: a spherical cap acts as a mirror and rests on four electrostatic beam actuators. Upon actuation, these actuators launch the mirror into a free flight phase for rotation, after which it is actively caught. Repeated actuation cycles achieve large rotations. In contrast to traditional designs, all structural connections are omitted and the mirror moves freely. In combination with the mirror's spherical geometry, the design features continuous stable positions over a large deflection range.

This case study demonstrates the same methodology as proposed for thermomechanical models in COMPAS. However, this purely mechanical model does not include temperature dependence, which qualifies it for an intermediate case study to implement the methodology.

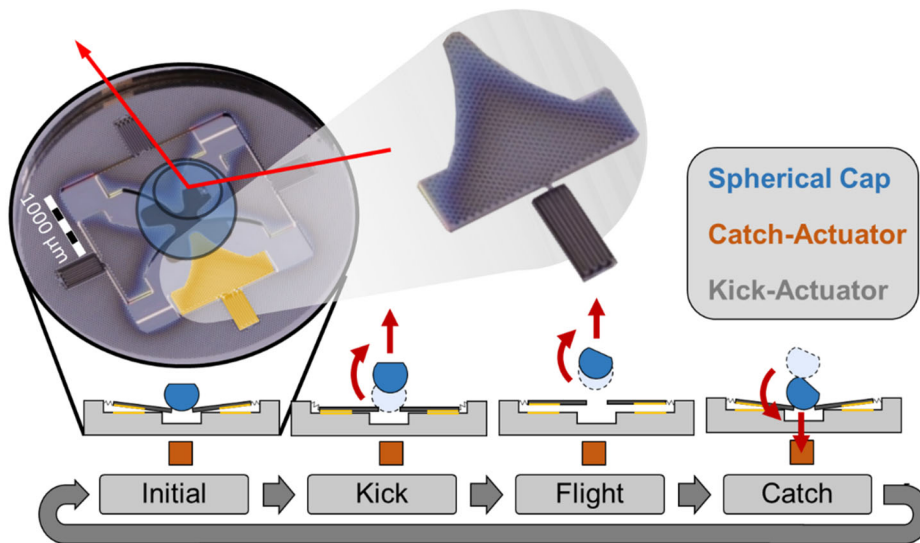


Figure 68 Operating principle of the microsystem [4] [5]: a spherical cap rests on four electrostatic beam actuators. Actuating the beams into pull-in transfers momentum to the spherical cap. After a free flight phase, the mirror is caught into its stable resting

For this case study, the beam actuator is loaded with an out-of-plane downwards force at its tip, causing mechanical contact to the supporting chip. A 1602-dimensional FEM model establishes the reference solution and provides the mathematical model for subsequent MOR. Projection-based MOR by POD creates a five-dimensional reduced order model that deploys TPWL to efficiently handle nonlinearities. Figure 69 illustrates this workflow.

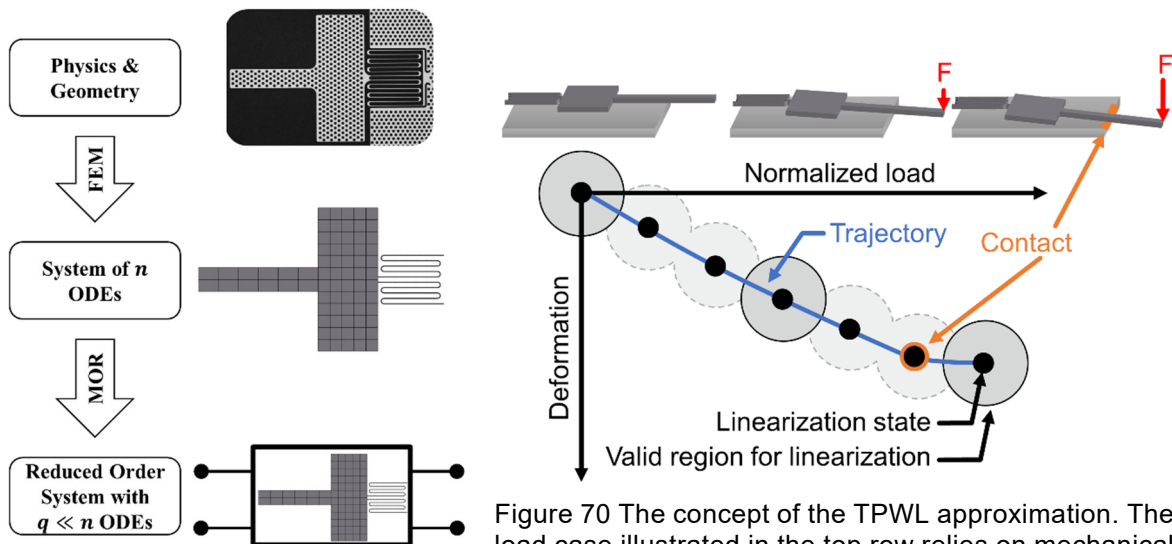


Figure 69 Workflow of modeling: FEM models the beam actuator as a high-dimensional system of ordinary differential equations. Subsequently, MOR constructs an accurate surrogate model of drastically smaller dimension.

Figure 70 The concept of the TPWL approximation. The load case illustrated in the top row relies on mechanical contact, rendering the model nonlinear. The TPWL approximation replaces the original system with a combination of linearized ones, which are obtained at different states along the trajectory. The linearized models' range of validity is indicated by circles at their linearization states.

Figure 71 compares the tip's displacement computed by the FEM model, the TPWL model, and the TPWL reduced order model. Both approximations perform extremely well, as the lines are

indistinguishable. The relative error in the bottom plot confirms this observation as no error exceeds  $10^{-4}$ . All relative errors have two sections separated by the contact event at a normalized load of 0.66. For each section, the minimum error coincides with sampling positions and reaches maximum values in between. In general, the relative error between the TPWL model and its reduced version is the lowest, identifying the TPWL approximation as the main source for deviation.

Table 8 lists the total computational time for each of the three models. The FEM model is the slowest with 23.5 s, while the TPWL model only requires half the time. However, the TPWL reduced order model achieves a speedup factor of more than 250 compared to the FEM solution.

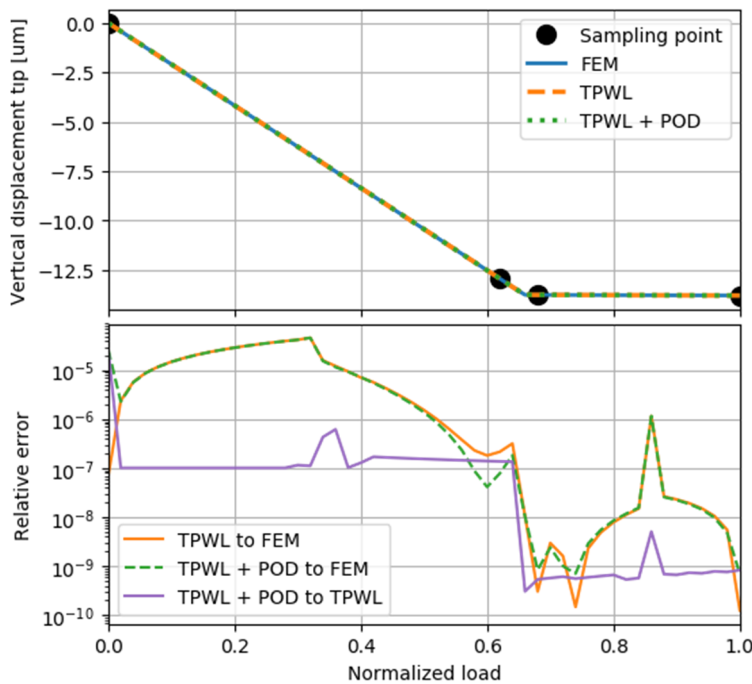


Table 8 Computational times on Intel® Core™ i5-7600, 32 GB RAM.

Model	Elapsed time [s]
FEM	23.5
TPWL	12.5
FEM + POD	$84.0 \cdot 10^{-3}$

Figure 71 Comparison of the beam's vertical tip displacement over the normalized load. The FEM solution constitutes the reference, which the TPWL model and its reduced version approximate. The plot also highlights sampling positions for linearized models utilized

## 7.5. Extension to thermomechanical practical difficulties and possibilities.

TPWL is based on training data and only remains reliable for similar load cases. Therefore, the method is more suited for i.e. feedback-control and not for predictions. In order to build a TPWL-approximated mode for the latter case, all cycles that are to be represented need to be part of the training data acquired by the FOM. This step provides all necessary results so that a TPWL-approximated ROM cannot provide additional benefits. Other methods for nonlinear model order reduction referred to as hyperreduction evaluate a subset of most significant nonlinearities and approximate the remaining nonlinear terms based on their results. This approach is more physics-based as FOM-level nonlinearities are considered and therefore, offers better prediction quality. However, these methods require full access to the analytic expression for nonlinear terms which are hardly compatible to commercial software. Another alternative based on easily available snapshots are ANNs. However, their extrapolation characteristics for trajectories not included in their training data remains questionable, especially for sensitive applications such as creep.

A significant impediment to applying TPWL in a mechanical simulation involving thermal cycling loads (e.g., NXP wafer-level chip-scale package) is the manner in which ANSYS handles the thermal load. Currently, there is a lack of accessibility and control over this thermal load. This issue is apparent in the tutorial where a Linear Perturbation step is utilized to capture the system matrices at various time steps under loading conditions. Please check Figure 72.

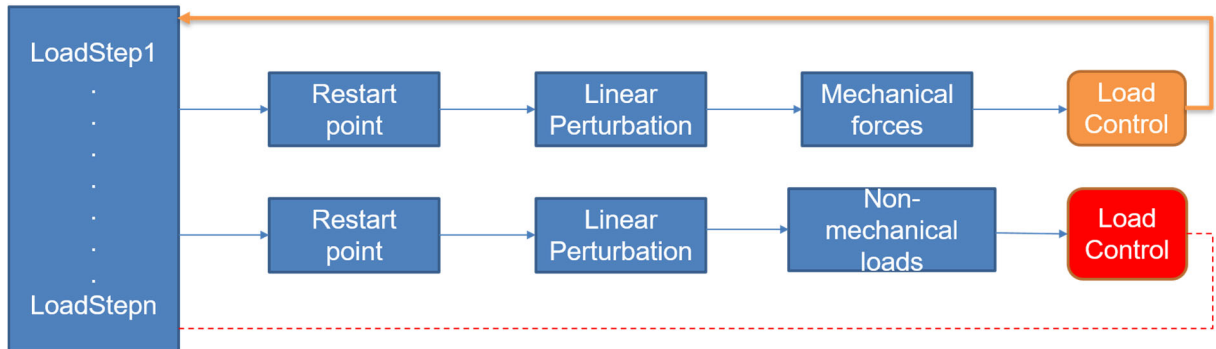


Figure 72 The schematic depicts the workflow for each time step in ANSYS. Notably, the user lacks control over non-mechanical loads, encompassing thermal loads.

Following our examination of how ANSYS handles thermal loads—wherein they are incorporated into the definition of total strain and potentially addressed on both sides of the equilibrium. The governing partial differential equations of elastoplastic behavior over a continuous domain  $\Omega$ , considering infinitesimal strain theory and isotropic materials can be written as follow:

$$\begin{aligned}
 \varepsilon(\mathbf{u}) &= H\sigma + \varepsilon^{th} + \varepsilon^p \text{ in } \Omega, \\
 -\text{div } \sigma &= \mathbf{f} \text{ in } \Omega, \\
 \varepsilon^p &: (\tau - \sigma) \geq 0 \forall \tau \text{ with } \mathcal{F}(\tau) \leq 0 \text{ in } \Omega, \\
 \mathbf{u} &= 0 \text{ on } \Gamma_D.
 \end{aligned}
 \tag{55}$$

Let's consider Formulation is based displacement not mixed(Compatibility to be investigated), more over let's consider elastic and plastic strains combined in one nonlinear function depending non linearly on the strain and so on the displacement  $F(u)$ , and let the strain tensor is symmetric, then the above equation will yield to :

$$\begin{aligned}
 \sigma &= F(u)(\varepsilon(\mathbf{u}) - \varepsilon^{th}) \text{ in } \Omega, \\
 -\text{div } \sigma &= 0 \text{ in } \Omega, \\
 \mathbf{u} &= 0 \text{ on } \Gamma_D.
 \end{aligned}
 \tag{56}$$

Then we can substitute first line in the second line.

$$\begin{aligned}
 -\text{div} \left( F(u)(\nabla(\mathbf{u}) - \alpha \cdot (T - T_{ref})) \right) &= 0 & \text{in } \Omega \\
 \mathbf{u} &= 0 & \text{on } \Gamma_D.
 \end{aligned}
 \tag{57}$$

## 8. Development of a Data-Based Reduced Order Modelling

### 8.1. Introduction

In this section, the method developed jointly by Eindhoven University of Technology and Siemens AG is introduced. The method is a model order reduction (MOR) technique that is characterized by the following features:

First, the technique is designed for the reduction of large-scale nonlinear dynamical models. Nonlinear dynamical models are relevant in scenarios where linear models are insufficient to accurately predict the behavior of the simulated system.

Second, the technique is non-intrusive, i.e., it only requires snapshots of simulation. This makes it particularly attractive for integration with commercial finite element analysis (FEA) software packages, which often do not provide access to the model equations. Simulation snapshots are always available.

A motivating example application that is considered through this section is that of modeling solder joints (Figure 73). Solder joint failure is one of the most occurring failure modes in automotive electronics components. Thus, simulation of solder joint behavior is an important ingredient in the virtual design and prototyping phase. The difficulty lies in the observation that solder joint behaves nonlinearly. Linear ROMs are insufficient to capture such behavior and hence a nonlinear modeling approach must be pursued.

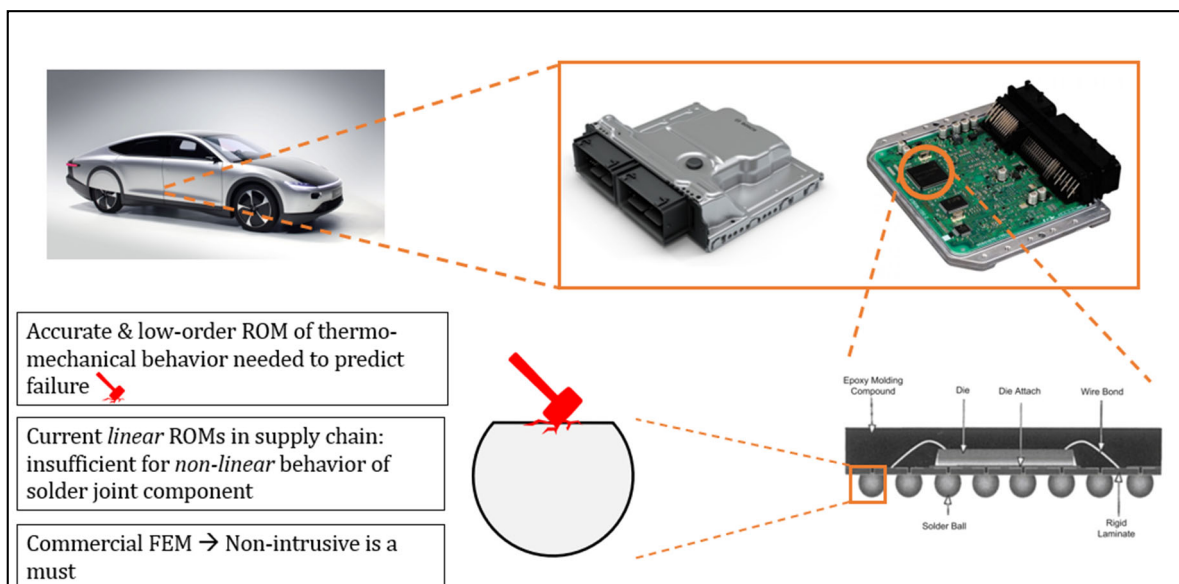


Figure 73: overview of the example application of the nonlinear MOR technique. We consider the problem of modelling solder joint – which behave nonlinearly and are critical for assessing structural integrity of components in automotive systems.

### 8.2. Method

The method can be seen as an optimization-based procedure that fits a given ROM structure to a set of simulation snapshots. Let the full-order model (FOM) be given in state-space form as

$$\dot{x} = f(x, u)$$

where  $x$  is the semi-discretized state-space and  $u$  are the input parameters of the simulation such as (time-varying) boundary conditions or material parameters. We are interested in rapid evaluation of trajectories of  $x$  for many different input trajectories  $u$ . In the solder joint creep example,  $x$  could represent the creep strain and temperature through the solder joint, while  $u$  could represent the ambient temperature. In practice, the size of  $x$  can become prohibitively expensive for such multi-query studies. The MOR technique we have developed will discover a ROM of the following form:

$$\begin{aligned} x &\approx Vx_r \\ \dot{x}_r &= f_r(x_r, u; \theta) \end{aligned}$$

where  $V \in \mathbb{R}^{n \times r}$  is the *reduced state basis* and  $x_r$  is the reduced state of size  $r$ . The parameter vector  $\theta$  parametrizes the reduced-order state evolution function  $f_r$ . As an example, consider the following ROM structure:

$$f_r(x_r, u; \theta) = A(\theta)x + H(\theta)x \otimes x + B(\theta)u$$

where  $\otimes$  denotes the Kronecker product, and  $A$ ,  $H$  and  $B$  are matrices whose elements consist of the elements of  $\theta$ .

Simulation of  $x_r$  by solving the ROM is much faster, after which an approximation of the full-order solution can be recovered through  $V$ . The quality of the approximation will depend on  $V$  and  $\theta$  and they should thus be chosen in a way to maximize the approximation quality. We assume in the sequel that we have access to a set of  $N$  simulation trajectories  $\{x_i, u_i\}_{i=1}^N$  simulated using the FOM.

In the remainder of this section, we will discuss how we make the choice of  $V$  and  $\theta$  based on this dataset, starting with  $V$ .

### 8.2.1. Selection of $V$

The selection of  $V$  such that  $x \approx Vx_r$  is achieved using Proper Orthogonal Decomposition (POD). We first collect the simulation trajectories of the full state into a data matrix:

$$X := [x_1(t_1), \dots, x_N(t_{M_N})]$$

where  $x_i(t_j)$  represents the state snapshot of the  $i$ -th simulation at the  $j$ -th timestep. The number of timesteps in each of the  $N$  simulations is denoted by  $M_i$ ,  $i = 1, \dots, N$ . Based on this data matrix, we can find a projection basis  $V$  that approximately satisfies the following equality:

$$X \approx VV^T X$$

If the error between  $X$  and  $VV^T X$  is measured in the Frobenius norm, then the solution is given by the Singular Value Decomposition (SVD) of  $X$ . The singular values of the  $X$  can guide the choice of the  $r$ .

### 8.2.2. Selection of $\theta$

To select an optimal  $\theta$ , we solve the following optimization problem:

$$\min_{\theta} \|\dot{X}_r - f_r(X_r, U; \theta)\|_2 + \lambda \|\theta\|_1$$

where  $\lambda$  is a regularization parameter that can prevent overfitting. The data matrices  $X_r$  and  $U$  are defined similarly to  $X$  in the previous section. The time-derivative data matrix  $\dot{X}_r$  is not typically directly available (unless the solver used to calculate the state trajectories also outputs  $\dot{x}$ ). Thus, a finite-difference approximation is often used to approximate this data matrix.

The above optimization problem is denoted in literature as *operator inference*. It was first proposed in the paper in “Data-driven operator inference for nonintrusive projection-based model reduction” by B. Peherstorfer and K. Willcox. Often, model structures are considered that are linear in the parameter  $\theta$ . The resulting optimization problem then becomes a regularized linear least-squares problem:

$$\min_{\theta} \|\dot{X}_r - A(\theta)X_r - H(\theta)X_r \otimes X_r - B(\theta)U\|_2 + \lambda \|\theta\|_1$$

### 8.3. Results

The proposed method is implemented in MATLAB and tested on a 1D model of a solder joint with a nonlinear creep law. The selected creep law is the Garofolo creep law, stating that the creep strain  $\varepsilon_{cr}$  evolves according to

$$\dot{\varepsilon}_{cr} = C_1 \sinh(C_2 \sigma_v)^n e^{C_3 T}$$

where  $C_1, C_2$  and  $C_3$  are material parameters,  $\sigma_v$  is Von Mises stress and  $T$  is temperature. The 1D model is discretized using the Finite Difference Method (FDM) as shown in **Figure 74**.

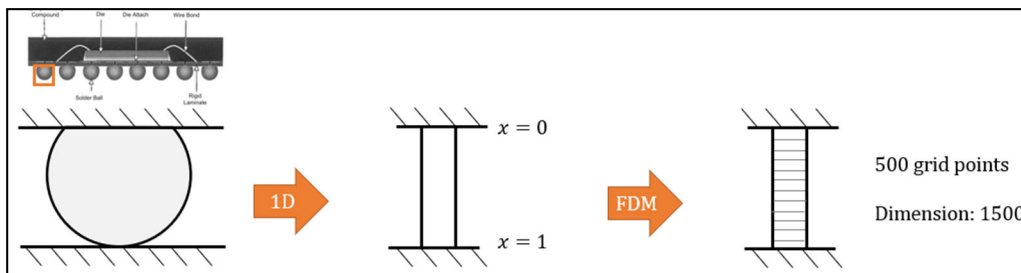


Figure 74: 1D modelling of solder joint using Finite Difference Method (FDM).

The input parameter  $u$  of the model was the initial profile of the displacement. 4 simulations were performed for different random displacements, and 1 simulation was performed to validate the ROM. Based on the singular values of  $X$ , the ROM order was set to  $r = 16$ . A quadratic model structure of the following form was then used to find the ROM:

$$\dot{x}_r = A(\theta)x_r + H(\theta)x_r \otimes x_r$$

with

$$x_r(0) = V^T u$$

To assess the quality of the ROM, the relative 2-norm of the error between the FOM and ROM solutions is plotted for 1 of the training (Figure 75) and 1 of the validation datasets (Figure 76).

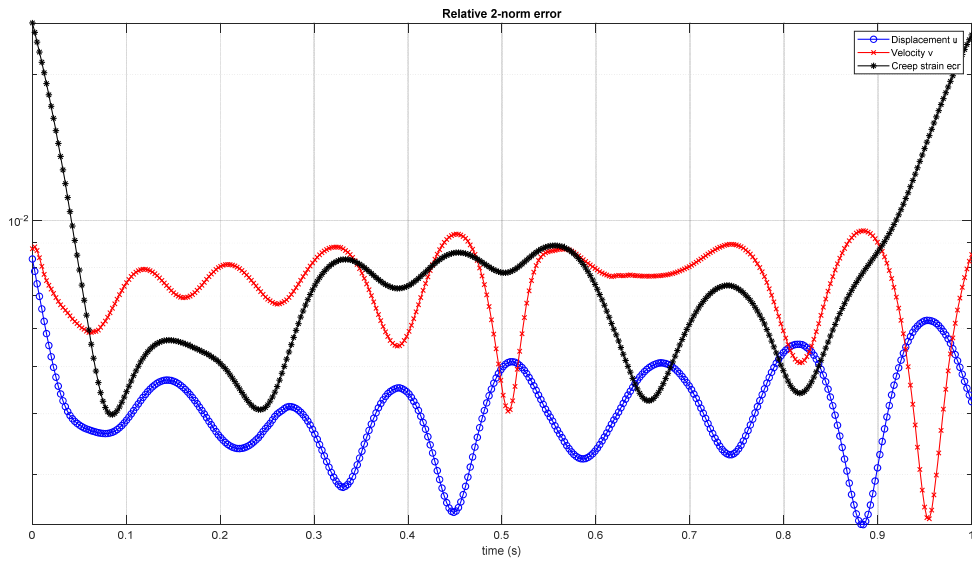


Figure 75: accuracy of the ROM for a sample of the training dataset

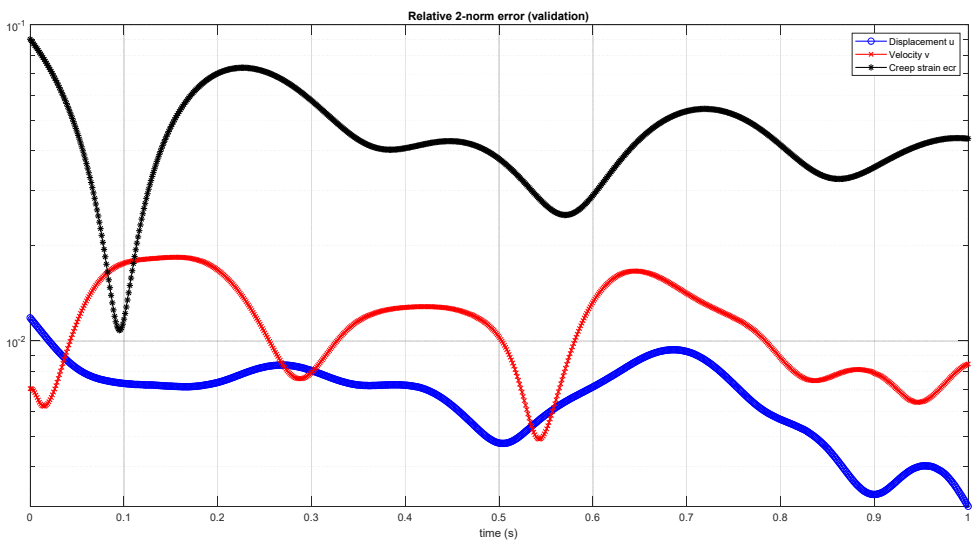


Figure 76: accuracy of the ROM for the validation dataset

## 9. Conclusion and Outlook

This comprehensive investigation delves into the realm of model order reduction (MOR) applied to diverse aspects of thermal and mechanical simulations within the microelectronics domain, with a particular emphasis on the models supplied by Infineon and NXP. The synthesis of our findings unfolds in a narrative manner, encapsulating the nuances of each explored facet.

Our exploration and achievements commenced with the successful application of MOR to linear single-domain thermal and mechanical chip models from Infineon Technologies. The results yielded exceptional approximation accuracy, extending to the computation of mechanical stresses and deformations induced by thermal strains in the reduced space. This inclusive analysis demonstrated a commendable correspondence across different models, shedding light on the vast potential inherent in the proposed methodology. Subsequent endeavors will pivot towards a sustained exploitation of this MOR scheme for thermal analysis, coupled with a dedicated assessment of its efficacy in dynamic problem-solving, such as eigenvalue analysis and frequency response.

The investigation then traversed the reduction journey of a linearized coupled thermo-mechanical Infineon model within ANSYS using the industrial software MORiA. This endeavor revealed the accuracy of Reduced Order Models (ROMs), which were generated through a Krylov-subspace based MOR method, strategically employing an expansion point at 0 Hz. The ensuing verification process encompassed the extraction of temperature, displacement, and stress results from the ROMs. These ROMs, validated through system-level simulations in ANSYS Twin Builder, exhibited commendable accuracy when compared to their Full Order Model (FOM) counterparts. The analysis further delved into probing the impact of non-zero expansion points through a MOR algorithm developed in MATLAB. The validation process, using time-domain simulations in Simulink, offered additional robustness to the proposed methodology.

Simultaneously, our exploration extended to conducting tests on various meta-modeling methods, including SoS and StaticROM Builder, aimed at generating a nonlinear compact model for the Infineon package. In parallel, solutions were introduced to preserve film coefficients and material parameters symbolically in parameterized finite element models. These efforts culminated in the successful creation of parametric reduced order models, catering to both single and multi-material domain parameters. Noteworthy attention was devoted to the nuanced selection of optimal expansion points and dimensions, elucidating their pivotal role in constructing efficient and accurate reduced models. This phase of the investigation harmonized with the overarching goals of the COMPAS project, securing the preservation of material properties in symbolic form within reduced order models, with subsequent endeavors slated for the reduction of fully nonlinear reliability models.

Another dimension of our exploration unfolded with the proposition of a substructuring approach, significantly alleviating the computational burdens associated with dynamic analyses of coupled thermo-mechanical circuit models. Leveraging a penalty-based coupling scheme and Lagrangian formulation, we meticulously assembled reduced order models, capturing the dynamic intricacies of circuit boards. The successful eigenvalue analysis of Infineon and NXP chip models on standard computational equipment marked a transformative milestone, diverging from conventional supercomputer reliance. This established assembly procedure not only streamlined the treatment of non-conforming interfaces but also bolstered the dynamic performance evaluation

of diverse design configurations. This innovative framework bears promise for augmenting design and analysis processes related to complex electronic components, heralding a more efficient and accessible era in computational mechanics methodologies.

A generalized methodology for reducing nonlinear dynamical systems also took center stage in our exploration. Demonstrating robustness and compatibility with commercial software, this approach found its exemplification in the thermomechanical model, portraying efficiency and computational advantages through model order reduction. The case studies involving the BGA and MEMS beam actuator underscored the methodology's practicality and versatility. Despite inherent challenges such as the "curse of dimensionality" and limitations in certain load cases, the proposed approach showcased robustness and efficiency in addressing complex nonlinearities across diverse engineering scenarios. Leveraging a finite element open-source implementation empowered us with crucial control over thermal loads, enabling the subsequent application of Trajectory Piecewise Linear within the proximity of an effective nonlinear reduced-order model.

In a parallel strand, a non-intrusive model reduction technique emerged as a potent solution for nonlinear models. This technique, requiring solely simulation snapshots, proved its generality by successfully applying it to the reduced-order modeling of solder joint creep. Its adaptability to a broad class of nonlinear model structures underscored its potential significance in diverse engineering applications.

In conclusion, our multifaceted investigation culminated in a nuanced understanding of MOR applications, encapsulating versatility, accuracy, and potential advancements in addressing challenges across various engineering scenarios in microelectronics. The proposed methodologies hold the promise of reshaping computational mechanics methodologies for enhanced efficiency and accessibility. This comprehensive synthesis underscores the potential transformative impact of MOR on diverse aspects of microelectronics design and analysis, ushering in a new era of computational efficiency and applicability.

In the future we hope to enable the reduction of general nonlinear multiphysical FE models. First steps will be the application of TPWL to coupled domain Ansys models and further development of parameterised Krylov-based superelements, which are described in more details in D4.3. We foresee that the final goal will be reached by a combination of machine learning and MOR.

## 10. Bibliography

- [1] R. W. Freund, "Krylov-subspace methods for reduced-order modeling in circuit simulation," *Journal of Computational and Applied Mathematics*, vol. 123, p. 395–421, 2000.
- [2] T. Bechtold, E. Rudnyi and J. Korvink, Fast Simulation of Electro-thermal MEMS: Efficient Dynamic Compact Models., 10.1007/978-3-540-34613-5. ed., 2006.
- [3] E. K. J. Rudnyi, Model Order Reduction for Large Scale Engineering Models Developed in ANSYS. In: Dongarra, J., Madsen, K., Waśniewski, J. (eds) Applied Parallel Computing. State of the Art in Scientific Computing., PARA 2004. Lecture Notes in Computer Science, vol 3732 ed., Berlin, Heidelberg.: Springer, 2006.
- [4] E. Zukowski, J. Wilde, E.B. Rudnyi, J.G. Korvink, "Model reduction for thermo-mechanical simulation of packages," *International Workshop on Thermal Investigation of ICs and Systems*, pp. p134-138, 27-30 September 2005.
- [5] I. ANSYS, Ansys® Academic Research Mechanical, Release 21.2, Help System, Mechanical APDL Theory Reference, ANSYS, Inc., 2021.
- [6] M. Thoben, X. Xie, D. Silber, and J. Wilde, "Reliability of Chip/DCB Solder Joints in AlSiC Base Plate Power Modules: Influence of Chip Size," *Microelectronics Reliability*, Vols. 41.9-10, p. 1719–1723, 2001.
- [7] J. Benzler, *Automotive Electronics –Trends and Requirements for Reliable Design*, 2014.
- [8] R. W. Freund, "Krylov-subspace methods for reduced-order modeling in circuit simulation," *Journal of Computational and Applied Mathematics*, vol. 123, no. 1-2, p. 395–421, 2000.
- [9] C. Yuan, C. Ummnakwe, I. Zawra and T. Bechtold, "COMPAS SharePoint>Documents>Work packages>WP2>1\_Infinion training models," 2022. [Online].
- [10] C. de Villemagne and R. E. Skelton, "Model reductions using a projection formulation," *International Journal of Control*, vol. 46.6, p. 2141–2169, 1987.
- [11] E. B. Rudnyi, "MOR for ANSYS," in *System-level modelling of MEMS*, Weinheim, Germany, Wiley VCH Verlag GmbH & Co. KGaA, 2013, pp. 425-438.
- [12] C. Yuan, C. Ummnakwe, I. Zawra and T. Bechtold, "COMPAS SharePoint>Documents>Work packages>WP2>T2.1 - Projection-based MOR for linearized thermo-mechanical models," 2022. [Online].
- [13] A. C. Antoulas, Approximation of large-scale dynamical systems, 2005.

- [14] L. a. R. E. a. K. J. Feng, "Preserving the film coefficient as a parameter in the compact thermal model for fast electrothermal simulation.," *IEEE Trans. on Comp.-Aided Design of Int. Circ. and Sys.*.
- [15] B. e. a. Lohmann, Model Order Reduction in Mechanical Engineering. Model order reduction., Berlin, Boston: De Gruyter, 2.
- [16] M. N. P. Gunupudi, "Multi-dimensional model reduction of VLSI interconnects.," in *Proceedings of IEEE Custom Intergrated Circuits Conference*, 2000.
- [17] L. .. S. O. C. a. C. ., .. a. L. K. H. a. W. J. Daniel, "A multiparameter moment-matching model-reduction approach for generating geometrically parameterized interconnect performance models," *IEEE Transactions on Computer-Aided Design of Integrated Circuits and Systems*, Vols. vol. 23, , no. no. 5, pp. pp. 678-693, 2004.
- [18] T. a. H. D. a. R. E. B. a. G. M. Bechtold, "Efficient extraction of thin-film thermal parameters from numerical models via parametric model order reduction.," *Journal of Micromechanics and Microengineering*, vol. Volume 20, no. Number 4, 2010.
- [19] M. E. P. Baumann, "Interpolation-based parametric model order reduction for material removal in elastic multibody systems.," *Multibody Syst Dyn* , vol. 39, p. 21–36, 2017.
- [20] "C. D. Yuan, O. S. Jadhav, E. B. Rudnyi, D. Hohlfeld, T. Bechtold," in *Proc. EuroSimE*, 2018.
- [21] X. X. D. S. J. W. M. Thoben, "Reliability of Chip/DCB solder joints in AISiC base plate power modules: influence of chip size.," *Journal of Micromechanics and Microengineering*, vol. Volume 20, no. Number 4, pp. p121-1223, 2001.
- [22] S. Gugercin, A. Antoulas and C. Beattie, "H2 Model Reduction for Large-Scale Linear Dynamical Systems.," *Journal on Matrix Analysis and Applications*, vol. vol. 30, p. pp. 609–638.
- [23] M. R. a. J. White, "piecewise-linear approach to model order reduction and fast simulation of nonlinear circuits and micro-machined devices.," *IEEE Transactions on Computer-Aided Design of Integrated Circuits and Systems*, p. 22 (2):155–170, 2003..
- [24] J. L. a. M. C. Sunyoung Im, "Surrogate modeling of elasto-plastic problems via long short-term memory neural networks and proper orthogonal decomposition.," *Computer Methods in Applied Mechanics*, vol. Volume 385, 2021.
- [25] E. Yoo, "Parametric model order reduction for structural analysis and control.," 2010. [Online]. Available: <http://www.ct.tkk.fi/publications/drjanne/main.htm>.
- [26] M. Farny, M. Olbrich, C. Ament and M. Hoffmann, "Kick & Catch : Coaction of an electrostatic kick and magnetic catch system for the rotation of a sphere.," *18th International Conference on New Actuator Systems*, ACTUATOR 2022:.

- [27] M. Farny and M. Hoffmann, "Kick & Catch: elektrostatisches Rotieren einer Kugel," *MikroSystemTechnik Kongress*, no. VDE Verlag GmbH: Stuttgart-Ludwigsburg, p. pp 274–277., 2021.